AD-A179 377 TECHNICAL REPORT FOR THE PERIOD 1 OCTOBER-31 DECEMBER 1986(U) SCIENCE APPLICATIONS INTERNATIONAL CORP ARLINGTON VA CENTER FOR SEISMIC STUDIES FEB 87 1/2

UNCLASSIFIED SAIC-87/1504 MDA903-84-C-0020 F/G 8/11 NL

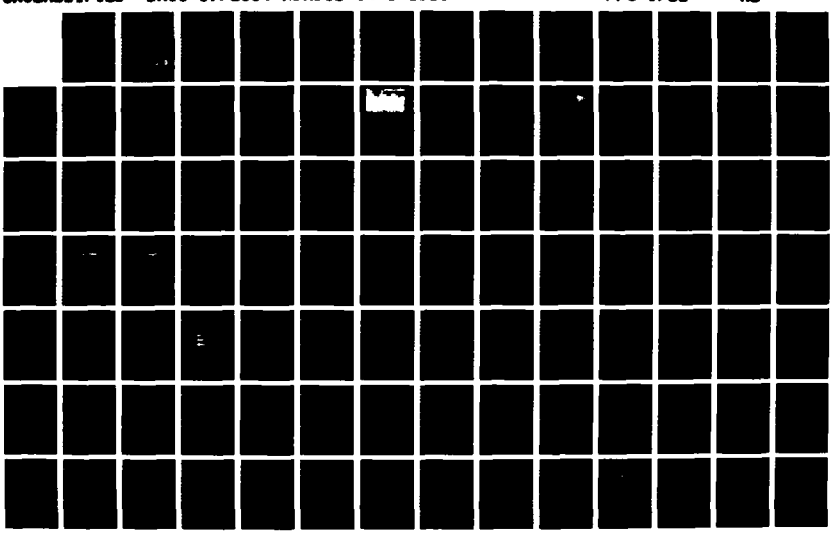


1.0
1.1
1.25
1.4
1.6
1.8
2.0
2.2
2.8
3.2
3.6
4.0

Technical Report C87-01
February 1987

TECHNICAL REPORT FOR THE PERIOD 1 OCTOBER – 31 DECEMBER 1986

Center Staff

SPONSORED BY
DEFENSE ADVANCED RESEARCH PROJECTS AGENCY

Center for Seismic Studies
1300 N. 17th Street, Suite 1450
Arlington, Virginia 22209-3871
Telephone: (703) 276-7900

Technical Report C87-01
February 1987

TECHNICAL REPORT FOR THE PERIOD 1 OCTOBER – 31 DECEMBER 1986

Center Staff

Sponsored by:
DEFENSE ADVANCED RESEARCH PROJECTS AGENCY
Monitored by:
Defense Supply Service – Washington
Under Contract No. MDA 903-84-C-0020

Science Applications International Corp.
1300 N. 17th St., Suite 1450
Arlington, VA 22209

UNCLASSIFIED
SECURITY CLASSIFICATION OF THIS PAGE

ADA179377

REPORT DOCUMENTATION PAGE

Form Approved
OMB No. 0704-0188
Exp. Date: Jun 30, 1986

1a REPORT SECURITY CLASSIFICATION Unclassified	1b RESTRICTIVE MARKINGS
2a SECURITY CLASSIFICATION AUTHORITY	3 DISTRIBUTION/AVAILABILITY OF REPORT Unlimited
2b DECLASSIFICATION/DOWNGRADING SCHEDULE	
4 PERFORMING ORGANIZATION REPORT NUMBER(S) SAIC-87/1584, Technical Report C87-01	5 MONITORING ORGANIZATION REPORT NUMBER(S)
6a NAME OF PERFORMING ORGANIZATION Science Applications International Corporation 6b OFFICE SYMBOL (If applicable)	7a NAME OF MONITORING ORGANIZATION Defense Supply Service - Washington
6c ADDRESS (City, State, and ZIP Code) Center for Seismic Studies, SAIC 1300 N. 17th Street, Suite 1450 Arlington, Virginia 22209-3871	7b ADDRESS (City, State, and ZIP Code) Room 1D245, The Pentagon Washington, D.C. 20310
8a NAME OF FUNDING/SPONSORING ORGANIZATION Defense Advanced Research Projects Agency 8b OFFICE SYMBOL (If applicable) STO/GSD	9 PROCUREMENT INSTRUMENT IDENTIFICATION NUMBER MDA-84-C-0020
8c ADDRESS (City, State, and ZIP Code) 1400 Wilson Boulevard Arlington, Virginia 22209	10 SOURCE OF FUNDING NUMBERS PROGRAM ELEMENT NO: PROJECT NO: A04882 TASK NO: WORK UNIT ACCESSION NO:
11 TITLE (Include Security Classification) Technical Report for the Period 1 October - 31 December 1986 (Unclassified)	
12 PERSONAL AUTHOR(S) G. Bulin, A. Campanella, P. Dysart, H. Israelsson, A. Jurkevics, J. Pulli , C. Romney and A. Ryall	
13a TYPE OF REPORT Technical Report 13b TIME COVERED FROM 10/1 TO 12/31/86	14 DATE OF REPORT (Year, Month, Day) 1987 February 15 PAGE COUNT 112
16 SUPPLEMENTARY NOTATION	

17 COSATI CODES			18 SUBJECT TERMS (Continue on reverse if necessary and identify by block number)
FIELD	GROUP	SUB-GROUP	Seismology, Network, Nuclear Monitoring, Polarization, Regional, Attenuation, P-Wave, GSE

19 ABSTRACT (Continue on reverse if necessary and identify by block number)

Work on network design and capability assessment during this reporting period has focused on defining the seismological criteria for selecting stations of a global seismic network to achieve a specified minimum verification capability. The design criteria are defined with a view toward minimizing the gap between detection threshold and the threshold for recording seismic waves used for discriminating earthquakes from explosions. In a complementary study, the *Seismic Network Assessment Program for Detection* (SNAP/D) was used to estimate the contribution to network detection capability on a continent-by-continent basis.

(Continued on attached sheet)

20 DISTRIBUTION/AVAILABILITY OF ABSTRACT ☒ UNCLASSIFIED/UNLIMITED ☐ SAME AS RPT ☐ DTIC USERS	21 ABSTRACT SECURITY CLASSIFICATION Unclassified
22a NAME OF RESPONSIBLE INDIVIDUAL Ann U. Kerr	22b TELEPHONE (Include Area Code) (202) 694-3624 22c OFFICE SYMBOL STO/GSD

DD FORM 1473, 84 MAR 83 APR edition may be used until exhausted
All other editions are obsolete

SECURITY CLASSIFICATION OF THIS PAGE
UNCLASSIFIED

19. Abstract - *(Continued)*

Research to improve analysis of regional seismic data is currently focused on determining various waveform "signatures" of events that occur frequently at the same location. Examples being studied at the Center include repeated explosions at mines in the western U.S.S.R. and Scandinavia, presumed underwater detonations off the coast of Norway, and northern European earthquake sequences. Procedures being tested as signature elements include the formation of particle-motion parameters from the six terms of the three-component covariance matrix, plus spectral, cepstral and autoregressive analyses.

A review of evidence for high-quality propagation of seismic waves at regional distance ranges in the U.S.S.R. was conducted in response to a request from DARPA. The available data are consistent with maximum Q_α of about 2,000 for regional seismic waves. In both the Baltic shield and central Asia, high-frequency signals from small events are observed to about 500-600 km, but disappear into the noise at larger distance ranges.

A study comparing the slope of M_{L_g} *vs.* m_b for NTS with that for the eastern Kazakh test site found differences suggestive of differences in L_g generation, and leads to questions about the use of M_{L_g} as a site-independent measure of explosion yield.

In work to support U.S. participation in the GSE, the Center staff helped in revising the *Sourcebook for Seismic Waveform Data Exchange*, participated in workshops, held technical exchanges with visitors, prepared data for use in demonstrating procedures and formats to other participants, and established links for acquiring foreign bulletin data. X.25 communications links were successfully tested between the Center and Norway, New Zealand, Japan, Australia, Canada, the Federal Republic of Germany, Sweden and Finland.

Other special reports during this reporting period included a draft study of technical and functional characteristics of a potential global seismic monitoring system, a report summarizing technical questions surrounding verification of the Threshold Test Ban Treaty, a *User's Introduction and Software Guide to the Center for Seismic Studies*, an evaluation of the RSTN system, and a technical note covering analysis of a Novaya Zemlya event that occurred during the recent Soviet nuclear testing moratorium.

In the area of system development, new memories were installed on the Center's VAX machines, classified operations were transferred to a Sun workstation, and routine archiving of NORESS data was initiated.

Table of Contents

1. FOREWORD 1-1

2. NETWORK CAPABILITY AND DESIGN 2-1

   2.1. Network Performance and Station Selection Criteria 2-1
   2.2. Detection Capabilities of Continental Networks 2-18

3. RESEARCH TO IMPROVE ANALYSIS OF REGIONAL SEISMIC DATA 3-1

   3.1. Particle-Motion Signatures for Source Identification 3-1
   3.2. Characteristics of P-Waves from a Mine in the Soviet Union 3-12
   3.3. Autogregressive Analysis of Earthquakes and Explosions 3-18
   3.4. High-Frequency Propagation in Shield/Platform Regions 3-28

4. SUPPORT OF DARPA PROGRAM 4-1

   4.1. Comparison of mb and mb(Lg) for NTS and Eastern Kazakh 4-1
   4.2. Discrimination and the 1 August 1986 Novaya Zemlya Event 4-11
   4.3. Evaluation of the RSTN System 4-29

1. FOREWORD

Work on network design and capability assessment during this reporting period has focused on defining the seismological criteria for selecting stations of a global network to achieve a specified minimum verification capability. In an example presented in Section 2.1, network design criteria are given which maximize the capability to detect and locate explosions, optimize the detection of signals used to identify shallow earthquakes by the m_b:M_s method, and provide for sufficient station coverage to determine the depth of deep-focus earthquakes. The design criteria are also defined with a view toward minimizing the gap between detection threshold and the threshold for recording seismic waves used for discriminating earthquakes from explosions. The presentation is illustrated with examples based on data collected during the Group of Scientific Experts, U.N. Conference on Disarmament, Technical Test (GSETT) in 1984-85.

In Section 2.2, the *Seismic Network Assessment Program for Detection* (SNAP/D; Ciervo *et al.*, 1983) was used to estimate the contribution to network detection capability on a continent-by-continent basis. In this analysis, the total number of stations used during the GSETT was redistributed to provide even coverage in continental regions, and the influence of each continental network on total capabilitity was determined, as well as the detection capability for events occurring on that continent. Results showed, for example, that stations in Africa would be important in monitoring other parts of the globe, while a network in South America contributes primarily to monitoring of events in that region.

Section 3 describes research to improve analysis of regional seismic data, currently focused on the use of *case-based reasoning* to identify the *signature* of events that occur frequently at the same location. Examples being studied at the Center include repeated explosions at mines in the western USSR and Scandanavia, presumed underwater detonations off the coast of Norway, and northern European earthquake sequences. In Section 3.1, particle-motion signatures are formed from the six terms of the three-component covariance matrix, as a function of time for different frequency passbands. The diagonal terms of the matrix represent the signal envelope, and the off-diagonal cross terms are important in identifying seismic phases and propagation effects. These signatures capture much of the important information contained in three-component seismograms, and retain it in a compressed form that can be automated to measure similarity of events in a given area.

Section 3.2 discusses spectral and cepstral features of explosions at a mine in the western Soviet Union, near Leningrad. The spectra are scalloped, with peaks separated by 3 Hz, and the mean cepstrum for the mine blasts confirms a positive secondary peak with about a 0.3 second delay. The note speculates that this may be associated with delayed firing of multiple explosions in the mine.

Section 3.3 compares time-varying autoregressive spectral parameters for TFO recordings of NTS explosions and a group of nearby earthquakes. The analysis reaffirms

previous results of Bennett and Murphy (1986), which indicated that the explosion P_g and L_g waves were depleted in high frequencies relative to the same phases for the earthquakes. However, P_n for the explosions had peak frequency as large or greater than that for the earthquakes. The difference is attributed to differences in near-source lithology for the two types of events.

Section 3.4 reviews evidence for high-quality propagation of seismic waves at regional distance ranges in the USSR, including evidence presented by Evernden *et al.* (1986) to support a value of Q_α = 9,000 in network capability assessments. The Evernden *et al.* interpretation requires assumptions about differences in the seismic source spectrum for earthquakes and explosions, and about the structure of the M-discontinuity. A more straightforward interpretation of the available data -- high-frequency USGS and ECTN recordings of earthquakes in eastern North America, data from a Soviet wide-angle reflection profile in the Caucausus Mountains, earthquake records made on selectable-frequency seismic systems (*ChISS*) in central Asia, and NORESS recordings of earthquakes and explosions in the Baltic shield -- is consistent with maximum Q_α of about 2,000 for regional seismic waves. In both the Baltic shield and central Asia, high-frequency (> 20 Hz) signals from small ($m_b \leqslant 3$) events are observed to about 500-600 km, but are lost in the noise at larger distance ranges.

A major part of the Center research program has been to respond to short-term DARPA requirements for special studies, including reviews aimed at integrating results developed by other research groups for some particular area of the program. Much effort during the last quarter of 1986 was devoted to preparing for, and conducting preliminary experiments in computer-to-computer transfer of seismic waveform data. This work included revising and republishing the *Sourcebook for Seismic Waveform Data Exchange* (GSE/JAPAN/24), preparing for and participating in workshops, technical exchanges with visitors, preparing waveform data for use in demonstrating procedures and formats to other participants, and establishing new links for acquiring foreign bulletin data. X.25 communications links were successfully tested between the Center and Norway, New Zealand, Japan, Australia, Canada, the Federal Republic of Germany, Sweden and Finland.

In other work to support the DARPA/GSD program, a draft paper was prepared defining technical and functional characteristics of a potential future global seismic monitoring system for consideration by the UN Committee on Disarmament, Group of Scientific Experts (GSE). An 89-page report by A. Ryall, titled *Yield Verification Research, 1965-1985, and the DOD Technical Review Panel*, summarizing technical questions surrounding verification of the Threshold Test Ban Treaty, was submitted to DARPA in October 1986 and is being reviewed for general distribution. A draft document titled *User's Introduction and Software Guide to the Center for Seismic Studies* was completed. This document contains information on all Center-supported software and additional research programs that could be of use to researchers using Sun workstations. The *User's Introduction* was sent to Finland and a few other users; after comments are received it will be available to Center users.

Other reports prepared in response to DARPA requests include the review of high-frequency propagation given above in Section 3.4, and several notes presented in Section 4. Section 4.1 is a note comparing the slope of M_{Lg} *vs.* m_b for NTS with that for the eastern Kazakh test site. Differences in this value for the two test sites are suggestive of differences in L_g generation, and lead to questions about the use of M_{Lg} as a site-independent measure of explosion yield. Section 4.2 describes the analysis of a Novaya Zemlya event that occurred during the recent Soviet nuclear testing moratorium, using various discrimination techniques being tested as DARPA workstation tools at the Center. The results illustrate the difficulty of identifying a well-recorded seismic event, with magnitude equivalent to a tamped underground nuclear explosion of a few kilotons, located in a stable geologic region, near a well-studied test site. Section 4.3 contains an evaluation of the RSTN system, based on Center experience in receiving and processing on-line data from this system since 1984. The technical note addresses selected questions relative to site selection and performance, instrument characteristics and communications for the RSTN system.

In the area of system development at the Center, 16 Mbyte main memories were installed on the VAX machines HUGO and BENO. Classified operations were transferred to a Sun 3/160 (HELIOS) in December, after receipt of government approval of a new security guide. Further work on the NORESS data acquisition system succeeded in eliminating the few remaining programming bugs, and routine archiving of NORESS data commenced. The earlier plan to archive waveform segments containing only events selected from the NORESS bulletins was postponed indefinitely. A number of waveform analysis programs for the Sun computers were developed as part of the research program; several of these appeared to be of potential use to others and were, accordingly, documented and demonstrated to DARPA and visitors to the Center.

2. NETWORK CAPABILITY AND DESIGN

2.1. A NOTE ON NETWORK DESIGN: MEASURES OF NETWORK PERFORMANCE AND CRITERIA FOR STATION SELECTION

2.1.1. Introduction

Studies of the capabilities of seismic station networks to monitor underground nuclear explosions are usually limited to estimates of given station networks. That is to say the geographical coordinates and noise characteristics of the seismological stations are given, and the capability of the network to detect seismic events is then calculated. From the point of view of monitoring, the reverse problem of determining the station network that satisfies given desirable performance criteria is also relevant. This problem is seldom addressed, partly because of its complexity and also because of the fact that widely accepted performance criteria are not available.

An *ideal* station network would perform uniformly with regard to basic seismological functions like event detection, location, depth determination and identification. It would, for example, detect events down to a certain magnitude regardless of location within a specified target area. All detected events just above this threshold would be located with about the same satisfactory accuracy, depths would be determined within an acceptable uncertainty, and identification parameters would be recorded for all detected events. In other words, the capability would be independent of geographical location and there would be a minimum gap between the thresholds of various seismological functions.

In practice, however, seismic networks do not usually perform in such a uniform and balanced manner. This is illustrated by the GSETT network (with the target area being the whole world), which had an event detection threshold that varied considerably with region, and a significant gap between detection on the one hand and epicenter determination, depth estimations, and recording of identification parameters on the other. Moreover, a large number of the reported station detections could not be associated with any seismic event detected and located by the network.

The problem of selecting seismological stations for a monitoring network can be formulated as follows. Select the minimum number (n_s) of sites (with co-ordinates, $\phi_i,\lambda_i;i=1,2,...,n_s$) for seismological stations in a given area (A_s), so that a specified performance will be obtained for monitoring seismic events in a given target area (A_e). A variant of this problem is to select the sites for a given number of stations to that the performance is optimized in some sense.

In order to get some insight into this problem we attempt in this note to define measures of network capabilities and performance criteria that can be used to select stations for a network with desirable capabilities.

2.1.2. Monitoring Tasks

A monitoring network could be designed for several seismological tasks and emphasis could vary between tasks depending on evasion scenarios: decoupling, hide-in-earthquake, and multiple shots. Hypothetical networks have been tailored to counteract one or more of such evasion scenarios (Hannon, 1983; Evernden *et al.*, 1986).

In the following we consider monitoring of events with magnitudes greater than $m_b \approx 4.0$, based on observations in the *teleseismic* distance range. Short of a general solution to the station selection problem we will tailor the tasks for different source types. The network in this example will be designed to maximize the capability to detect explosions and to detect signals used to identify shallow earthquakes by the m_b:M_s method, and deep earthquakes by focal depth. In addition, emphasis is placed on minimizing the unassociated station signal detections. This leads us to consider the following monitoring tasks:

- *Explosions:*

  The system should be designed to maximize the capability to detect and locate explosions. Moreover, the depth has to be estimated so that the explosions can be identified to have shallow source focus. For simplicity it is assumed that the explosions are carried out in hard rock and are fully decoupled.

- *Shallow earthquakes:*

  Identification is made primarily on the basis of depth. For shallow earthquakes the m_b:M_s criterion is also important. Signal detections at individual stations from shallow earthquakes have also to be associated with detected and located events with high probability. In other words the number of unassociated station detections originating from shallow (and deep) earthquakes should be minimized. In principle it is thus not necessary to optimize the capability of detection, location, or depth estimation for shallow earthquakes.

- *Deep earthquakes:*

  It is assumed that the occurrence of deep earthquakes is confined to a sub-region of the target area. The most important function is depth estimation, *i.e.*, again it would in principle not be necessary to optimize the capability to detect and locate deep events, but the depth of events that are detected and located has to be determined so that a possible explosion depth can be ruled out. The number of unassociated station detections originating from deep earthquakes (together with those from shallow earthquakes) should also be minimized.

The tasks in relation to source type can be summarized by the following table:

TASK	SOURCE TYPE		
-	Explosion	Shallow Quake	Deep Quake
Event Detection	*		
Signal Association		*	*
Epicenter Location	*		
Depth Estimation	*		*
Source Identification (Surface Waves)		*	

The functions listed in the table require different kind of information from the seismic recordings. A network designed to optimize only one of the tasks may therefore not necessarily perform in an optimum manner for another. Consider for example the case for which the area, A_e, consists of one site only (one pair of coordinates). Then the azimuthal coverage of the stations around the site largely determines the location accuracy, whereas appropriate coverage of certain epicentral distance intervals is important for the depth estimation based on surface reflections *(pP, sP)*. Siting of the stations to optimize the detection capability is mainly determined by the amplitude attenuation as a function of distance, which may result in a station distribution that is non-uniform in azimuth and distance. If the target area, A_e, is not just one pair of coordinates but for example a continent the situation becomes more complicated. Because of this trade-off between the tasks, selection of the stations taking several tasks into account has to be based on some kind of 'compromise' between tasks. One of the tasks above, detection of surface waves, can however be optimized independently of the others provided the long period stations are not necessarily to be co-located with short period stations. On the other hand, it may from a seismological point of view be desirable to maintain such a co-location of different kinds of instrumentation.

2.1.3. Measures of Performance

In order to design criteria for selecting stations of a network, measures of performance of the various functions discussed above have to be specified. The specification below is illustrated with calculated examples for the GSETT network which had global coverage (*i.e.*, the area A_e is the whole world in these examples). Thus, the target area is the whole world, and not just the Eurasian continent.

2.1.3.1. Event Detection

The event detection capability of a given seismic network (with co-ordinates $(\phi_i,\lambda_i), i=1,2,...,n_s$) is usually described in terms of magnitude thresholds (m_b) at a certain probability, p, which is often chosen to be 90%. A seismic event detection requires here by definition that signals are detected at a sufficient number of stations to determine the epicenter of the event. The detection threshold is a function of the geographical co-ordinates (Φ,Λ) of the area to be monitored A_e, *i.e.*, $m_b=m_b(\Phi,\Lambda|\, p)$. Station selection could be based on obtaining at least a certain minimum threshold, m_{b0}, throughout the area, A_e, *i.e.*:

$$m_b(max)=\underset{\Phi,\Lambda}{Sup}\left\{ m_b(\Phi,\Lambda);(\Phi,\Lambda)\in A_e \right\} \leqslant m_{b0}$$

This means that in some parts of A_e the threshold could be significantly below m_{b0}, whereas in other parts it could be significantly higher but still not greater than m_{b0}. A station selection could, however, also aim at obtaining a minimum average threshold with as uniform a capability as possible specified by a maximum standard deviation of the threshold, σ_0:

$$\overline{m}_b=\int_{A_e} m_b(\Phi,\Lambda)\,d\Phi\,d\Lambda \Big/ \int_{A_e} d\Phi\,d\Lambda \leqslant m_{b0}$$

and

$$\sigma^2(m_b)=\int_{A_e} (m_b(\Phi,\Lambda)-\overline{m}_b)^2\,d\Phi\,d\Lambda \Big/ \int_{A_e} d\Phi\,d\Lambda \leqslant \sigma_0^2(m_b)$$

The detection probability at a certain magnitude, $p=p(\Phi,\Lambda|\, m_b)$, can be used in a similar way as the magnitude threshold to formulate station selection criteria.

The following magnitude thresholds were calculated for the GSETT network (Israelsson, 1986):

Region	Max	Mean	S.D.
World	4.59	4.22	0.22
Eurasia	4.22	3.99	0.18

2.1.3.2. Association of Station Detections

Association of station detections from naturally occurring earthquakes are usually not considered in seismic network assessments, but since unassociated station detections

may be considered as false alarms, the function of association is included here. The average of the total number of unassociated detections at the stations of the network for a given time period, $N_u(tot)$, is here used as a measure of performance, and this average should not exceed a certain maximum rate, N_{u0}, *i.e.*,

$$N_u(tot) \leqslant N_{u0}$$

There are other ways to define the number N_u. For example, if a significant part of the unassociated station detections can with high probability be determined to be originating from events outside the area of interest, A_e, it could be sufficient to use the number of unassociated station detections, $N_u(A_e)$, that with high probability originate from events in the area A_e as a measure of association.

The total number of unassociated teleseismic station detections for the GSETT were 7000, which gives a daily average of 120.

2.1.3.3. Epicenter Determination

The location capability of a network is usually described by estimated location errors for a given magnitude, m_b, at a given confidence level, p, which can be equal to the probability for the detection threshold (i.e, 90%). The error is some parameter of the estimated error ellipse, like length of maximum axis or area. If we use the length of the maximum axis of the error ellipse, $l(\Phi,\Lambda|\, m_b,p)$ as a measure then the criterion for location can be written in an analogous way to that for detection above:

$$l(max) = \underset{\Phi,\Lambda}{Sup}\left\{ l(\Phi,\Lambda|\, m_b=m_{b0});(\Phi,\Lambda)\in A_e \right\} \leqslant l_0$$

with l_0 denoting a maximum acceptable length of the largest axis of the error ellipse. Again, the location error could be much smaller than l_0 in some parts of A_e, and significantly larger in other parts but still not greater than l_0. If uniformity is emphasized, average location errors and associated standard deviations could be used rather than extreme values like $l(max)$, as indicated above for the detection threshold.

For the GSETT, examples using the world and the Eurasian continent as A_e gave values of 52 and 23 km, respectively, for $l(max|\, m_{b0}=4.6 \text{and} p=0.90)$ in a SNAP/D simulation.

A more strict criterion would be to use $l(max)\leqslant l_0$ for all detected events above the magnitude detection threshold.

2.1.3.4. Depth Estimation

We use the lower and upper ends of the confidence (e.g., 90%) interval for the estimated depth, which are denoted h_{lo} and h_{hi} respectively as a description of the depth estimation capability. They are both functions of event location (Φ,Λ), depth (h), and magnitude (m_b), *i.e.*, $h_{lo}=h_{lo}(\Phi,\Lambda,h,m_b)$ and $h_{hi}=h_{hi}(\Phi,\Lambda,h,m_b)$. We assume that only depths of earthquakes in a sub-region $A_e(deep)$ of the target area, below a certain depth, h_1, and of explosions anywhere in A_e above a certain maximum depth h_e need to be considered. The depth, h_1 corresponds to a certain reduction in the generation of surface waves and reduced capability to determine M_s (see discussion below). For example, if $dM_s/dh \approx -0.008$, (Marshall and Basham, 1972) a depth of 40 km corresponds to an M_s reduction of about 0.3. The depth h_e corresponds to a maximum depth below which underground nuclear explosions can not realistically be set off (say, 25 km).

As measures of the network capability to estimate depth we then use:

$$h_{lo}(min)=\underset{\Phi,\Lambda}{Inf}\left\{ h_{lo}(\Phi,\Lambda|\, h=h_1,m_b=m_{b0}),(\Phi,\Lambda)\in A_e(deep)\right\}$$

and

$$h_{hi}(max)=\underset{\Phi,\Lambda}{Sup}\left\{ h_{hi}(\Phi,\Lambda|\, h=h_e,m_b=m_{b0}),(\Phi,\Lambda)\in A_e\right\}$$

It is assumed that if $h>h_1$ then $h_{lo}(d)>h_{lo}(h_1)$, and that if $h<h_e$ then $h_{hi}(d)<h_{lo}(h_e)$.

The values for the GSETT network for the two target areas (world and Eurasian continent) were: $h_{lo}(\min|\, m_{b0}=4.60;h=100km)=-47$ and $=15$ km respectively and $h_{hi}(\max|\, m_{b0}=4.60;h=0km)=582$ and $=261$ km respectively.

2.1.3.5. Determination of Surface Wave Magnitudes

The capability of determining M_s for shallow earthquakes $(d<d_1)$, can be described by the M_s detection threshold in a similar way as the detection threshold, m_b is used. It can also be more directly related to the task of compilation of identification parameters. The aim is to determine surface wave magnitudes for all shallow earthquakes that are detected and located, which can be formulated as follows. Assume also that estimates of the coefficients a and b of the linear relation between m_b and M_s for each Φ,Λ or sub region of A_e are available:

$$m_b = a(\Phi,\Lambda) + b(\Phi,\Lambda)\cdot M_s$$

close to the detection threshold for m_b in that sub region. The difference between the m_b threshold (also denoted m_b) and the 'equivalent' m_b threshold for surface waves from shallow earthquakes and derived from the actual M_s threshold (this M_s threshold is also

denoted M_s) using the linear relation above:

$$\Delta m_b(\Phi,\Lambda) = m_b - (a+b\cdot M_s)$$

is a function of the co-ordinates Φ,Λ and the following measure can be used for compilation of surface wave magnitudes:

$$\Delta m_b(min) = \underset{(\Phi,\Lambda)}{Sup}\left\{ \Delta m_b(\Phi,\Lambda);(\Phi,\Lambda)\in A_e \right\}$$

The differences in detection thresholds between surface and body waves for the GSETT network were, for the whole world and the Eurasian continent, 0.46 and 0.18, respectively. This is based on the assumption that m_b=1.26+0.74·M_b, which was obtained from m_b:M_s data for the GSETT.

2.1.4. Criteria for Station Selection

The measures of performance defined above can be summarized by a a six component performance vector, $\overline{c}$:

$$\overline{c} = (m_b(max),N_s(tot),l(max),h_{l_0}(min),h_{h_i}(max),\Delta m_b(max))$$

The components of this vector takes the following calculated values for the two GSETT examples:

$$\overline{c}(world) = (4.6,120,52,-47,582,0.46)$$

and

$$\overline{c}(Eurasia) = (4.2,120,23,15,261,0.18)$$

The values of the components of this vector can also be used to formulate criteria for selection of stations for a network. This is illustrated in the following. Each component is associated with a task and its value represents a desired minimum performance. We use calculations for the GSETT data to determine the regions in which this network would have the following minimum performance:

$$\overline{c}=(4.0,10,10,25,25,0.0)$$

These calculated examples are only included as an illustration and should not be construed as an assessment of the GSETT network for global monitoring. Most of the calculations were made with the SNAP/D program and extensions of the "Networth" approach.

• *Signal Association and Event Detection*

The maximum acceptable magnitude detection threshold for the example vector above leads to the following requirement for detection of explosions:

$$m_b(max) \leqslant m_{b0}=4.0$$

Figure 1 shows the areas (unshaded on the map) of the world for which this inequality is fulfilled for the GSETT network. These areas are limited to Europe and some parts of North America. The "grey" areas indicate regions where the inequality is not fulfilled and the different degree of shading also indicate how close the threshold of the network is to the desired minimum threshold (m_{b0}=4.0). The lighter the shading the closer to the threshold.

The "false alarm" criterion for unassociated station detections described in Section 2.1.3.2 above:

$$N_u(tot) \leqslant N_{u0}$$

has been modified in *Figure 2* to map the percentage of unassociated station detections as a function of region, and it is assumed to be acceptable for 15% or less or the station detections to be unassociated.

• *Epicenter Determination*

The value of the maximum acceptable location error of the performance vector in the example above gives the following criterion for location capability:

$$l(max|\ m_b=m_{b0}) \leqslant l_0 = 10$$

The regions where the inequality is satisfied, are shown as unshaded areas in *Figure 3*, for m_{b0}=4.0 and 5.0. In fact, it is satisfied only for m_{b0}=5.0 in very limited areas in Europe and Eastern Asia. The degree of shading in *Figure 3* is proportional to the location error: the larger the error the darker the shading. From the degree of shading as indicated by the scale in the top of *Figure 3* it can be seen that if l_0=50 would be an acceptable location accuracy the location criterion would be satisfied by the GSETT network for detection threshold of m_{b0}=5.0 over the entire globe.

• *Depth Estimation*

Since depth estimates are used to identify the seismic events, it is important that the depth estimation criteria are satisfied for all events that are detected in order to minimize the gap between event detection and identification. The calculated

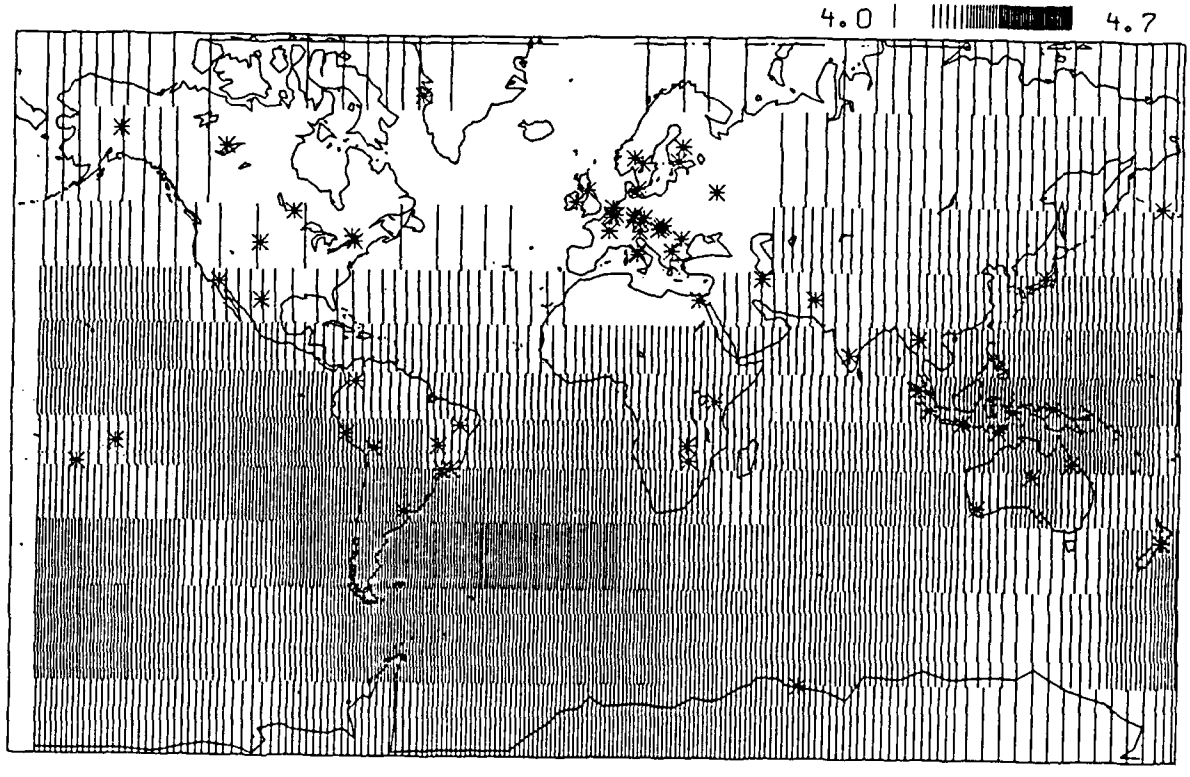

Figure 1. Detection capability of the GSETT network compared with a m_b - threshold of 4.0. The stations are indicated by asterisks. Grey and dark areas outline parts of the world where the GSETT is above m_b=4.0.

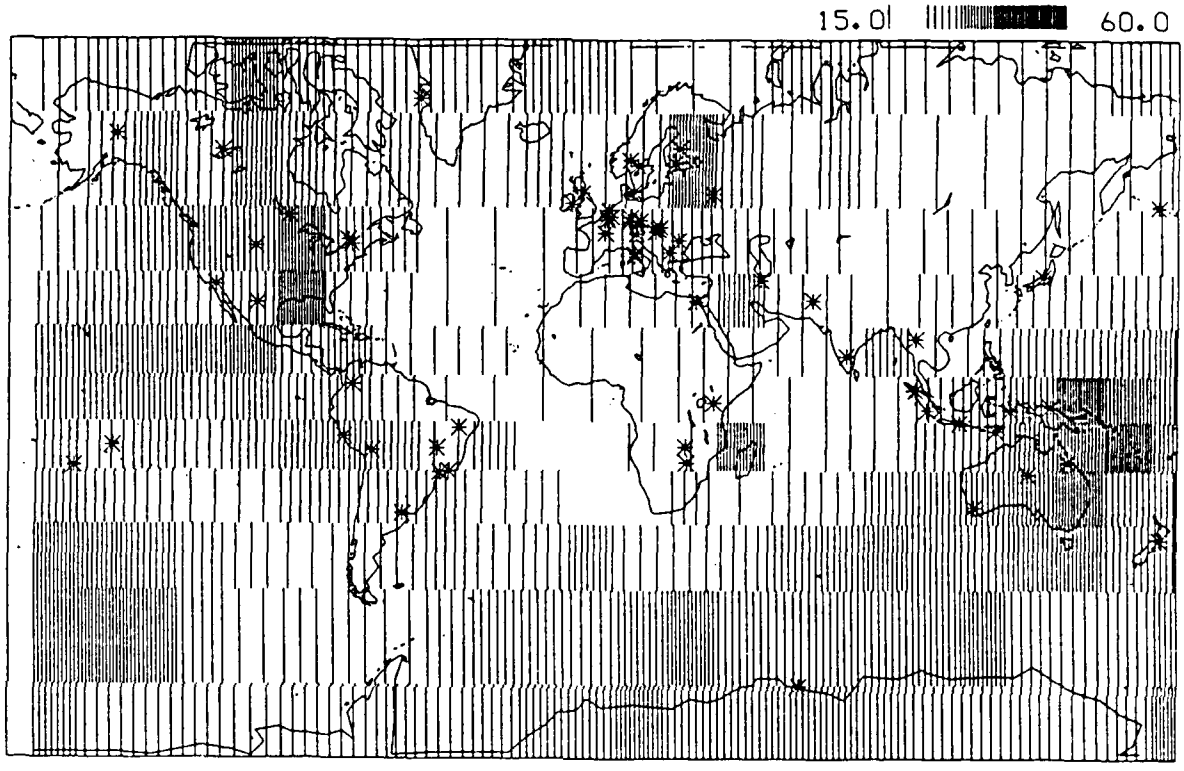

Figure 2. Percentage of unassociated station detections of the GSETT network compared with a maximum of 15%. Grey and dark areas outline parts of the world where the percentage for the GSETT network would be higher than 15% assuming an exponential magnitude distribution of the events with a b - value of 1.0.

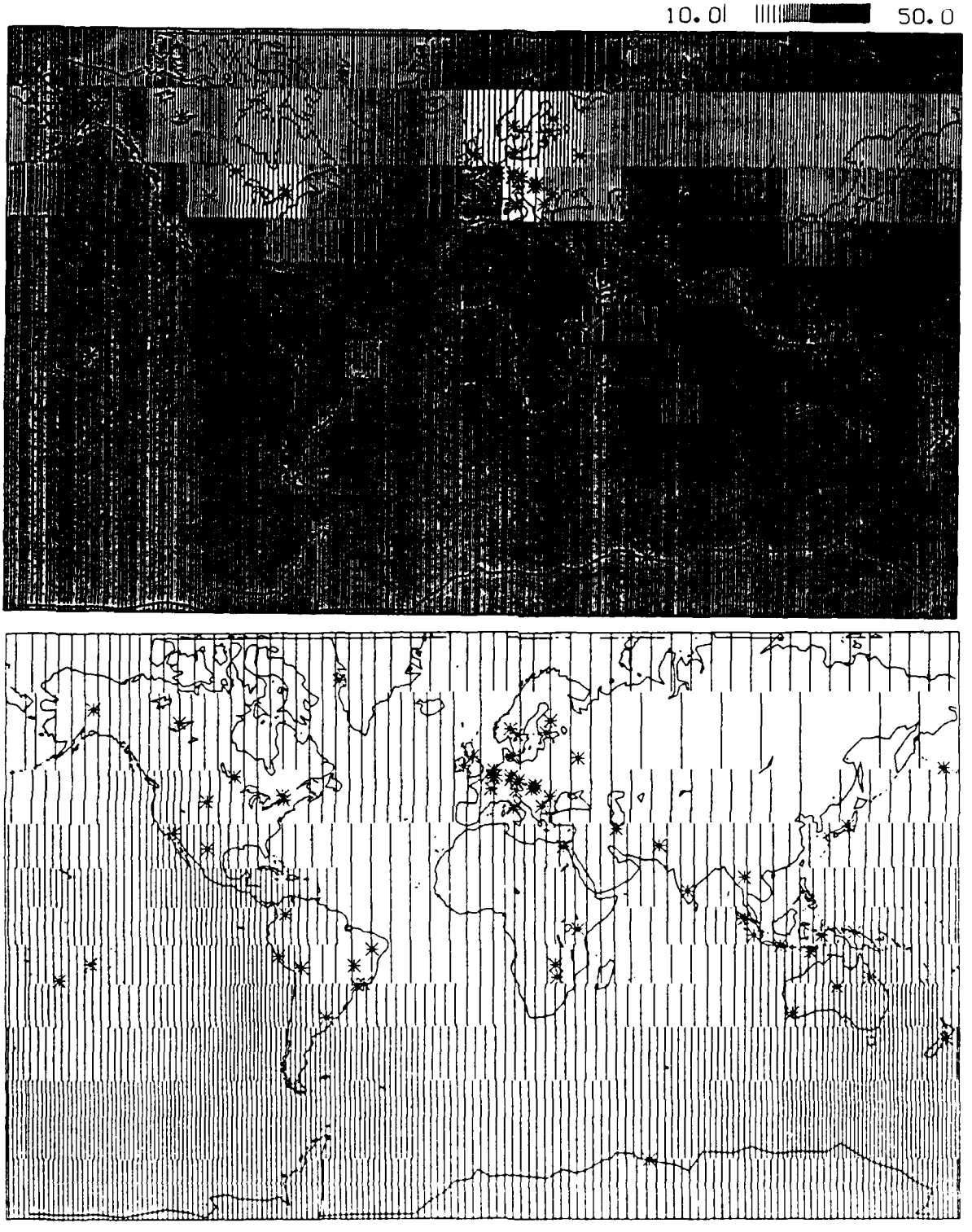

Figure 9. Location errors for the GSETT network compared with a 10 km error for events with m_b=4.0 and m_b=5.0. Grey and dark areas outline parts of the world where the GSETT location error is larger than 10 km.

examples below are therefore made for depth estimates based on first arrival times, since they will always be available for detected events. Even if depth phases provide more reliable estimates their observability and the confidence with which they can be positively identified are not very well known.

In the example in *Figure 4* for explosions we use:

$$h_{hi}(max|\ m_b=m_{b0}) \leqslant 25$$

where h_{hi} is the upper limit of the confidence (90%) interval of the depth estimate for m_b=4.0 and 0 km depth. The inequality is satisfied in only very limited areas in Europe and North America.

For deep earthquakes (*i.e.*, $d>d_1$ and $(\Phi,\Lambda)\in A_e(deep)$) we use the ineqaulity:

$$h_{lo}(min|\ m_b = m_b(threshold))>25 = h_e$$

where h_{lo} is the lower limit of the confidence (90%) interval of the depth estimate for events with magnitudes at the detection threshold and depth at 100 km *(Figure 5)*. In this case the criterion is largely satisfied in areas where stations are located. The improved depth estimation capability in these areas reflects the importance of arrival time measurements at distances around 10 degrees or closer. This also suggests a network with a somewhat higher station density than that of the existing GSETT network (Roy, 1984).

- *Surface Wave Detection*

The m_b:M_s-method is assumed in this example to be the main criterion for discriminating between shallow earthquakes and explosions. As for the depth estimates described above, a minimum gap between the thresholds of event detection and that for applying this method is therefore important.

The maximum likelihood technique for magnitude calculations makes it possible in theory to virtually close this gap, since magnitude estimates only need to be based on information on detecting and non-detecting stations and not on the amplitude measurements themselves. This means that the m_b:M_s criterion can in principle be applied for any event where station detections are obtained as long as information on station noise amplitudes are available.

Station selection based on the criterion:

$$\Delta m_b(min)\leqslant m_0=0.0$$

for shallow earthquakes (with $h\leqslant h_1$=25 km) will make detection of surface waves likely.

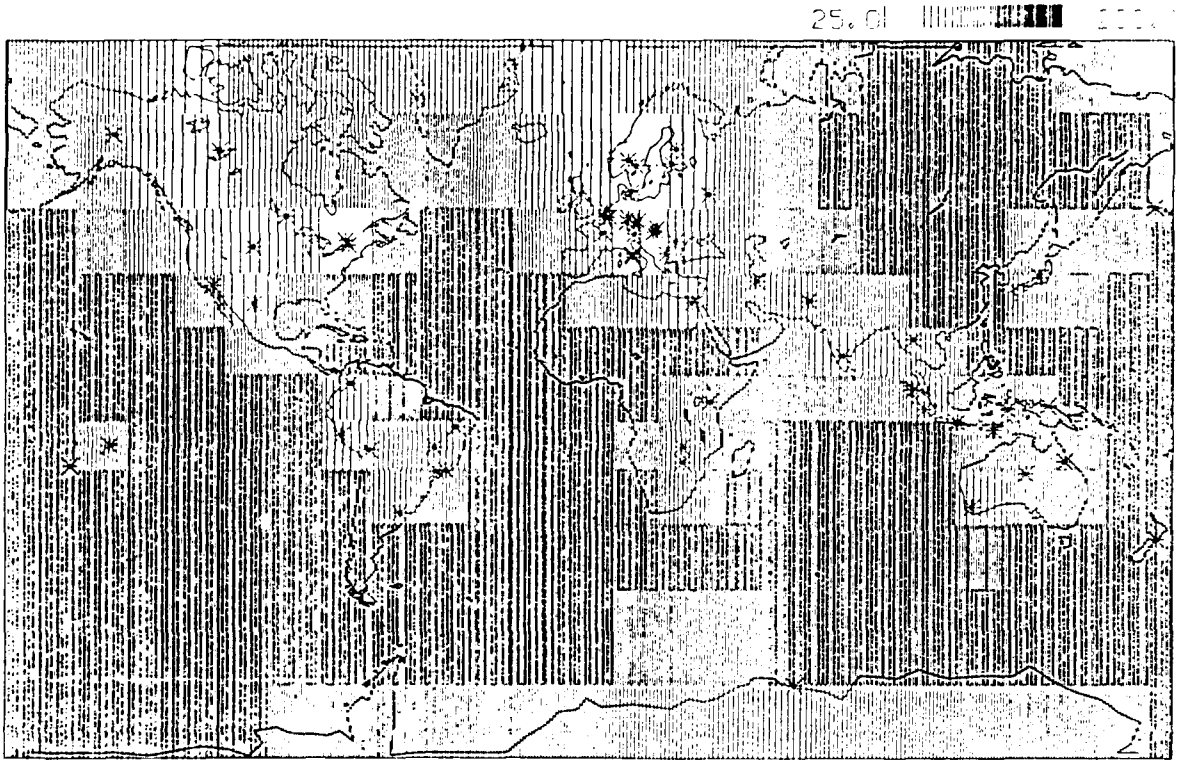

Figure 4. The the upper limit of the confidence (90%) interval of the depth estimate for a m_b=4.0 event at 0 km depth in relation to a 25 km depth. Grey and dark areas outline the parts of the world where the estimated depth is larger than 25 km.

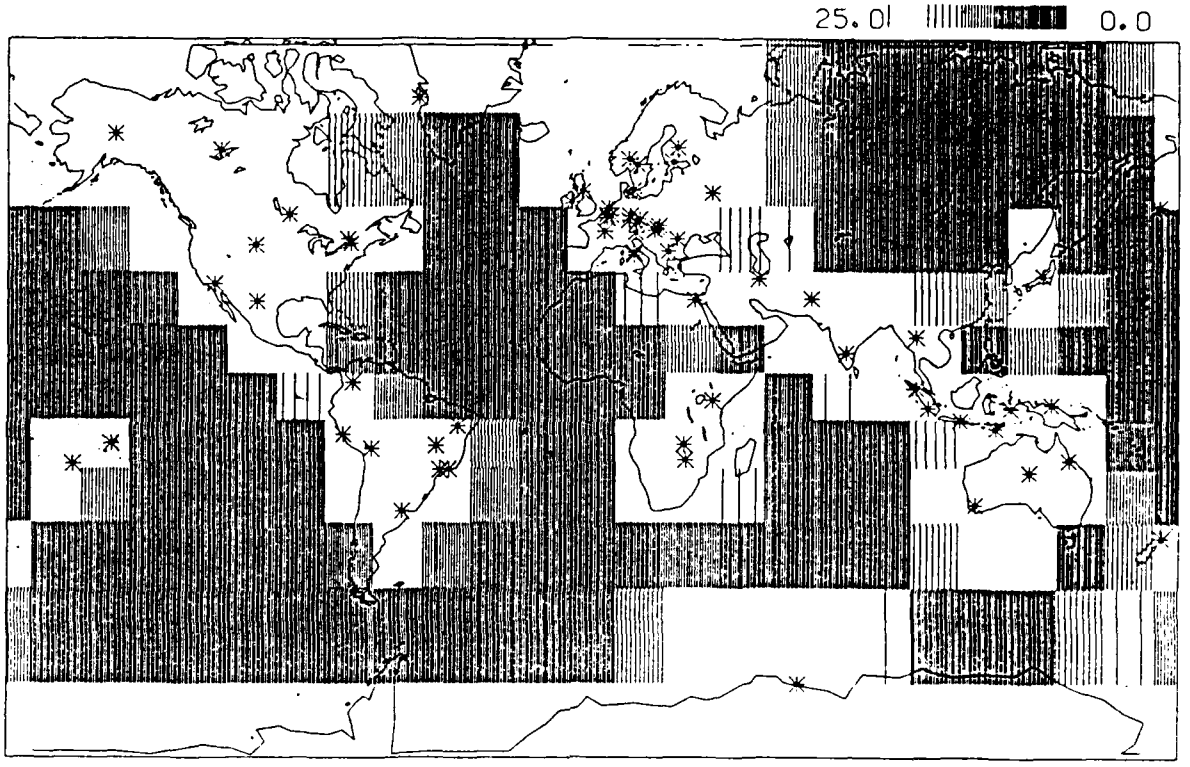

Figure 5. The the lower limit of the confidence (90%) interval of the depth estimate for events with magnitudes at the detection threshold and depth at 100 km in relation to a threshold of 25 km. Grey and dark areas outline parts of the world where the confidence interval in below 25 km and thus sufficiently deep.

The map in *Figure 6* shows the geographical distribution of Δm_b for the GSETT. The criterion above is satisfied only in limited areas in the Southern Hemisphere and interestingly enough not in Europe where the station density is high.

It may be desirable to have a larger value than 0.0 for $\Delta m_b(max)$, depending on the importance attached to actually detecting surface waves from explosions, even if negative evidence or absence of surface waves could be employed (Elvers, 1974). This would require, however, that the M_s detection threshold of routine reporting networks, and also that of the GSETT network, would have to be lowered significantly. It has been suggested that, even given numerous high-quality long-period stations, the M_s threshold may be lowered only to $M_s \approx 3.5$ (Marshall, 1985). On the other hand, there are examples for which this threshold has been obtained for more modest networks. For example, a network of only 23 long period stations give an estimated 90% cumulative threshold for M_s determination of 3.4 (Johansson, 1982). It appears that surface wave detection is an area where there still are considerable uncertainties about the performance of a global network.

2.1.5. Concluding Remarks

Desirable performance of a global monitoring system has previously been expressed only in rather general terms for research purposes. For example, such a system should aim at a magnitude detection threshold of $m_b \approx 4.0$. However, no precise specification in *seismological* terms of desirable performance of the various functions has gained wide acceptance.

In this note we define *seismological* criteria for selecting stations of a global network that tailor the seismological tasks to source types and require a certain minimum performance. This will not necessarily result in uniform geographical capabilities, but ensures that a certain prescribed minimum capability will be obtained throughout a given target area. In some regions the capability may well be lower than the prescribed minimum, whereas in others it may only be equal to this minimum.

Apart from standard functions (like event detection, location, and identification) association of signal detections at the stations is included among the seismological tasks. The tasks are also selected with a view of minimizing the gap between detection thresholds and thresholds for recording parameters for event identification. In particular, magnitude estimates of m_b and M_s based on the maximum likelihood method eliminates in principle the gap between detection and identification for shallow earthquakes.

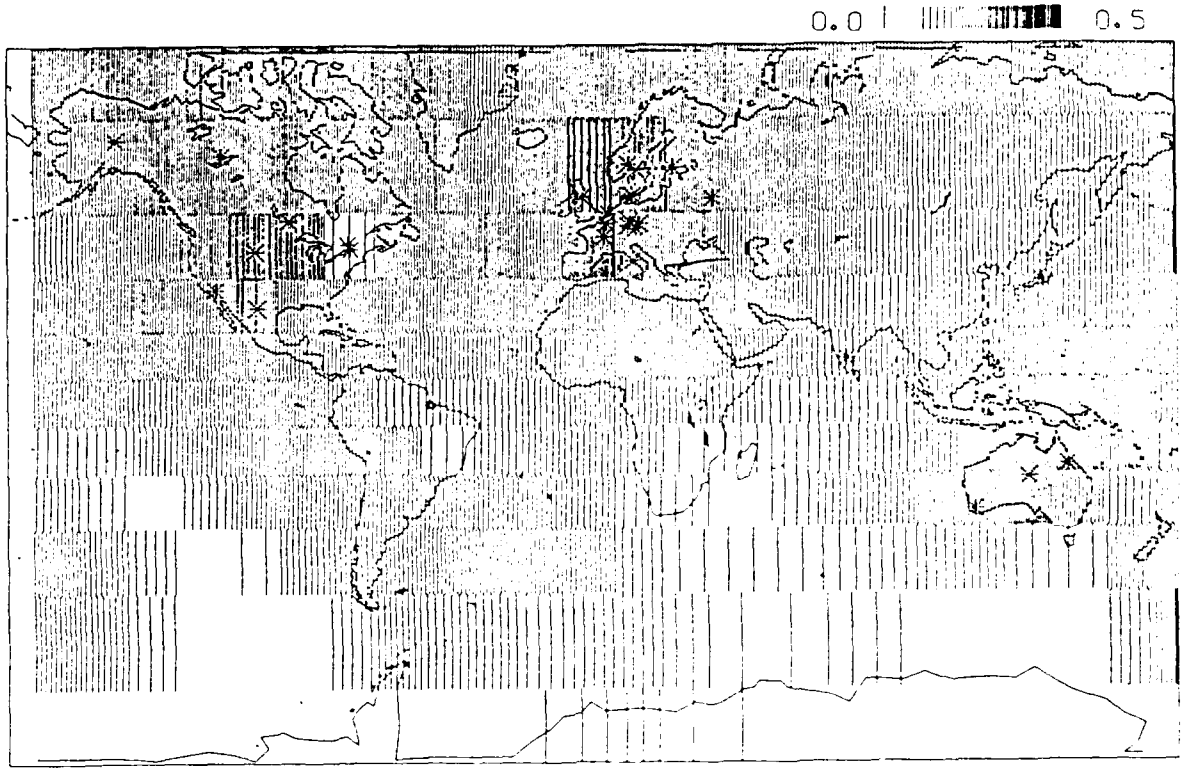

Figure 6. The map shows the value of Δm_b as defined in the text for the GSETT network. Locations of long period stations are indicated by asterisks in the map. Grey and dark areas outline parts of the world where the detection capability for short period body waves is higher than that for long period surface waves for shallow earthquakes.

The presentation is illustrated with examples based on the GSETT network. These examples, which outline geographical regions where given example criteria are fulfilled, indicate that a higher station density in large parts of the world and a significantly increased number of long-period stations as compared with the original GSETT network would be necessary in order to narrow the observed gap between thresholds for detection and recording of M_s magnitudes for event identification.

Hans Israelsson

REFERENCES

Elvers, E. (1974). Seismic event identification by negative evidence, *Bull. Seism. Soc. Am.*, *64*, 1671-1684.

Evernden, J.F., C.B. Archambeau and E. Cranswick (1986). An evaluation of seismic decoupling and underground nuclear test monitoring using high-frequency seismic data, *Reviews of Geophysics, 24*, 143-215.

Hannon, W.J. (1983). Seismic verification of a Comprehensive Test Ban, *Energy and Technology Review*, Lawrence Livermore National Laboratory, May 1983, 51-65

Israelsson, H. (1986). Simulations with a program for seismic network assessment, *Quarterly Technical Reports, 1 July - 30 September and 1 October - 31 December 1985*, Technical Report C86-5, Center for Seismic Studies, Arlington, VA.

Johansson, P. (1982). Common data base experiment - long period surface wave signals, *National Defense Research Institute, Stockholm, Report C-20462-T1.*

Marshall, P.D., and P.W. Basham (1972). Discrimination between earthquakes and underground explosions employing an improved Ms scale, *Geophys. J. Roy. astr. Soc.*, *28*, 431-458.

Marshall, P.D. and A. Douglas (1985). Earthquake or explosion: teleseismic monitoring - where are we now?, *The VELA Program: A Twenty-five Year Review of Basic Research (Ed. A.U.Kerr)*, Defense Research Projects Agency, 633-657.

Roy, F. (1984). Source depth estimation using multi-station waveform data, *Bull. Seism. Soc. Am.*, *74*, 1623-1643.

2.2. DETECTION CAPABILITIES OF CONTINENTAL NETWORKS

In designing a seismic network, there are a number of capabilities to be considered, including detection threshold, location accuracy, focal depth accuracy and so on. Each of these capabilities can contribute to the definition of an overall figure of merit that can be used to compare different networks. This study examines one such network characteristic: the capability of a network on one continent to detect seismic events on other continents. Understanding this capability should be useful as a guide in determining where an additional investment in stations might contribute the most to a global network.

Seismic networks used in this study were evenly distributed over seven major continents. Three networks, with each continent having proportionally increasing and decreasing numbers and locations of stations, were employed. The detection threshold was based on the 90% probability of detecting *P* or *PKP*, assuming all stations had a noise level equal to the median noise measured during the GSETT. The mean magnitude threshold was computed at locations separated by 15 ° latitudes and longitudes for the selected network of stations, meeting the selected multiwave detection criteria. These magnitude threshold values were then weighted according to the area covered by their values (polar latitudes have less weight than equatorial latitudes). A mean magnitude value was calculated for all continents, worldwide and continent-by-continent. The standard deviation, minimum, and maximum magnitudes were also computed.

Three detection criteria were used in this study: detection of phase *P* out to 100 ° at four stations; detection of phase *P* or *PKP* out to 180 ° at four stations; and detection of phases *P* and/or *PKP* out to 180 ° at four stations. The low mean magnitude threshold for networks in North America, Africa, Asia, South America, and Australia, is attributed to the detection criterion of phases *P* and *PKP*.

The mean magnitude threshold had an overall range of 2 magnitude units when examining the networks worldwide. The continents of North America, Africa, and Asia showed a decrease in mean magnitude threshold of 0.3 when the number of stations on a continent was doubled. Doubling the number of stations on the continents of Europe, South America, Antarctica, and Australia lowers the mean magnitude threshold by 0.5 units of magnitude.

Standard deviations for magnitude values indicate that more stations in a network on a continent are not necessarily better. Only in Africa, Asia, and South America do the seismic networks with the greatest number of stations have the smallest standard deviation in magnitude. Standard deviation increased with increasing number of stations in North America, Europe, Antarctica, and Australia.

In what follows, we examine just one of the three global networks. The total number of stations used was 68, a number comparable to that used in the GSETT of 1984. The networks on each continent were analyzed separately (see Table 1). Looking at the first row in Table 1 we see that stations on the continent of North America produce

a mean magnitude threshold of 4.66 on North America. Continuing across the row, these same stations produce a mean magnitude threshold of 5.21 on the African continent, 5.08 in Asia, and so on. Because the station density was the same on each continent, the magnitude thresholds on a given continent derived from stations on the same continent might be expected to be the same, but thresholds were actually found to vary from 4.42 to 4.96. This variation may be due to the number of stations per continent and to the coarse grid spacing used for station locations.

Table 1. Mean magnitude thresholds for the seven continents

Continents on which stations were located	NA	AF	AS	EU	SA	AN	AU
NA	4.66	5.21	5.08	4.89	4.97	6.27	5.78
AF	5.01	4.60	4.81	4.75	4.85	4.83	5.19
AS	4.63	4.73	4.42	4.63	5.45	5.31	4.77
EU	5.47	5.38	5.32	4.96	5.68	-	5.81
SA	5.26	5.38	5.76	5.60	4.76	5.45	-
AN	-	5.45	5.72	-	5.31	4.94	5.29
AU	5.91	5.56	5.19	-	5.75	5.12	4.47

-means not geometrically possible
NA - North America; AF - Africa; AS - Asia; EU - Europe
SA - South America; AN - Antarctica; AU - Australia

We see from the second row in the table that the continent which has the strongest influence on worldwide detection of seismic events is Africa. This continental network produces low thresholds on most other continents (*Figure 1*). On the other hand, Table 1 and *Figure 2* indicate that the South American continental network by itself has a high thresholds for events on the other continents, although very important for detecting events in South America.

Europe and South America are best covered by other continental networks as indicated by the lower magnitude values in the columns. Coverage will be improved with a finer distribution of stations.

Antoinette Campanella

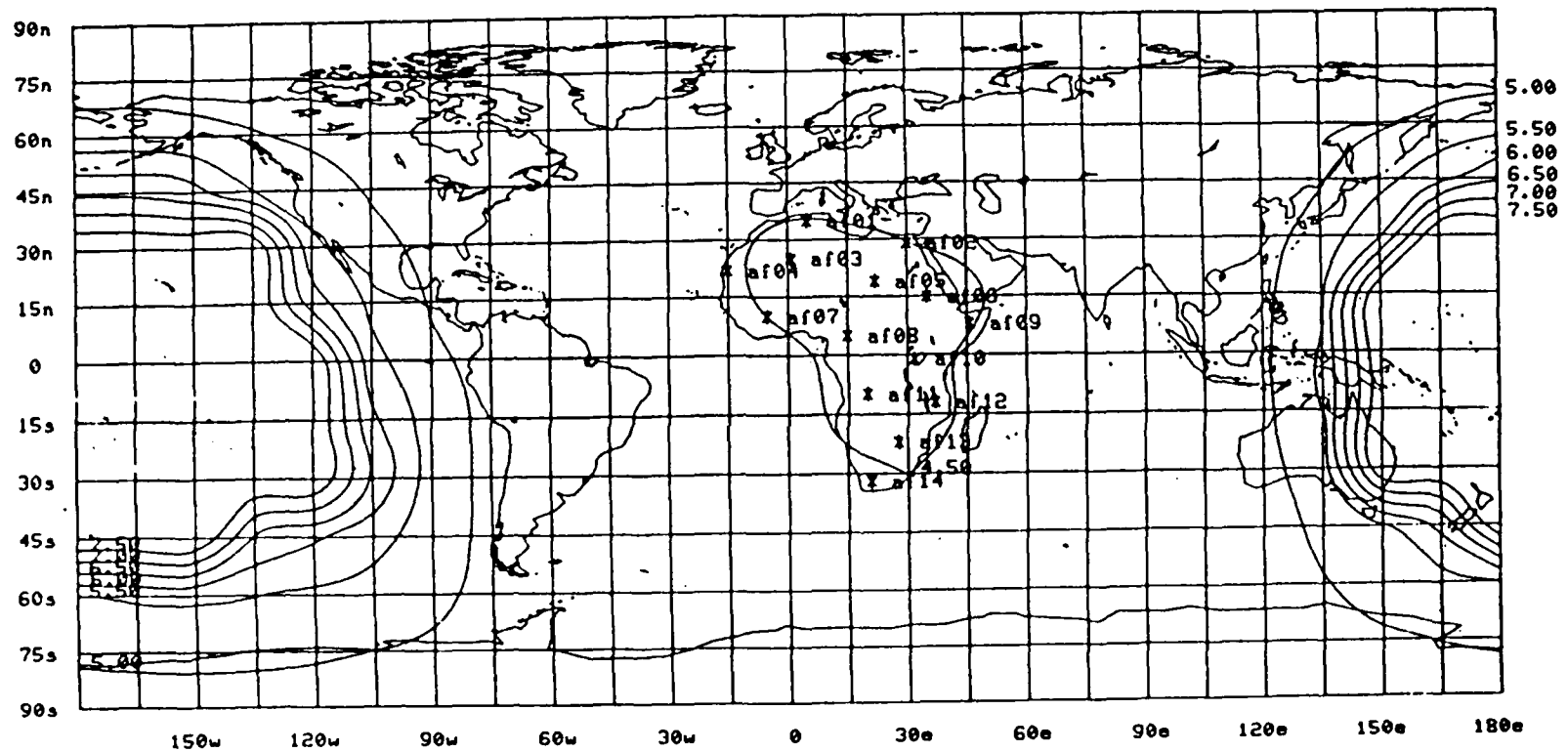

Figure 1. Detection threshold of African continent network, based on median noise levels reported during the GSETT in 1984 and using detection criterion of P and/or PKP at four stations. Contours are labeled with body wave magnitudes, m_b , at which events can be detected with a 90% confidence level. Note the low detection threshold surrounding Africa.

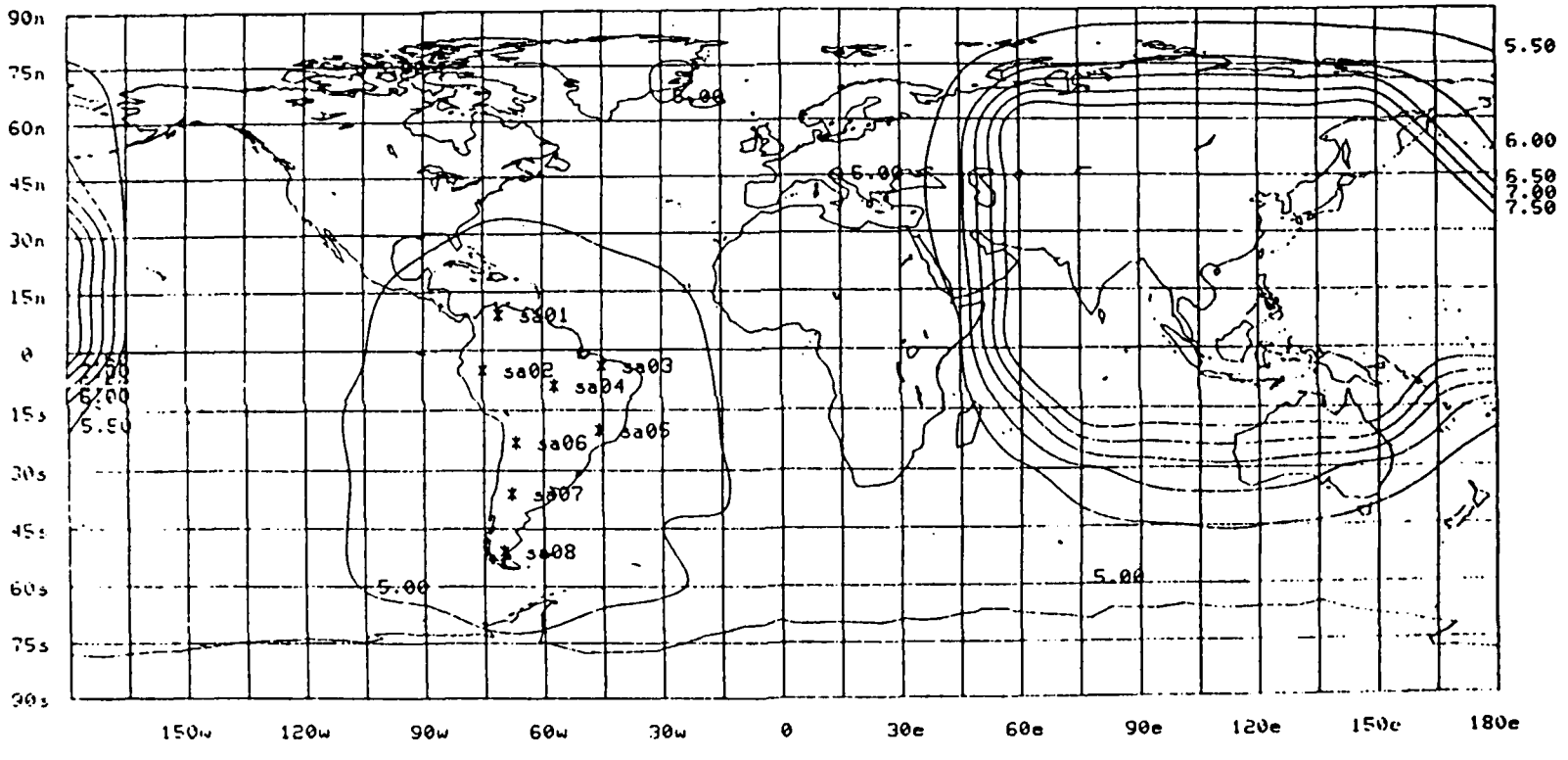

Figure 2. Detection threshold of South American continent network

3. RESEARCH TO IMPROVE ANALYSIS OF REGIONAL SEISMIC DATA

3.1. PARTICLE-MOTION SIGNATURES FOR SOURCE IDENTIFICATION

3.1.1. Introduction

In regional seismic monitoring, many of the events recorded are from fixed sources such as active mines. Events occuring at such fixed sources may be difficult to distinguish from those occurring nearby simply on the basis of epicenter locations. A careful examination of seismograms recorded at one receiver from several events at the same source often shows a remarkable similarity in the time histories. This is because the source, propagation and receiver effects on the seismic waves are nearly the same. Experienced analysts can often recognize a new event and associate it with a unique source simply by examining the waveforms.

This technical note presents a technique for automatically identifying events on the basis of recorded waveform characteristics. The idea is to extract a particle-motion "signature" from recorded seismograms and compare it with reference signatures from candidate sources. A reference signature is constructed by averaging together several event signatures known to be from the same source. Identification is performed by cross-correlating the signature of the unknown event with the reference signatures. A high correlation indicates a large degree of similarity in the ground motions. The same technique can also be used to automatically identify seismic phases from a particular region. In this case, a signature is constructed for a short data segment containing one particular seismic phase which is then correlated against a reference signature.

Examples are given of particle-motion signatures for NORESS recordings of several events in southern Norway. The signatures are used to identify events from a particular mine and also to identify different seismic phases. The results presented here are preliminary and meant to illustrate the idea of using particle-motion signatures for source identification. Work on this topic is currently in progress.

3.1.2. Computing Particle-Motion Signatures

A seismic signature for use in source or phase identification should satisfy certain criteria. It should compress the information in the original signals into a smaller data-space, it should be easy to compute, and it should contain as much information as possible characterizing the source and propagation effects on seismic waves. The approach used here is to form signatures from the seismic-wave particle motions as a function of time. The method is based on previous work by Jurkevics (1986a, 1986b) for polarization analysis. A brief description of the processing involved in computing particle-motion signatures follows.

In this application, particle-motion analysis is carried out in the time domain. A three-component seismogram is filtered into several passbands and the data in each band are windowed into short overlapping time segments. The bandwidth and window length determine the frequency and time resolution. The data window is tapered and its length is related to the pass-band center frequency in such a way that each frequency component is assumed to be purely polarized over several cycles duration. The covariance matrix in each time window is formed as the product of pairs of the three components of motion integrated over the window:

$$R_{ij} = \frac{1}{N}\sum_{t=1}^{N} S_{it}S_{jt} \qquad i,j = 1...3.$$

Here i and j are seismogram component indices, t is time index, N is the number of samples within a time window and S_{it} is sample t of component i. The covariance matrix R_{ij} is the 3x3 matrix of coefficients for a quadratic form which is an ellipsoid. R_{ij} is real and symmetric and contains six unique terms. In a polarization analysis, the eigenproblem for R_{ij} is solved, which gives the three principal axes of the polarization ellipsoid. Various useful polarization attributes can be extracted from the polarization ellipse. These attributes provide quantitative descriptions of the particle-motion ellipticity, orientation, etc.

When an array of M three-component sensors is available, the data redundancy can be exploited to stabilize the polarization estimates. In this case, the covariance matrices from all the three-component sensors in an array are averaged term-by-term before the polarization ellipse is computed. This gives an unbiased and consistent estimate of the covariance matrix. The variance of computed particle motions goes as $1/M$ when the scattering distortions and noise are uncorrelated between sensors. An added requirement in the covariance averaging is the application of time shifts to align the windows at the different sensors. An assumption is usually made that the coherent wavefronts are planar, so an frequency-wavenumber analysis can be used for the phase velocity. Recent results with NORESS data indicate that, for most regional events, the particle motions are sufficiently stationary and the analysis windows sufficiently long that the time shifting can be neglected for frequencies up to about 12 Hz.

A particle-motion signature is simply formed from the six coefficients of the covariance matrix. These coefficients are computed in sliding time windows and vary with time. When several passbands are used, a separate signature is obtained for each frequency interval. The polarization ellipse is not calculated *per se;* the vector ground-motion information is in its most compressed state as a covariance matrix. The three diagonal terms of the covariance matrix as a function of time are simply the envelopes of the three components of motion. The three off-diagonal terms are the cross-products between components and provide important information about the phase and orientation of particle motion. These cross terms are very useful for distinguishing seismic phases with different particle-motion characteristics. When several three-component sensors are used in an

array, the covariance matrices from each sensor can be averaged together for a more stable signature estimate.

An important motivation for using signatures instead of raw seismograms to compare signals is the saving in computation effort during the correlation stage. The correlations are the most burdensome part of the analysis, as the computation effort required to correlate two signals is proportional to the square of the number of samples. Consider the case of NORESS short-period data with a sampling interval of .025 seconds. When a pair of three-component seismograms are correlated, the effort is proportional to $3(L/.025)^2$, where L is the signal length in seconds. The sampling rate of the particle-motion signatures is determined by the time increment between adjacent windows. Experience with NORESS regional data has shown that the signatures are well sampled using a .4 or .5 second increment between windows. For a signature sampling of .4 seconds the signature correlation effort is $6(L/.4)^2$, since six covariance terms are used. Thus the correlations require 128 times more effort for the raw seismograms than for the signatures. The overhead in computing the signatures themselves is proportional to $6(L/.025)^1$ and is insignificant relative to the correlation effort for $L > 15$ seconds.

3.1.3. Examples Using NORESS Data

Examples are given here of using particle-motion signatures of NORESS short-period recordings to identify events from the Titania mine near the coast of southern Norway. Table 1 gives a list of the events used. The Titania mine is located 394 km from the array and has regular blasting activity. Events 1-5 have been positively identified as Titania mine blasts and are used to construct a reference signature. Event 6 is also a Titania mine blast but is not used in constructing the reference signature. Instead, event 6 will serve as a "new event" to be tested. Events have also been recorded at NORESS which are located just off the coast and at about the same azimuth from NORESS as the mine. Event 7 in Table 1 is one such event and will serve as a second test event. Table 1 shows the locations of these seven events as routinely computed by NORESS. The differences in the locations for all the events known to be from the same mine give an idea of the location accuracy from this type of array.

Table 1
Events Used in the Analysis

event	description	year/doy	time	latitude	longitude	magnitude
1	T-mine ref 1	1985/312	14:18:52	57.9	6.9	1.9
2	T-mine ref 2	1985/317	14:11:05	58.0	6.6	1.9
3	T-mine ref 3	1986/007	14:14:28	58.7	5.8	1.8
4	T-mine ref 4	1986/017	14:10:58	59.1	4.9	2.3
5	T-mine ref 5	1986/045	17:54:04	58.1	6.2	2.0
6	T-mine new event	1986/045	14:13:19	58.1	6.2	2.4
7	offshore event	1985/324	23:17:26	57.5	7.0	2.1

The upper part of *Figure 1* shows the Titania mine "reference" signature on the left and the "new event" signature on the right. Two seismograms are also plotted for reference; these are the short-period vertical components at sensor NRA0 for events 4 and 6 after bandpass filtering between 6 and 10 Hz. The six signature traces are the six covariance matrix coefficients as a function of time for a band 2.5 Hz wide centered at 4 Hz. The S_n and L_g phases are clearly visible in these signatures. The P_n waves have relatively smaller amplitudes at 4 Hz, but are stronger on the seismic traces which have been bandpassed at 8 Hz. The particle-motion signatures for a band 5.0 Hz wide and centered at 8 Hz were also computed but are not shown in *Figure 1.* The signature traces are labelled according to the two components of motion from which they are formed. Thus, "zz" represents the self-covariance of the vertical component, "zn" represents the cross-covariance between the vertical and north components, and so on. The self terms "zz", "nn" and "ee" simply yield the envelopes of the three components of motion and are always positive. The cross terms "zn", "ze" and "ne" may be negative and contain important information about phase and orientation of particle-motion.

The reference signature for the Titania mine was constructed by averaging signatures of the first five events in *Table* 1. These five signatures were time-aligned before being summed together. The signature on the right side of *Figure* 1 is for event 6 in *Table* 1. All the individual signatures were computed identically. Since three three-component sensors were in operation at NORESS during this period, NRA0, NRC4 and NRC7, the covariance matrices at the three sensors were combined for each event using the covariance averaging method described by Jurkevics (1986a). Note the strong similarities between the reference signature and the new event-signature. The L_g as well as S_n waves have very well-defined particle-motion histories which are similar for all these events. The P_n waves at 4 Hz have relatively smaller amplitudes and do not contribute much to these signatures.

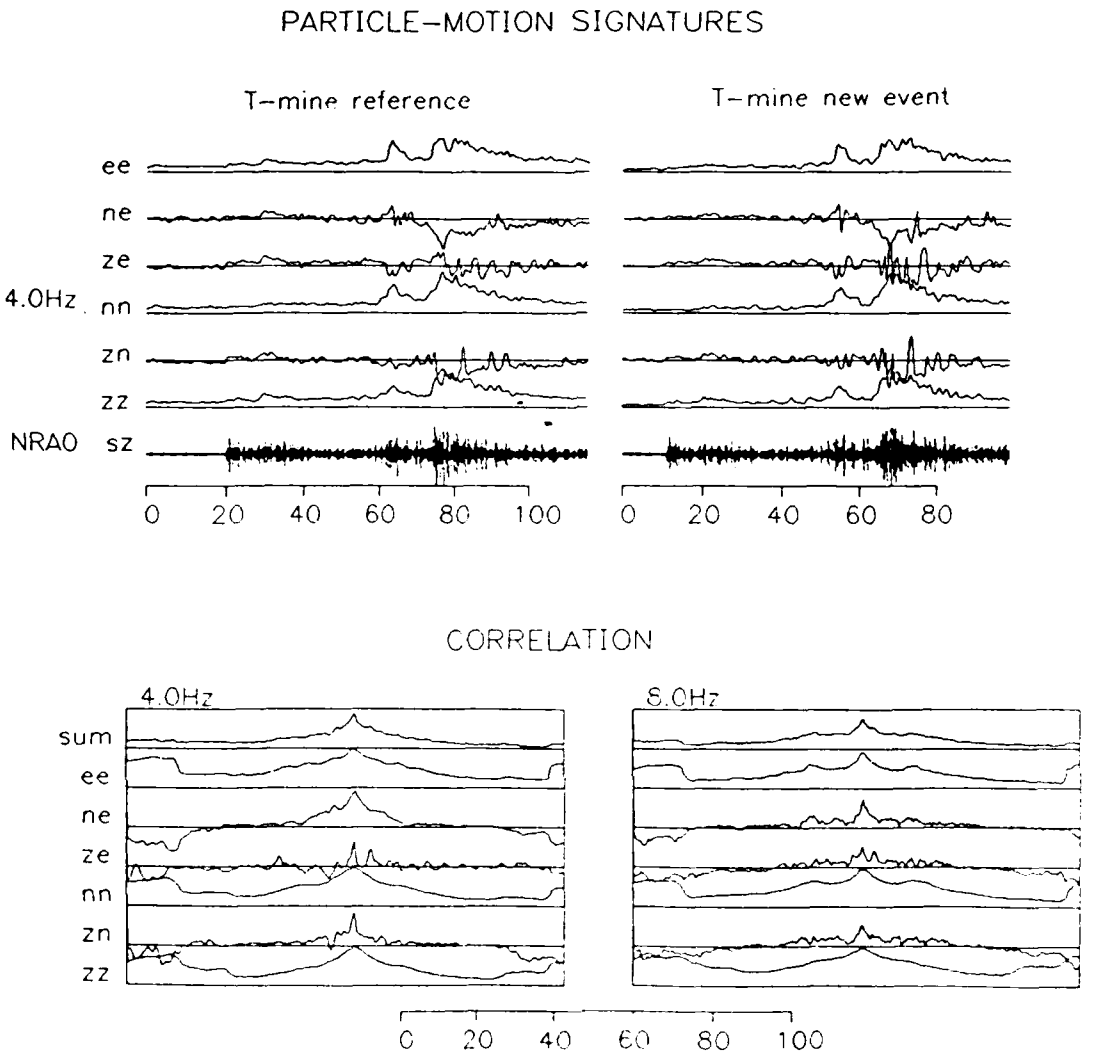

Figure 1. The particle-motion signatures at the top are for Titania mine events recorded at NORESS. The signature on the left is a reference formed by averaging signatures of five separate events from the mine. The signature on the right is for a new event from the same mine. The signatures shown are for a frequency band centered at 4 Hz. Short-period vertical seismograms of two mine events are also shown for a band at 8 Hz. The correlations at the bottom are a result of cross-correlating each of the signature traces for the reference and the new event. A summation of the correlation traces is also shown; this is the proposed measure of similarity. The correlations are peaked if the signatures are similar.

The lower part of *Figure 1* shows the cross-correlations between the two signatures. The correlations give a quantitative measure of similarity. The top correlation trace labelled "sum" is a summation of the six individual correlations shown directly below. This summation trace is the proposed measure of similarity between the signals. The individual trace correlations have been included to show the relative importance of the six covariance terms. The left side shows the correlations for the signatures in the band at 4 Hz and the right shows the correlations for the band at 8 Hz. The correlation functions have been energy-normalized so that the values are between 1.0 and -1.0. The correlation peak occurs when the two signatures are aligned in time. The peak of the correlation summation trace is close to 1.0 at 4 Hz and less at 8 Hz, indicating that the events are very similar at low frequencies and somewhat less similar at higher frequencies. The peaks of the summed correlations are about a factor of four above the background level.

Figure 2 shows a similar analysis using the Titania mine reference signature and that for the offshore event 7. The seismograms themselves in *Figure 2* show a large difference in the P, S and L_g waveforms between the events. The signatures reflect this difference. The correlation traces at the bottom of *Figure 2* do not have the same peaked response as those in *Figure 1*. Note that the correlation traces labelled "zz", "nn" and "ee", which are the correlations between the envelopes of each of the three components, reach values close to 1.0, but the cross terms "zn", "ze" and "ne" have much smaller values. Thus the cross terms are important for recognizing differences in the seismic wave motions.

Figures 3-5 show signatures and correlations of individual seismic phases for Titania mine events. The upper part of *Figure 3* shows the entire reference event on the left and a short segment containing the P_n wave of the Titania mine event 6 on the right. The signatures in *Figure 3* are for a frequency band 5 Hz wide and centered at 8 Hz. The scaling is somewhat different between the two signatures. The P_n signature was correlated against the entire reference event and the results are shown in the lower part of *Figure 3*. A strong peak in the correlation occurs when the P_n signature of the new event is aligned with the P_n wave of the reference signature. The correlation summations gradually decrease with time over the P coda and are very low at the times of the S_n and L_g arrivals. The individual correlation traces show that the envelope correlations "zz", "nn" and "ee" are not as useful in separating the phases as are the cross terms "zn", "ze" and "ne". *Figure 4* shows signatures and correlations for the Titania mine reference event and the S_n phase of the new event. The summation correlations show a strong peak at the time when the S_n phases align. The importance of the covariance cross terms is again apparent. *Figure 5* shows signatures for the Titania mine reference and for the L_g phase of the new event. The correlation traces peak when the L_g phases are aligned. The L_g corrrelation at 8 Hz is somewhat smaller than the peak at 4 Hz. The signature correlations in all three cases P_n S_n and L_g are quite peaked and clearly identify these phases from one another.

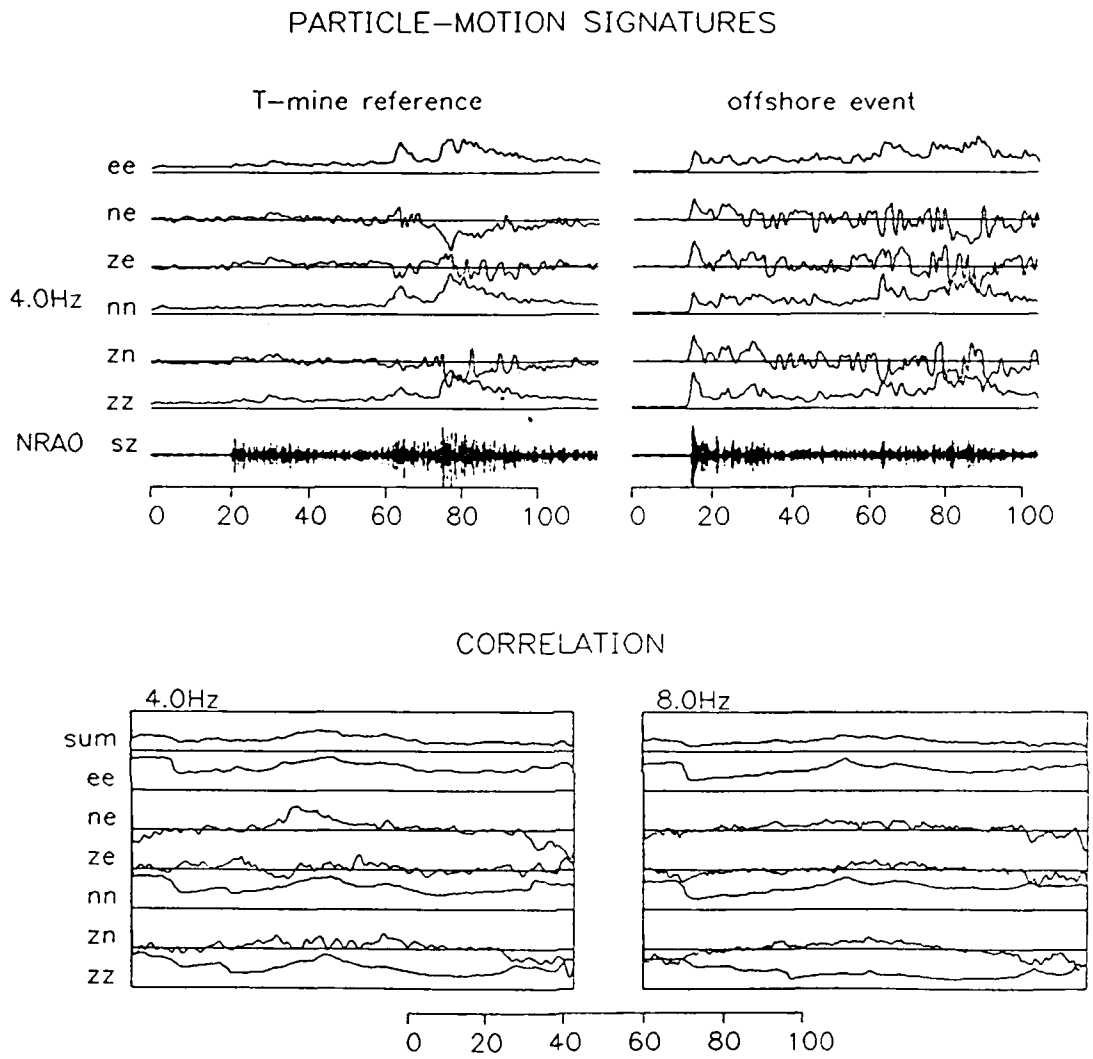

Figure 2. The signatures shown at the top are for the Titania mine reference and an event which was not a mine blast but was located off the coast in the vicinity of the mine. The signatures are quite different in this case; this is reflected by the poor correlations shown at the bottom.

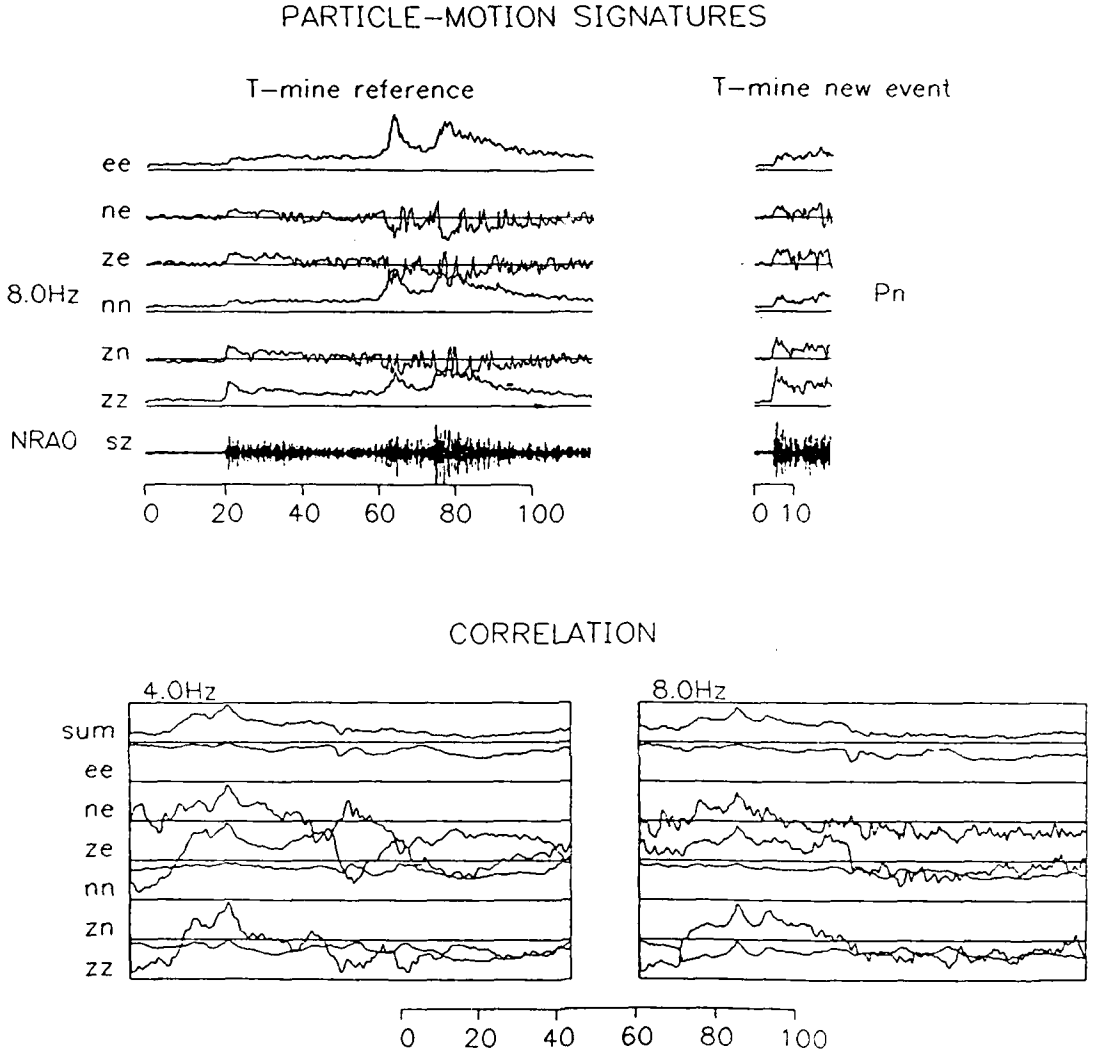

Figure 3. The signatures at the top are for the Titania mine reference and for a short segment containing the P_n phase of the new event from the mine. These signatures are shown for a frequency band centered at 8 Hz. The correlations at the bottom peak when the P_n segment of the new event is aligned with the P_n phase of the reference. There is some correlation between the P_n and reference P coda but little correlation between the P_n and the S_n or L_g. The individual correlations show that the covariance cross-terms are important for distinguishing the seismic phases.

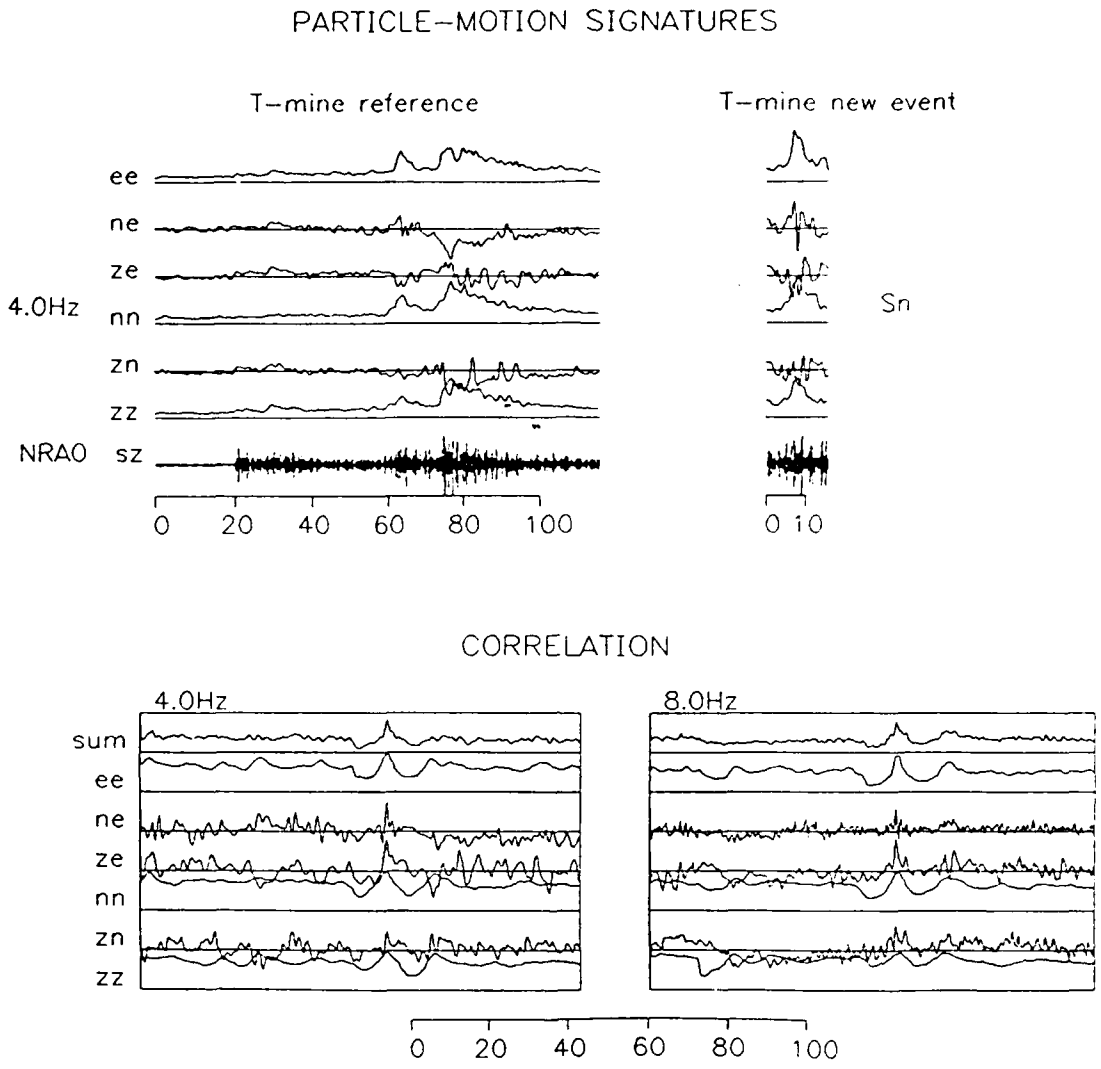

Figure 4. The signatures shown here are similar to those in *Figure* 4 except that the segment for the new event contains the S_n phase. The signatures are shown for a frequency band centered at 4 Hz. The correlations are peaked only when the S_n phases are aligned. The particle-motion signatures can clearly differentiate between S_n and P_n or L_g waves.

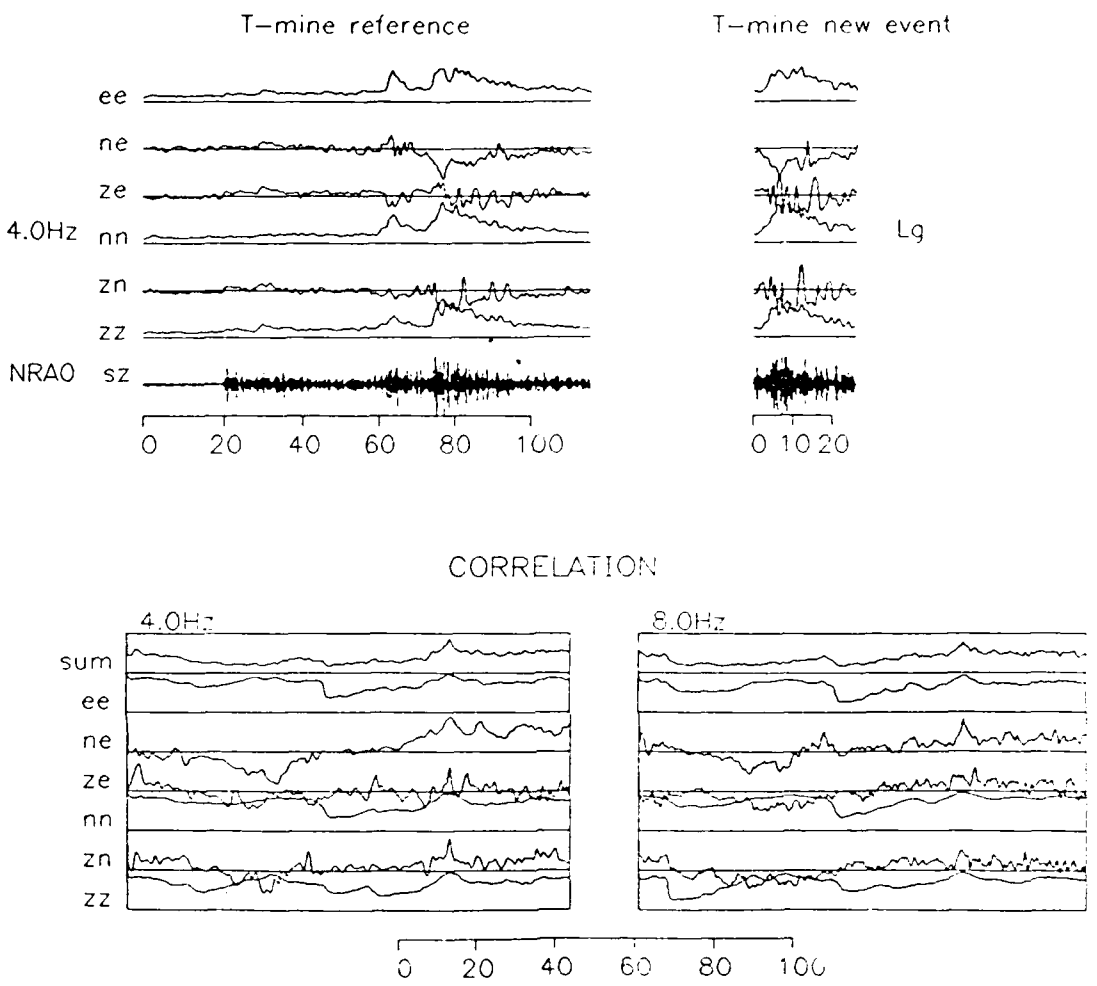

Figure 5. The signatures shown here are like those in *Figure* 5 except that the L_g phase segment for the new event from the mine is used. The correlations are peaked only when the L_g phases are aligned. The L_g correlation is stronger at 4 Hz than at 8 Hz.

3.1.4. Summary

Preliminary results have been presented in which particle-motion signatures are used to automatically identify events and individual seismic phases from a fixed source. The signatures used are the six terms of the three-component covariance matrix as a function of time and frequency. These signatures seem to capture much of the important information contained in three-component seismograms and retain it in a compressed form. The diagonal terms of the covariance matrix yield the signal envelopes. The off-diagonal cross terms are very important for providing particle-motion phase information and so distinguishing different seismic phases and propagation effects. The results so far are quite encouraging and show that different events from a fixed source have very similar particle-motion time histories. Seismic waves from nearby events not from the same source undergo different source and propagation effects and their signatures are different. Future work on this topic will concentrate on testing these concepts on a larger set of events from the Scandanavia region recorded at NORESS.

Andy Jurkevics

REFERENCES

Jurkevics, A. (1986). Polarization analysis using an array of three-component sensors: Part I -- theory, *Center for Seismic Studies Tech. Rept. C86-07*, 48-58.

Jurkevics, A. (1986). Polarization analysis using an array of three-component sensors: Part II -- application to NORESS, *Center for Seismic Studies Tech. Rept. C86-07*, 59-73.

3.2. CHARACTERISTICS OF P-WAVES FROM A MINE IN THE WESTERN SOVIET UNION

3.2.1. Introduction

In an earlier Quarterly Technical Report (Pulli, 1986), we discussed the use of pattern recognition in seismic analysis and illustrated this by comparing the waveforms from two adjacent clusters of events in southern Norway which were recorded by the NORESS array. Specifically, we compared the power spectra of Pn waves from a number of chemical explosions at the Titania Mine with those from a set of events off the coast. (In that report, we stated that the events off the coast of Norway were presumably microearthquakes, however we now have reason be believe that these events may have been underwater explosions conducted during naval exercises.) We showed that the power spectra of the Pn waves from Titania Mine explosions were very similar and that all of the spectra had peaks at 6 Hz or more. The power spectra of the Pn waves for the offshore events all peaked at 4 Hz. Thus, the difference in the Pn spectra could be used to identify events from each source area. This difference also was a quantifiable explanation of how a seismic analyst might visually recognize the difference in the waveforms from the two source areas.

3.2.2. Analysis

Since the last report we have analyzed approximately 50 other events recorded by the NORESS array and have found that distinct and repeatable waveform characteristics can be observed for groups of events. This study is still ongoing, and a full report will be presented in later Technical Reports. For this brief note, we would like to show an example of distinct waveform features from explosion sources at a mine in the western Soviet Union. In this case, the waveforms have features which likely may be used to discriminate between an explosive source and an earthquake source. These features are also quantifiable, and easily expressed as a series of numbers or vectors. They can then be stored in a database and indexed by event, so that subsequent events in the same area can be analyzed and compared to the reference events for identification purposes.

The mine is located at latitude 61.5 ° N, longitude 30.4 ° E near Lake Ladoga, north of Leningrad. The distance to the NORESS array is 1020 km. Analysts at NORESS refer to this mine as "V3". *Figure 1* shows an unfiltered seismogram for an explosion at V3 which occured on June 4, 1986 at 09:06:31. A prominent feature of signals from this mine is the large amplitude Pn wave. *Figure 1* also shows a blowup of the Pn waveform for the entire NORESS array as well as the beam. *Figure 2* is a similar plot for an explosion at this mine on June 12, 1986 at 09:30:55. Pn waves from this mine are distinctive in that they arrive as a "wavepacket" of nearly monochromatic frequency. The predominant frequency of this wavepacket is about 3.5 Hz. Pn waveforms for events from this mine also correlate quite well through the 8th cycle.

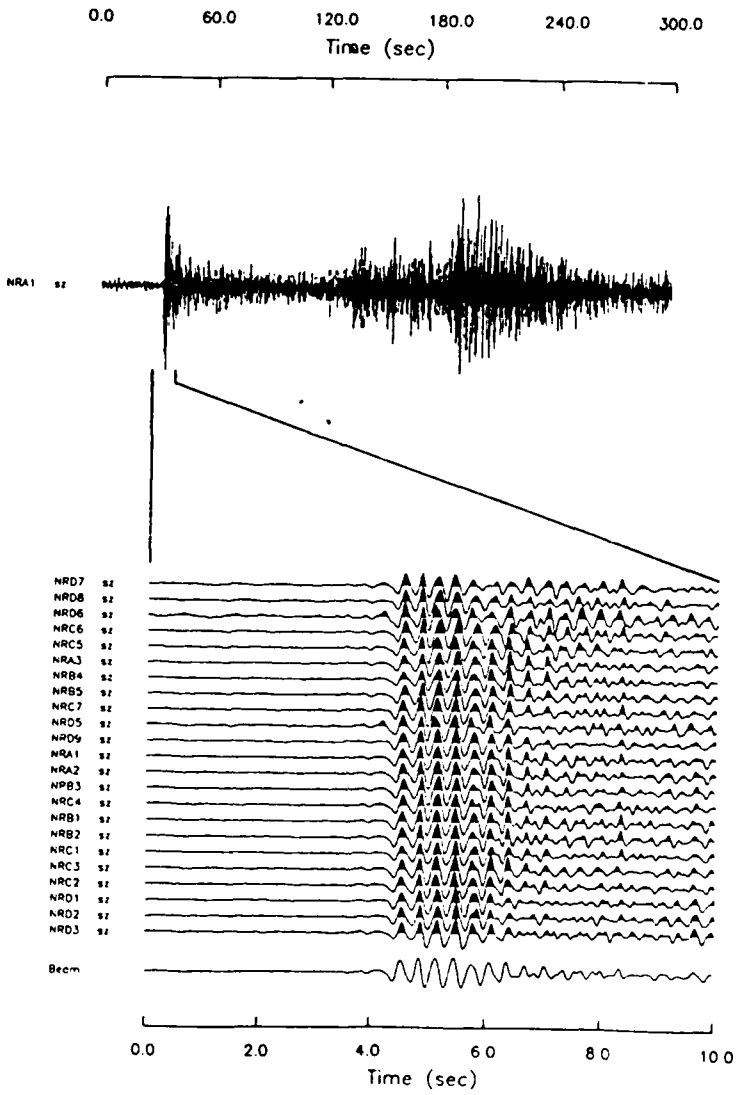

Figure 1. Unfiltered seismogram at site NRA1 of the NORESS array for a chemical explosion at mine V3, north of Leningrad. The explosion occured on June 4, 1986 at 09:06:31. Also shown is a blowup of 10 seconds of the Pn wave for all of the NORESS channels, as well as the corresponding beam.

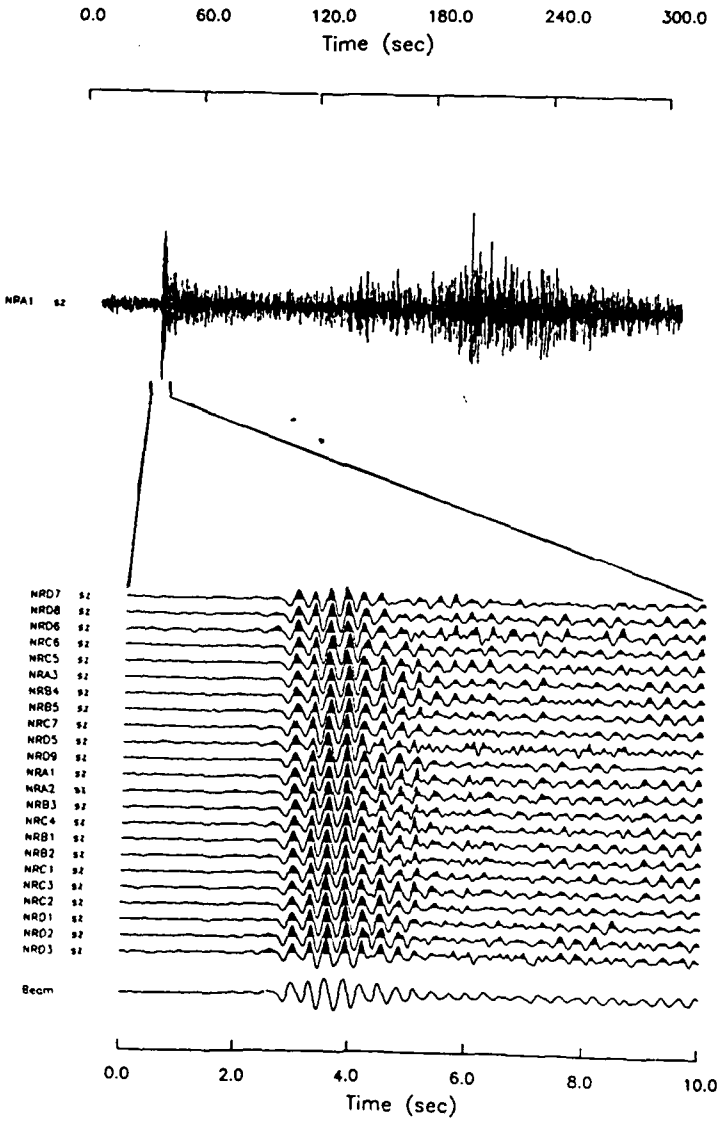

Figure 2. Unfiltered seismogram at site NRA1 of the NORESS array for a chemical explosion at mine V3, north of Leningrad. The explosion occured on June 12, 1986 at 09:30:55. Also shown is a blowup of 10 seconds of the Pn wave for all of the NORESS channels, as well as the corresponding beam.

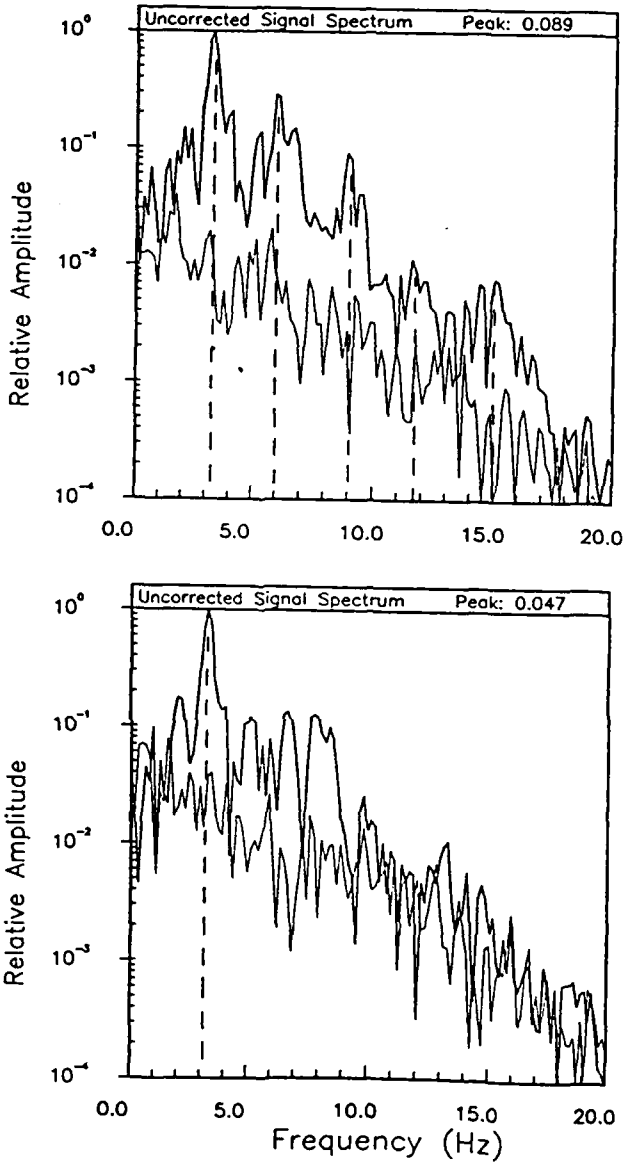

Figure 3. Amplitude spectra of the Pn waves for the two V3 mine explosions. The top spectrum is for the June 4 event, and the bottom is for the June 12 event. Note the scalloping of the spectra with peaks at 3, 6, 9, 12, and 15 Hz. If this scalloping is due to "ripple" firing at the mine, then the delay time between shots would be 0.33 seconds.

Figure 3 shows the Pn amplitude spectra (uncorrected for instrument response) for the two V3 explosions mentioned above. The spectra are scalloped at harmonic frequencies with peaks at 3, 6, 9, 12, and 15 Hz. Such a scalloping could be caused by delayed or "ripple" firing of charges at the mine site. Ripple firing is often used at quarries in the U.S. as a means of controlling the spread of crushed rock. If we assume that this scalloping is due to ripple firing, and that the polarity of each source is the same, then the 3 Hz scalloping pattern would be indicative of a charge delay of 0.33 seconds. We have also examined the high frequency (125 samples/second) NORESS data for these two events to determine if this scalloping continues beyond 20 Hz, but the signal-to-noise ratio is at most unity.

As further evidence of the polarity and delay time derived from the spectra of these two events, cepstra were also computed. *Figure 4* shows the mean cepstra of each event with the variance in cepstral amplitudes over the 24 element array. A coherent positive cepstral peak is seen at about 0.3 second in both cases, with the delay time for the June 12 event being slightly shorter.

The features we have shown for Pn waves from mine V3 provide important secondary information for source identification. With array or network monitoring, the primary information is the source location. However, once a location has been determined, means must be found for discriminating between source types. In the case of mine V3, the Pn waveforms have been shown to be repeatable, with spectral and cepstral analysis revealing multiple sources which may be indicative of ripple firing. These features can then be stored in a database as a sequence of numbers or vectors. For example, the spectral attributes for the June 4 explosion can be expressed as (3,1), (6, 0.3), (9, 0.09), (12, 0.01), (15, 0.007), (18, 0.0004) where the first entry equals the frequency and the second entry is the relative spectral amplitude. Once these attributes are stored in an appropriately indexed database, subsequent events at the same location can be similarly analyzed and their spectral attributes compared with those of previous events. In an area such as Scandinavia and eastern Europe with numerous earthquake and mining regions, a database of reference events can be quickly accumulated and used as a part of daily event analysis.

Jay J. Pulli
Paul S. Dysart

REFERENCE

Pulli, J.J.(1986). Expanded use of computers in regional seismic data analysis, *Center for Seismic Studies Tech. Rept. C86-07,* 29-38.

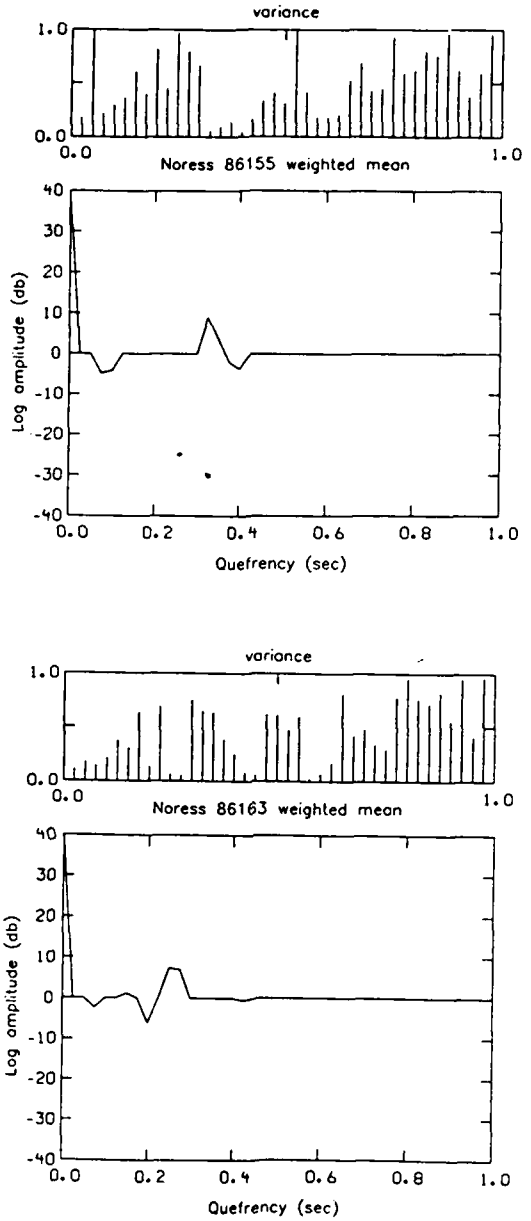

Figure 4. Cepstral analysis of the Pn waves for the two V3 mine explosions. A coherent cepstral peak at about 0.3 second can be seen in both cases.

3.3. AUTOREGRESSIVE ANALYSIS OF NTS EXPLOSIONS AND NEARBY EARTHQUAKES RECORDED AT TFO

3.3.1. Introduction

Spectral studies of Eurasian earthquakes, mine blasts, and underground nuclear explosions recorded at NORSAR and NORESS indicate that explosion source spectra are generally rich in high-frequency energy compared to spectra of earthquakes with similar magnitudes (Tjostheim, 1975; Dargahi-Noubary *et al.*, 1978; Dysart, 1986; Pulli and Dysart, 1986). In the case of regional data, this is true for both mantle (P_n and S_n) and crustal phases (P_g and L_g) with propagation paths largely within the Baltic shield. This observation would be expected from seismic source theory, given the shorter time duration of the explosive source. Consequently, the difference in the spectral content of explosions and earthquakes has been used as a basis for a number of successful short-period discriminants (*e.g.*, m_b:M_s and Variable Frequency Magnitude). However, in contrast to these observations in a shield region, studies of NTS explosions and nearby earthquakes recorded in the southwest U. S. have clearly shown that the spectra of NTS events are depleted in high-frequency energy compared to earthquakes of similar magnitudes (*e.g.*, Bennett and Murphy, 1986; Springer and Denny, 1976), an effect most probably due to the higher attenuating nature of the explosion source medium.

In this report, an attempt is made to show that the spectra of events recorded in the southwest U. S. are in many cases consistent with the difference in source type and source lithology. A set of time-varying autoregressive spectral parameters were computed for a subset of the data set analyzed by Bennett and Murphy to compare the spectral character of events recorded at or near NTS.

The results reaffirm the fact that the high-frequency spectra of NTS events are depleted; however, the peak frequencies of P_n and coda are in several cases greater than or equal to those of the earthquakes. This observation appears to be obscured in the later phases by path attenuation.

3.3.2. AR Parameters

The equivalence between the second-order AR system and a damped harmonic can be used to derive spectral parameters from the prediction coefficients. The four AR parameters used in this study are the peak frequency, damping factor, entropy and power. A detailed description of each is given by Dysart (1986). The peak frequency f_{max} and the damping factor γ are given by the equations

$$f_{max} = \cos^{-1} \frac{2\,Re(p_1)}{|p_1|^2 + 1} \qquad (1)$$

$$\gamma = 2\,(f_{\max}^2 - f_{res}^{2)\,\frac{1}{2}} \tag{2}$$

where

$$f_{res} = \tan^{-1} \frac{Im(p_1)}{Re(p_1)} \tag{3}$$

and P_1 is the pole of thhe second-order model (Oppenheim and Schafer, 1975). The two parameters $f_{\max}$ and γ are shown in *Figure 1* on sample maximum entropy spectra corresponding to the pole-zero plot above.

The peak frequency gives an estimate of the corner frequency or equivalently, the frequency where the main energy of the signal is concentrated. The damping factor, which is defined as the half pulse-width of the spectrum, indicates whether the signal is dominated by a single narrow band centered at the peak frequency (low value), or is more full-band in character (high value). As seen in *Figure 1*, a low value of the damping factor is indicative of a steep high-frequency falloff.

The entropy (h) is given by the formula,

$$h = 0.5 \log (\det[r_t]) \tag{4}$$

where $[r_t]$ in the expression for entropy is an estimate of the autocorrelation matrix, obtained either directly from the raw data or from the Burg estimate of the autocorrelation function (Ulrych and Bishop, 1975). The entropy can be considered a measure of the disorder or randomness of the time series, and the power is simply the variance of the underlying white noise. Of the four parameters shown here, the entropy is most sensitive to sudden changes in spectral content. The time-varying power simulates a time envelope. Both the entropy and the power are useful in picking the onset of P_g and L_g. In all, these four parameters provide a great deal of amplitude and frequency information at very little cost in computational effort.

3.3.3. Tonto Forest Observatory Data

Table 1 is a list of NTS explosions and nearby earthquakes analyzed in this report. *Figure 2* shows the location of the events and the recording station TFO. These eight events were chosen from those published by Bennett and Murphy for their similarity in magnitudes and clear P_n and P_g arrivals (*Figure 3*).

The TFO data were digitized at 20 samples per second and band-pass filtered from 1 to 5 hz. The NTS explosions show very little signal energy above 5 hz as shown by the averaged signal and noise spectra for P_n and P_g in *Figure 4*. Each of these four underground nuclear explosions was detonated in dry alluvium above the water table at depths ranging from 240 to 300 meters.

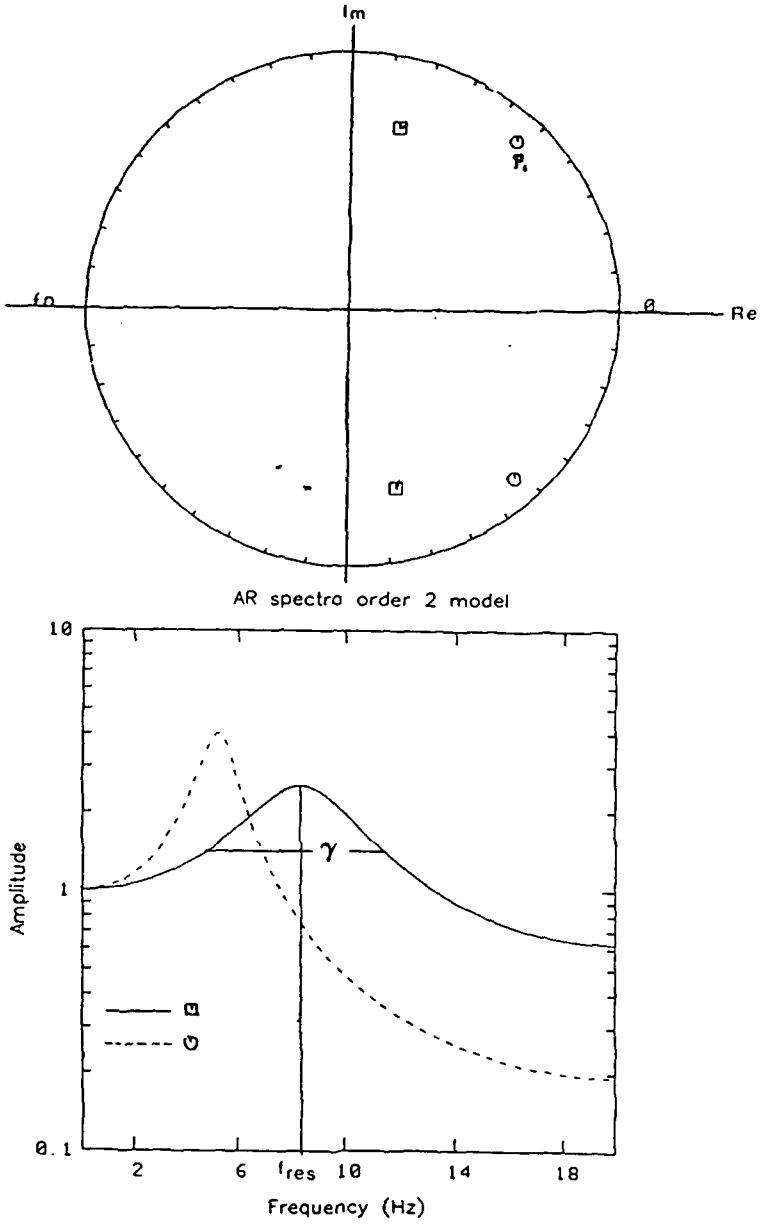

Figure 1. Pole-zero plot and maximum entropy spectra showing the peak frequency and damping factor.

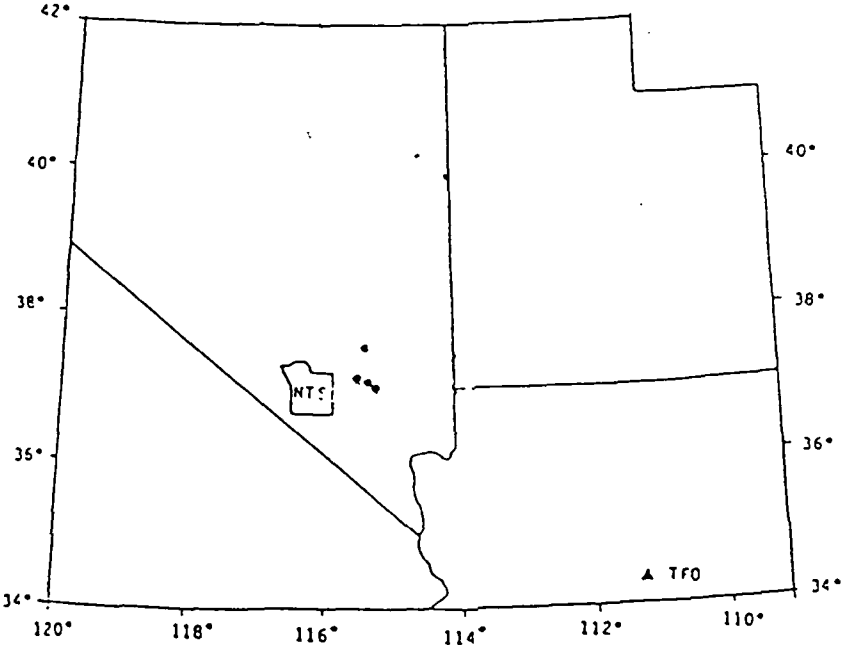

Figure 2. Map showing TFO, NTS and earthquakes epicenters.

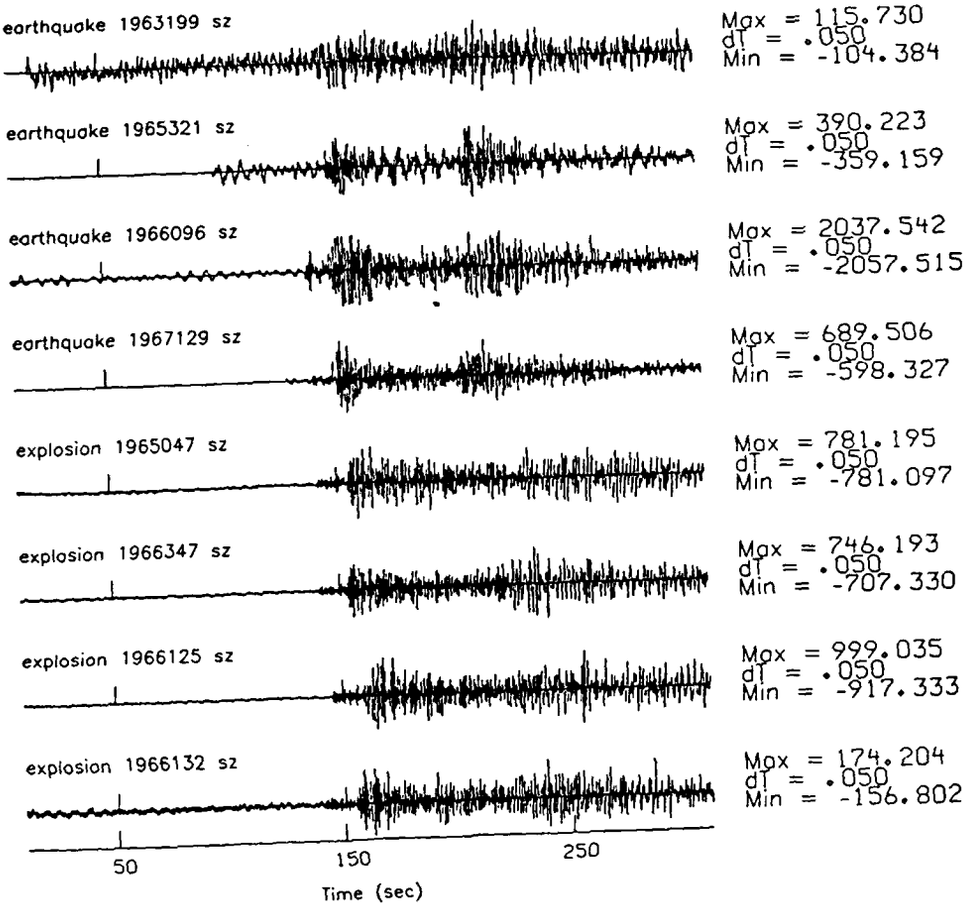

Figure 3. TFO data analyzed in this report.

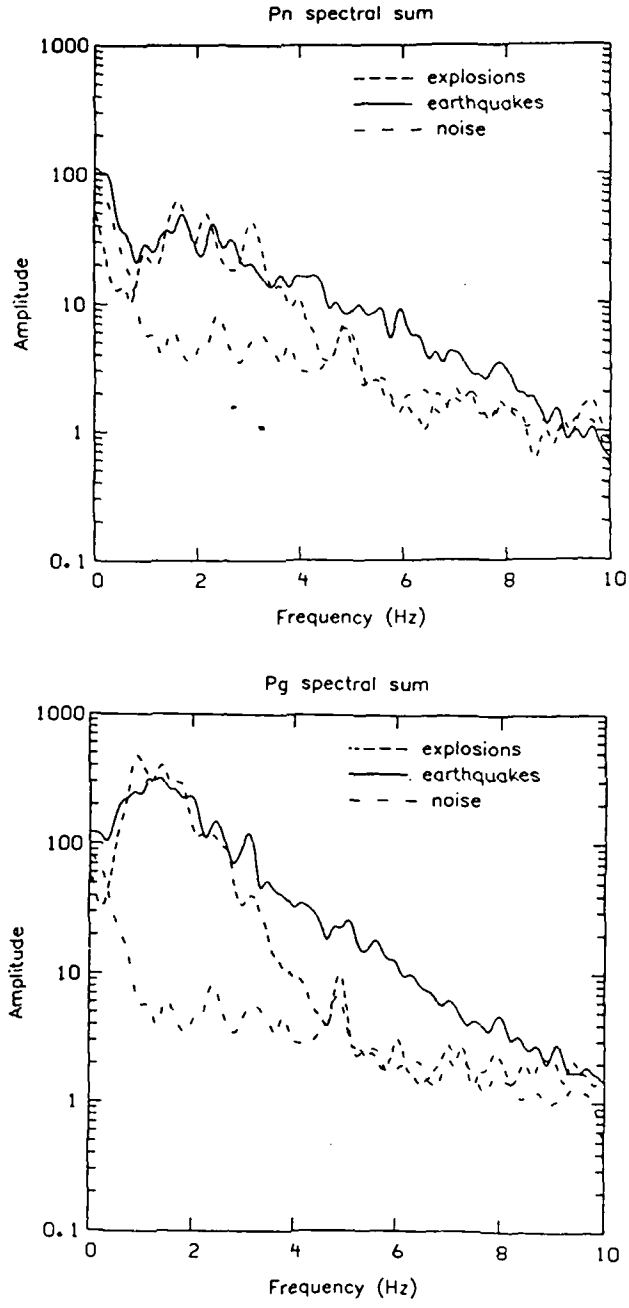

Figure 4. Averaged signal and noise spectra of P_n and P_g.

Table 1. TFO recordings analyzed in this report.

Event	Lat (N)	Long (W)	Date	Time	mb	Dist (deg)	Azi (StoE)
1963199	37.20	-115.60	Jul 18 1963	04:01:16.0	3.9	4.5	311.0
1965321	37.60	-115.20	Nov 17 1965	09:41:28.0	3.7	4.6	317.0
1966096	37.20	-115.40	Apr 6 1966	17:56:32.0	4.1	4.5	312.2
1967129	37.00	-115.00	May 9 1967	00:42:26.0	3.9	4.1	313.0
1965047	Merlin	NTS	Feb 16 1965	17:30:00.0	4.5	5.0	307.0
1966347	New Point	NTS	Dec 13 1966	21:00:00.0	4.6	5.0	307.0
1966125	Cyclamen	NTS	May 5 1966	14:00:00.0	4.2	5.0	307.0
1966132	Tapestry	NTS	May 12 1966	19:37:26.0	4.2	5.0	307.0

3.3.4. Results

In their analysis of discrimination capabilities in the western U. S., Bennett and Murphy were able to discriminate between NTS explosions and nearby earthquakes using the ratio of L_g amplitudes in the two frequency bands 0.5-1 and 2-4 hz. Their results clearly showed that L_g , P_n and P_g waves for NTS explosions have less high-frequency energy than a group of earthquakes with similar distances and magnitudes. The earlier study by Springer and Denny made the same observation on the basis of P_n and total wave train spectra of NTS explosions and one NTS earthquake. The following discussion suggests that a closer look at the variation in spectral content with time yields a picture which is more consistent with the theoretical spectra of earthquakes and explosions.

Figure 5 shows the time-varying AR parameters for several earthquake-explosion pairs. As the figures show, the P_g peak frequencies are generally lower for the explosions than for the earthquakes, but for P_n they are about the same or greater. In several of these examples, the plot of peak frequency as a function of time for the explosions actually crosses the curve for the earthquake as it moves from P_n to P_g and later phases. In general, the damping factors tend to be lower for the explosions than for the earthquakes, for both P_g and P_n. If γ is considered a relative measure of attenuation, then lower values indicate that the explosions have experienced greater near-source attenuation than the earthquakes.

The difference in source lithologies for earthquakes and nuclear explosions in the Southwest U. S. would be expected to cause greater attenuation of the explosions. The four NTS explosions in this study were detonated in a shallow alluvial layer, which would probably not support an earthquake of equal magnitude. The source lithologies for earthquakes and explosions in a shield region such as Norway are more likely to be similar.

These observations are consistent with the average P_n and P_g spectra in *Figure 4*. The P_n spectra show a much steeper falloff rate and a higher corner frequency for the

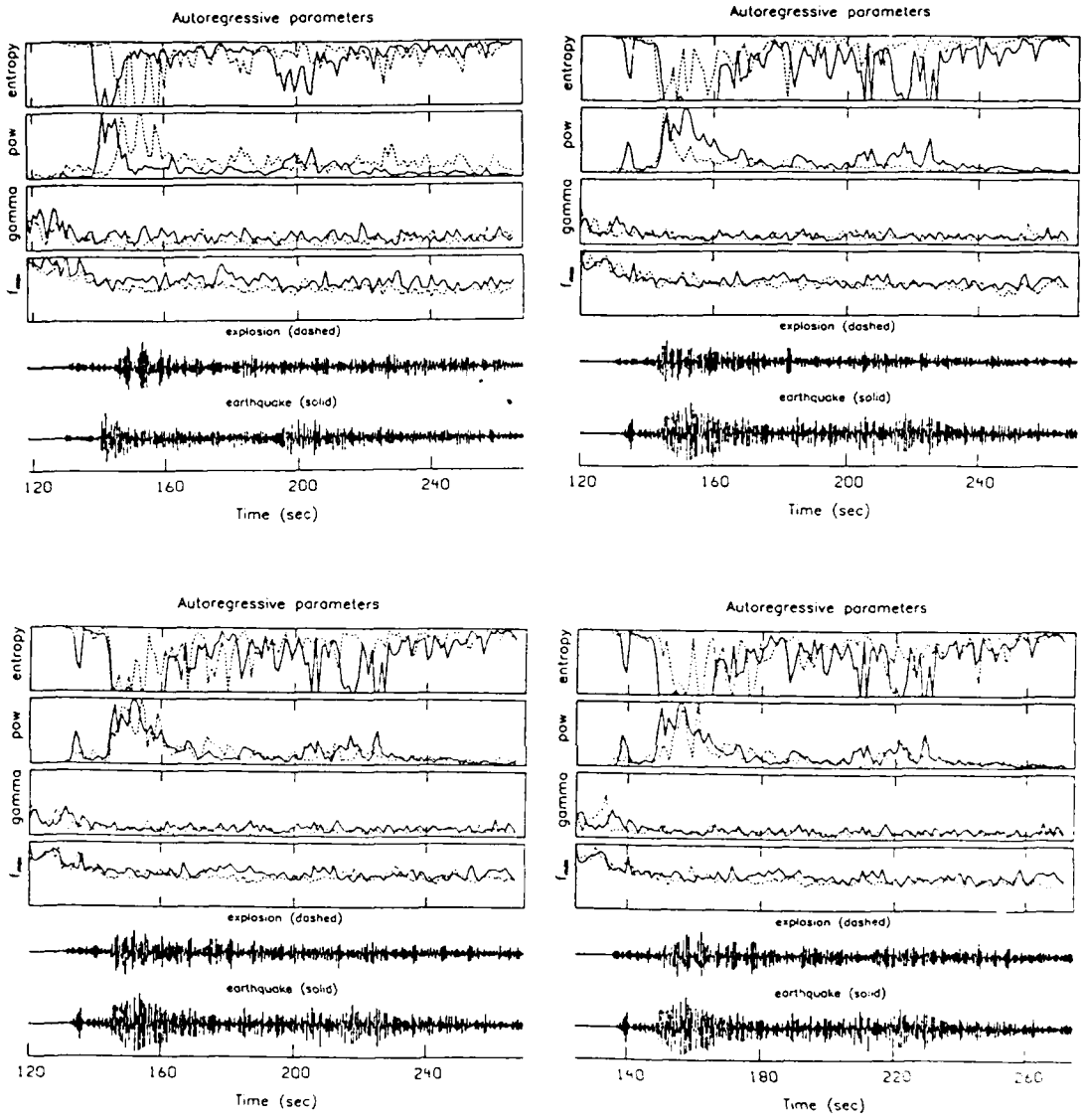

Figure 5. Examples of time-varying AR parameters for event pairs.

explosions. The average spectra of P_g waves shows about the same corner frequency for the explosions as for the earthquakes. The crustal phases appear to have suffered greater path attenuation which has made the interpretation of corner frequency difficult.

Given the probable effects of differences in near-source lithology, it is not supprising to find the explosion spectra depleted in high frequencies. In addition to the probable effect of the source medium, the NTS events are an average of 0.5 magnitude units larger than the earthquakes, and an average of 60 km farther from the recording station. In spite of all these factors which serve to deplete the high-frequency content of the explosions, the measurement of peak frequencies made here suggests that the spectra of P_n for earthquakes and explosions are not completely inconsistent with those expected from the two source types.

Paul Dysart

REFERENCES

Bennett, T. J. and J. R. Murphy, 1986. Analysis of seismic discrimination capabilities using regional data from western United States events, *Bull. Seism. Soc. Am., 76*, 1069-1086.

Dargahi-Noubary, G. R., P. J. Laycock and T. Subba Rao, 1978. Non-linear stochastic models for seismic events with applications in event identification, *Geophys. J. R. astr. Soc., 55*, 655-668.

Dysart, P. S., 1986. Autoregressive analysis of regional seismograms from earthquakes and explosions, *Center for Seismic Studies Technical Rept. C86-07*, 82-99.

Oppenheim, A. V. and R. W. Schafer, 1975. *Digital Signal Processing*, Prentice-Hall, inc., New Jersey.

Pulli, J. J., 1986. A note on the spectral interpretation of regional waveforms, *Center for Seismic Studies Technical Rept. C86-07*, 74-81.

Springer, D. L. and M. D. Denney, 1976. Seismic spectra of events at regional distances, Lawrence Livermore Laboratory Rept. UCRL-52048.

Tjostheim, D., 1975. Autoregressive representation of seismic P-wave signals with an application to the problem of short-period discriminants, *Geophys. J. R. astr. Soc., 43*, 269-291.

Ulrych, T. J. and T. N. Bishop, 1975. Maximum entropy spectral analysis and autoregressive decomposition, *Rev. Geophys. and Space Phys., 13*, 183-200.

ACKNOWLEDGEMENT

Brian Barker of S-cubed Reston, Va. provided the TFO data used in this study.

3.4. REVIEW OF EVIDENCE FOR HIGH-FREQUENCY PROPAGATION IN GEOLOGICALLY STABLE SHIELD/PLATFORM REGIONS

3.4.1. Introduction

In their evaluation of CTBT verification using high-frequency seismic data, Evernden *et al.* (1986) state as one of five major conclusions that "transmission of high-frequency P and S wave signals in the regional distance range in stable continental areas and shields is nearly as efficient as at 1 Hz, with effective Q factors in shield areas being about 9,000 and 4,000 for high-frequency P_n and S_n, respectively, while the effective Q for P_n waves in tectonic areas is about 1,000."

The authors state that "several lines of evidence support the inference of efficient high-frequency propagation in stable continental areas," but they cite only two examples -- a high-frequency recording of an earthquake in eastern Canada, and Soviet recordings of Moho reflections on a profile in Georgia and Azerbaijan. Their calculation of Q_α using the earthquake recording involves non-unique or questionable assumptions about the source spectrum and the character of Q, and their interpretation of the Soviet reflection data appears to be wrong. The two cases are described below:

- An earthquake in eastern Canada with magnitude $m_b(L_g) = 4.2$ was recorded by a USGS seismic station in New York at a distance of 190 km. The seismic station recorded digitally at a rate of 400 samples/second, and the system included a 100-Hz anti-aliasing filter. The displacement spectrum of the first 2.5 seconds of the P_n-wave as recorded on the vertical component of the system was interpreted as being flat below about 5 Hz and having an almost constant negative slope for higher frequencies (*Figure 1*). The displacement spectrum of a phase identified by the authors as S_n was flat to 2.6 Hz, with a negative slope for higher frequencies. To estimate Q using data from just the one station, Evernden *et al.* assumed a high-frequency spectral slope of f^{-3} and frequency-independent Q. With these assumptions the observed P-wave spectrum can be modeled using $Q_\alpha = 9{,}000$. For the S_n phase, they assumed f^{-2} for the high-frequency source spectrum, and obtain Q_β of 4,000. Had they assumed f^{-2} for the P-wave source spectrum, Q_α would have been about 2,000.

- Davydova and Mikhota (1973) present plots of amplitude as a function of distance, for band-filtered (<3, 5, 6-8, 8-14 and 14-30 Hz) recordings of P-waves reflected from the mantle. Evernden *et al.* use the ratio of amplitudes in the 5 and 14-30 Hz bands, calculated for distances of 50 and 300 km, and conclude that Q_α = 1,500-7,000.

Comments on this evidence, plus other studies involving anaysis of high-frequency data, are given below.

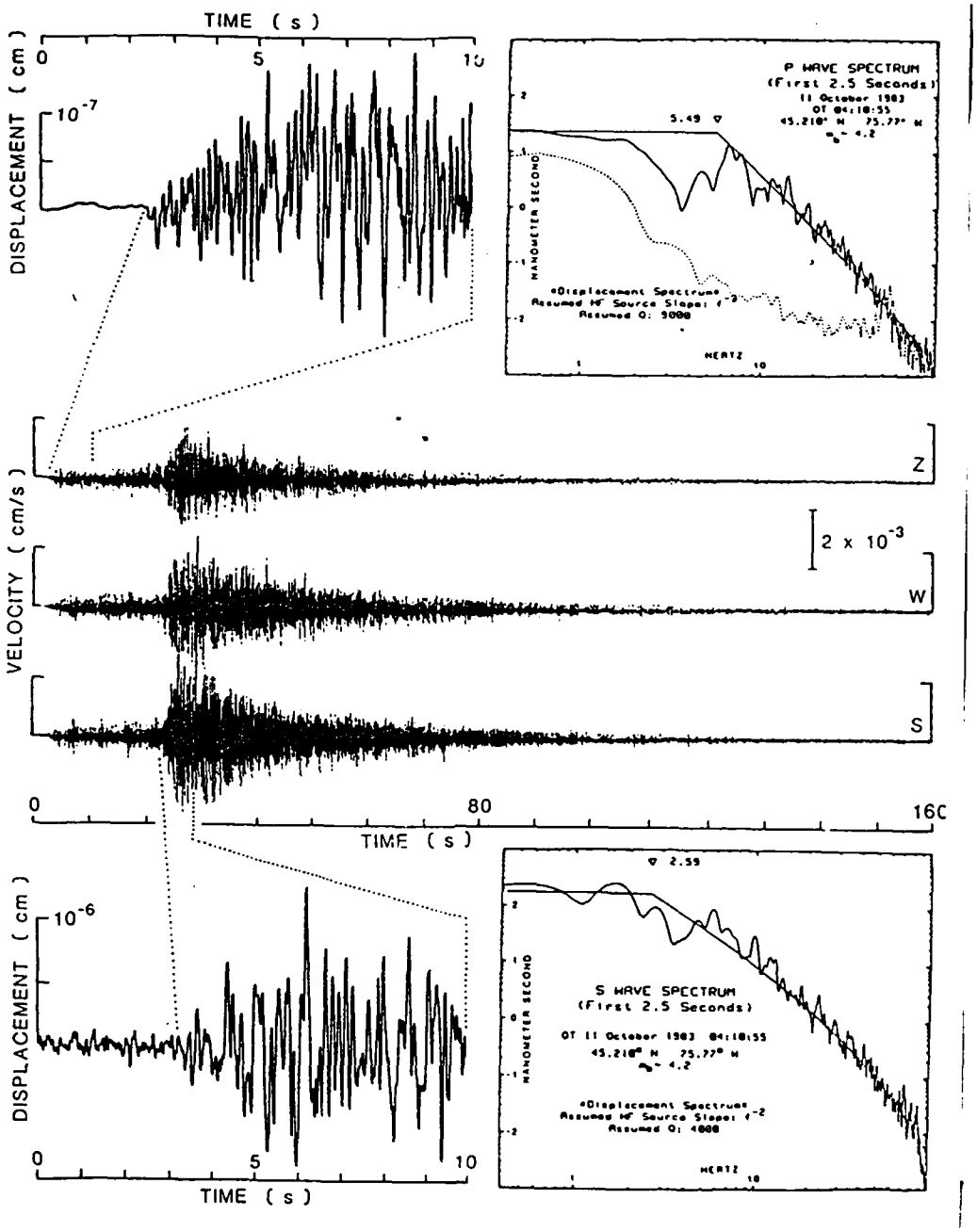

Figure 1. High-frequency ground motion recorded at 400 sps on a GEOS station in New York at distance 192 km from the 11 October 1983 Ottawa earthquake. Initial *P* and *S* arrivals at top and bottom left are displacement traces, obtained by integrating the velocity recordings in the center of the figure. Fourier spectra at top and bottom right were computed from the inferred displacements (Borcherdt, *et al.*, 1985).

3.4.2. The USGS Recording

Pulli (1986) reanalyzed Cranswick's high-frequency recording of the Ottawa earthquake and examined tradeoffs between the source corner frequency, the high-frequency slope of the source spectrum, and Q along the path. He makes the following points regarding this recording and the interpretation by Evernden *et al.*:

- There is a basic tradeoff between source spectrum and attenuation. *Figure 2* shows two theoretical spectra that match the observed spectrum equally well. One is based on the Evernden *et al.* model, having f^{-3} slope for the source spectrum, source corner frequency f_c = 10 Hz, and constant Q = 9,000. The other is for a source spectrum with f^{-2} slope, f_c = 10 Hz, and frequency dependent $Q = Q_0 f^{\eta}$, where η = 0.2. The value of Q_0 for this model is 750, *i.e.*, a *factor of twelve* smaller than the value of 9,000 found by Evernden *et al.* A slight shift in the assumed corner frequency or in η could bring the two curves into even closer correspondence at the higher frequencies.

- The tradeoff between source and path effects is explored by Pulli using theoretical spectra to illustrate (a) differences in constant Q, (b) differences in corner frequency, (c) differences in high-frequency slope of the source spectrum, and (d) differences in several parameters to produce essentially identical spectra.

- Pulli also notes that the P-wave signal was accompanied by a small burst of noise that limited the usable bandwidth to about 35 Hz. Evernden *et al.* noted the problem, but interpreted the spectrum out to 100 Hz.

3.4.3. The Soviet Data

Davydova and Mikhota (1973) present models of the M discontinuity to explain the character of reflected and refracted waves out to distances of several hundred kilometers along a DSS profile in the Rioni-Kura depression, a tectonically active area along the southwest side of the Caucausus Mountains in Georgia and Azerbaijan. Elevations along the profile were moderate, probably between sea level and 1,000 meters; however, elevations in the Caucausus range to the northeast exceed 3,000 meters in places. Crustal thickness is about 40 km under the depression, 50 km under the mountains, and there are major fault zones in the area of the profile (Shekinskii *et al.*, 1967). The level of seismicity in the region is moderate, according to the 1962 *Atlas of Seismicity in the USSR*.

On *Figure 9*, amplitude-distance curves are shown for five different frequency bands: <3, 5, 6-8, 8-14, and 14-30 Hz. The authors note that the maximum amplitude for supercritical reflections (large peak at about 140 km) is about the same for all frequency bands except 14-30 Hz, and that this amplitude is also about equal to that of the subcritical reflection at about 40 km. To explain this pattern, they propose that the Moho consists

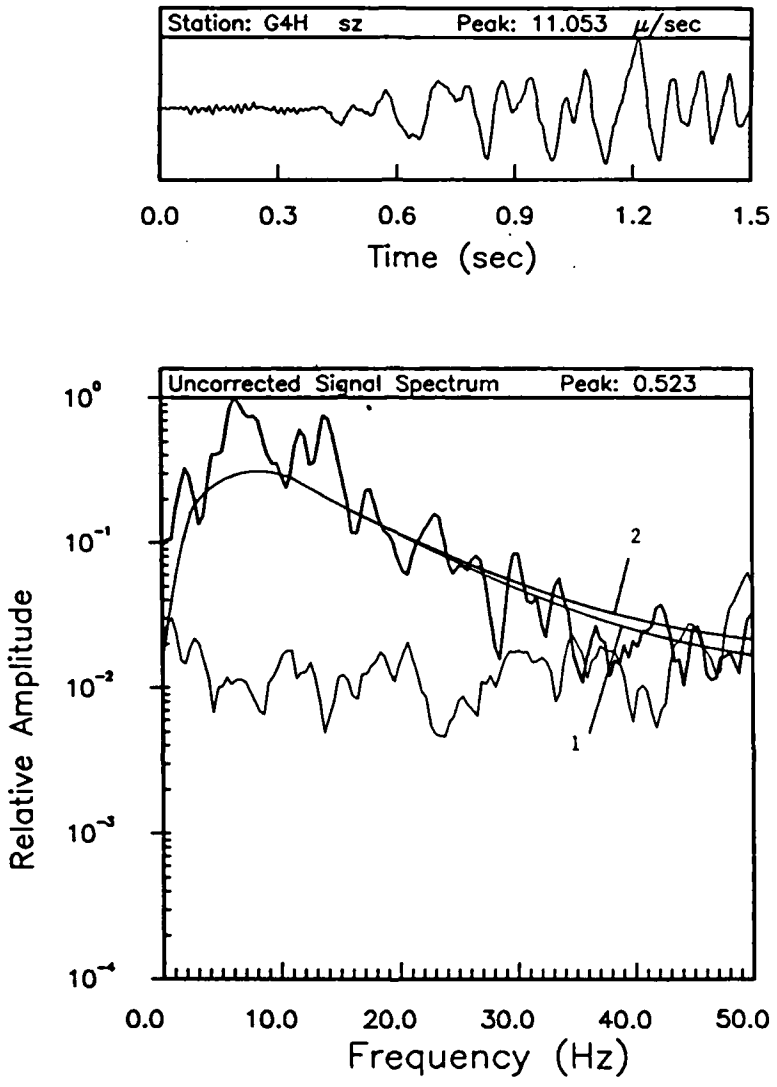

Figure 2. P_n waveform and spectrum for the 11 October 1983 Ottawa earthquake recorded at 400 sps by a GEOS station in New York at distance 192 km. The noise spectrum is also shown. Curve 1 is the theoretical curve for an f^{-3} source and frequency-independent Q of 9,000. Curve 2 is for an f^{-2} source, $Q_0 = 750$, and $\eta = 0.2$.

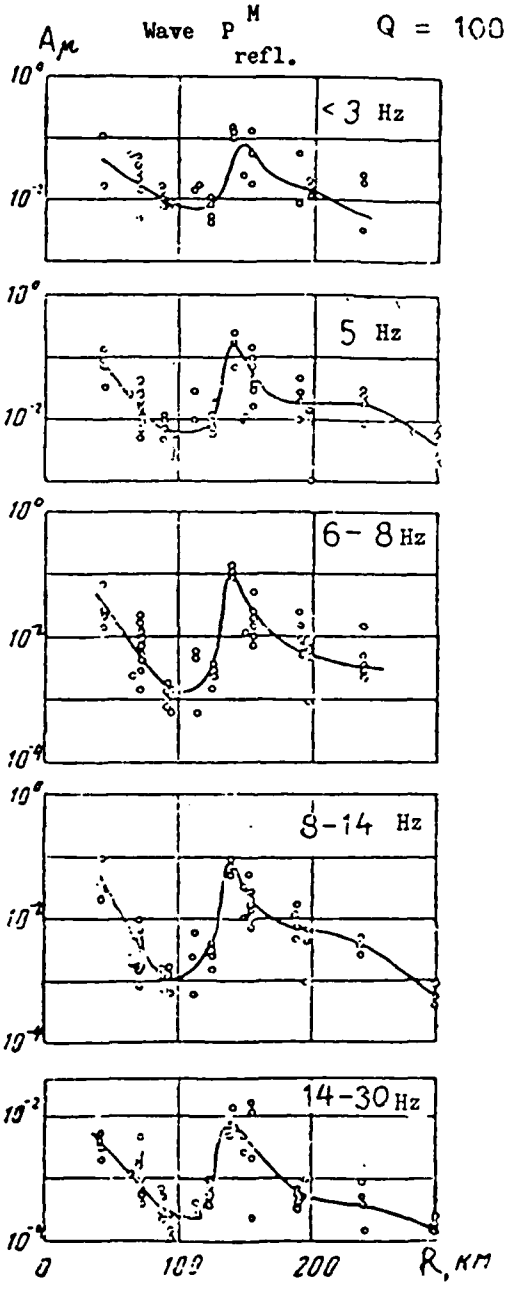

Figure 9. Observed amplitudes of *P*-waves reflected from the Mohorovicic discontinuity, in various frequency bands, obtained on a deep seismic sounding profile in the Riono-Kurinsk depression (Davydova and Mikhota, 1973).

of a "packet" of thin layers of alternating high and low velocity -- causing the ratio A_{max}/A_{min} to increase with increasing frequency up to a "resonance frequency" (about 20 Hz in this case), where "the reflection coefficients vary in a complex manner." Amplitudes measured from the curves on *Figure 3* for the 5 and 14-30 Hz bands are given in Table 1.

Table 1. Amplitudes measured from *Figure 3*

Distance, km	Ampl. (5 Hz) $x10^{-3}$	Ampl. (14-30 Hz) $x10^{-4}$
35	100	70
50	70	35
100	7.8	3.8
140	200	85
300	6.2	1.5

The main conclusion of the Soviet investigators was that the observed amplitudes were best explained by laminar structure of the M-discontinuity. They note that the ratio of A_{max}/A_{min} -- the peak amplitude at about 140 km divided by the amplitude in the trough at about 110 km -- increases with increasing frequency to about 20 Hz, and then decreases in the 14-30 Hz band. They interpreted this observation in terms of theoretical results by Fuchs (1968), who showed that a reflecting horizon with lamellar structure could lead to very complex behavior of the reflection coefficient as a function of frequency and angle of incidence of the wave (*Figure 4*). Numerous recent crustal reflection investigations support the idea that in many places the Moho may contain fine structure such as thin alternating high- and low-velocity lamellae, or gradients that change rapidly from one location to another (*e.g.*, Braile and Chiang, 1986).

In a different interpretation, Evernden *et al.* (1986) used *Figure 3* to support the contention that Q_α for P_n in stable geologic regions like the eastern US and large parts of the USSR is high -- of the order of 9000. However, their calculation involves a number of mistakes:

- The Soviet study is of reflected waves for which the entire path is in the crust; the results do not apply to the P_n phase, which propagates in the upper mantle.

- Their attenuation calculation was based on amplitude ratios [A(5 Hz)/A(14-30 Hz)] at 50 and 300 km. Amplitudes from these distances should not have been included in the same calculation because they represent different types of waves. As noted by the Soviet authors, the amplitude curve for distances less than 140 km represents subcritical reflections, which are highly dissipative because of energy loss to refracted arrivals transmitted across the Moho. In the range 150-300 km, however, the amplitude curve corresponds to supercritical reflections for which no

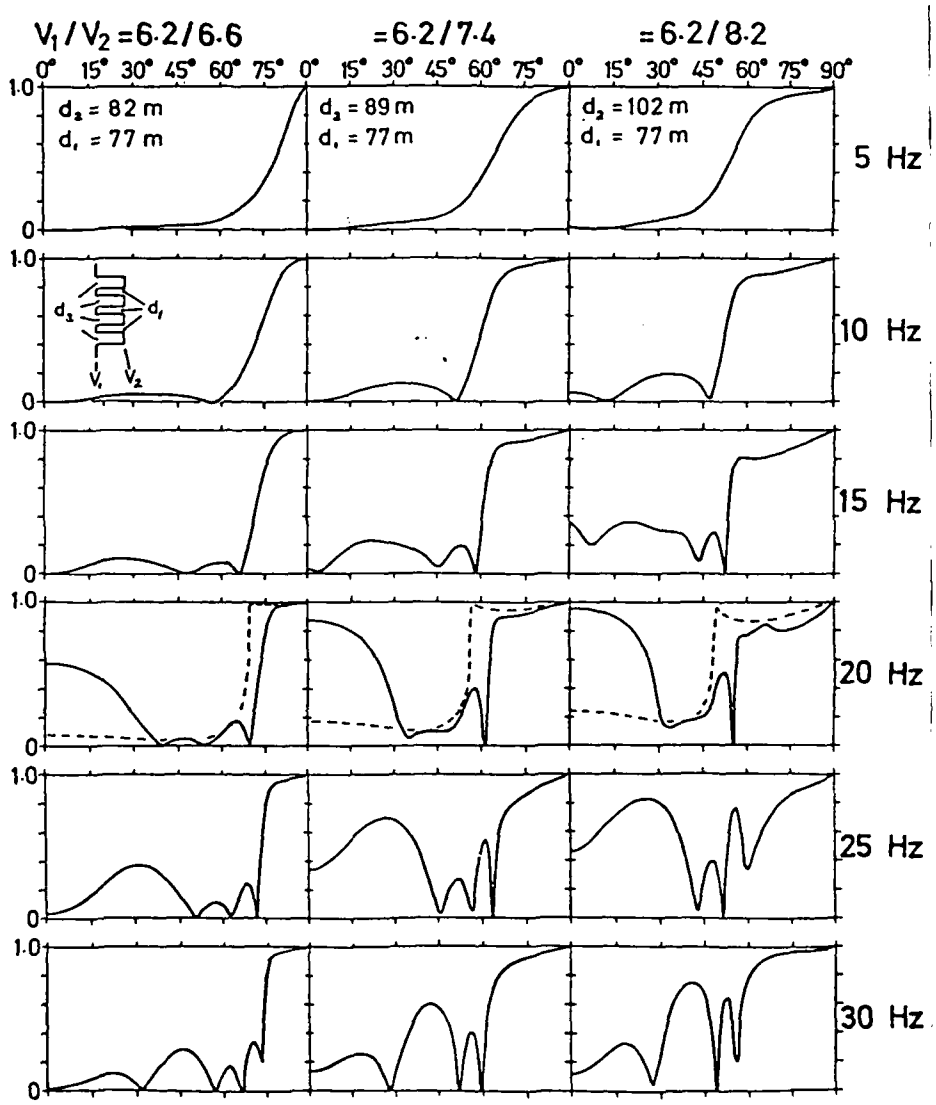

Figure 4. Reflection coefficient R_{PP} for boundary with four thin, high-velocity layers and three thin, low-velocity layers between two low-velocity half-spaces, as a function of the angle of incidence, for three different velocity contrasts, at six frequencies (Fuchs, 1968).

energy is transmitted across the Moho.

- A frequency of 20 Hz was taken to be appropriate for the 14-30 Hz band. Noting that maximum amplitudes remained constant over all the frequency bands from 3 to 14 Hz, and then decreased by a factor of ten in the 14-30 Hz band, it is more likely that energy in the latter band is peaked closer to 14 Hz than at a frequency close to the middle of the band.

- The authors ignored the possibility, which was the point of the Soviet paper, that the structure of the crust-mantle boundary affects reflection coefficients differently for different frequencies.

Recalculation of Crustal Q. Assuming Q is not frequency dependent, the amplitude of a seismic wave at distance R and frequency f can be written as

$$A(f,R) = A_0(f)\, R^{-n}\, e^{\frac{-\pi R f}{Qv}}, \tag{1}$$

where R^{-n} is a geometrical spreading factor, Q^{-1} is the intrinsic dissipation factor, and v is the average velocity along the path. Taking the natural logarithm of the ratio of amplitudes at a single distance and two frequencies yields the following:

$$\ln \frac{A(f_1,R_1)}{A(f_2,R_1)} = \alpha + \frac{\pi R_1}{Qv}(f_2 - f_1), \tag{2}$$

where

$$\alpha = \ln \frac{A_0(f_1)}{A_0(f_2)}.$$

Using equation (2), limiting the calculation to the supercritical reflections at 140 and 300 km, and solving for α and Q yields a "Q" of 1356. This value is given in quotes because the calculation still ignores the possibility that the structure of the Moho may be enhancing high-frequency amplitudes, as claimed by the Soviet authors; it should therefore be considered a maximum value. Use of equation (2) to calculate "Q" for the subcritical reflection at distances less than 140 km would be inappropriate because of signal loss across the boundary. Our calculation was based on the following:

- Amplitude ratios $A(5\ Hz)/A(14\text{–}30\ Hz)$ at 140 and 300 km were 23.5 and 41.3,

respectively, based on the measurements listed in the above table.

- Distances R used in the calculations were those for the ray path, not the shot-receiver distances. Using 40 km for crustal thickness, the values of R corresponding to 140 and 300 km are 161.2 and 310.5 km, respectively.

- For the highest-frequency band, 16 Hz was used instead of 20 Hz for the reason stated above.

- We assumed an average crustal velocity of 6.75 km/sec, identical reflection coefficients for the two frequency bands at a given angle of incidence, and frequency-independent Q.

3.4.4. Other Evidence

Several published reports deal with high-frequency propagation, and a figure published in a recent NORSAR technical report can be used to estimate Q for P_n waves propagating in the Baltic shield. These are summarized below.

- Hasegawa (1985) studied L_g waves recorded by SPZ instruments of the Eastern Canada Telemetered Network (ECTN), for Canadian shield earthquakes in the magnitude range $m_b(L_g)$ 2.8-5.2 and distance range 70-900 km. The recordings were digital, with a sampling rate of 60 Hz. Results indicated that for the vertical component of L_g waves propagating in the Canadian shield, $Q = 900\ f^{0.2}$.

- Chael (1986) analyzed RSNY recordings of the mainshock and 11 aftershocks ($m_b(L_g)$ range of 3.3-5.7) of the 1982 Miramichi, New Brunswick earthquake sequence. Comparison of theoretical and observed spectral ratios between the mainshock and aftershocks indicated that the source spectra of these events had high-frequency slope of f^{-2}, to frequency of at least 15 Hz. Theoretical spectral ratios for a source model with high-frequency slope of f^{-3} strongly disagreed with the data. The author concluded that, since both earthquakes and explosions have similar source spectra, the utility of a high-frequency discriminant (Evernden *et al.*, 1986) based on assumed differences in source spectra for these two types of events was dubious. Chael's results also cast doubt on the high Q_α found for the eastern US by Evernden *et al.*, because the finding was based on assumed high-frequency slope of f^{-3} for the 1983 Ottawa earthquake.

- Goncz and Dean (1986) analyzed P_n, S_n and L_g propagation in the eastern US using data from the five RSTN stations, over the distance range out to 30° and frequency band from 0.5 to 20 Hz. They concluded that the P_n attenuation corresponded to $Q = 640\ f^{0.5}$, which would correspond to constant Q of 2,024 and

2,862 at 10 and 20 Hz, respectively. They found L_g propagation to be about as efficient as that for P_n, $Q = 1{,}000\ f^{0.35}$, *i.e.*, 2,238 and 2,853 at 10 and 20 Hz. For S_n they obtained $Q = 825\ f^{0.8}$, which gives very high Q -- 5,205 and 9,063 -- at 10 and 20 Hz. Their analysis consisted of picking the maximum amplitude in the appropriate time window for a particular phase, on comb-filtered, rectified, vertical-component traces. All of the measurements for a particular phase (*e.g.*, 227 measurements of L_g amplitudes for 114 earthquakes) were used in a regression calculation that solved simultaneously for an average source function, station bias and attenuation coefficient ($\gamma = \pi f / Qvf^k$). Geometrical spreading was assumed to be as $R^{-5/6}$, at least for L_g, and the source function for all three phases was found to have slope proportional to f^{-3}. As in the Evernden *et al.* (1986) study, there is an obvious tradeoff between Q and the high-frequency source spectrum, with high apparent Q values linked to f^{-3} source rolloff.

- Nersesov *et al.* (1982) studied Central Asian earthquakes recorded by a variable-frequency (*ChISS*) seismic system at stations near Alma-Ata and Garm. The study involved analysis of recordings from 170 earthquakes in the northern Tien Shan range (distance range 20-220 km), plus about 240 recordings of earthquakes from seven source areas in Central Asia in the distance range 30-750 km. Magnitudes of the earthquakes were m_b = 3.6-4.1 (K = 7-9) for the first group and 3.1-5.4 (K = 5-14) for the second group (conversion from K to m_b was based on Soviet papers comparing NEIS m_b with Soviet K -- if NEIS m_b had been determined by maximum-likelihood calculations the minimum magnitudes could be 2.0 or less).

Figure 5 indicates that high-frequency signals decay very rapidly with distance, beyond about 150 km. For P-waves the effective coefficient of attenuation, corresponding to n_{eff} in the expression

$$A \approx R^{-n_{eff}},$$

was 3.6 for 11-Hz signals and 5.0 for 22-Hz signals; for Lg waves the corresponding values are 5.4 and 7.2, respectively. The authors summarize their results as follows:

> "For near distances (20-100 km) the slope of the curves for 0.8, 1.5 and 2.7 Hz are almost the same for both P (n_{eff} = 1.2) and S. For the 5.7 and 11 Hz curves there is some steepening of the slope (n_{eff} = 1.5-1.6), and for the 22-Hz curve the slope increases sharply, to n_{eff} = 2.5 for P and 2.0 for S.
>
> "In the range 120-300 km almost all the amplitude curves decrease in slope. The 0.8 Hz curve for P has a flat part ($n_{eff} \approx 0$). With increasing frequency the steepness increases and at 22 Hz reaches n_{eff} = 5. For S this trend is repeated, with the only difference that n_{eff} for this part of the 0.8 Hz curve is

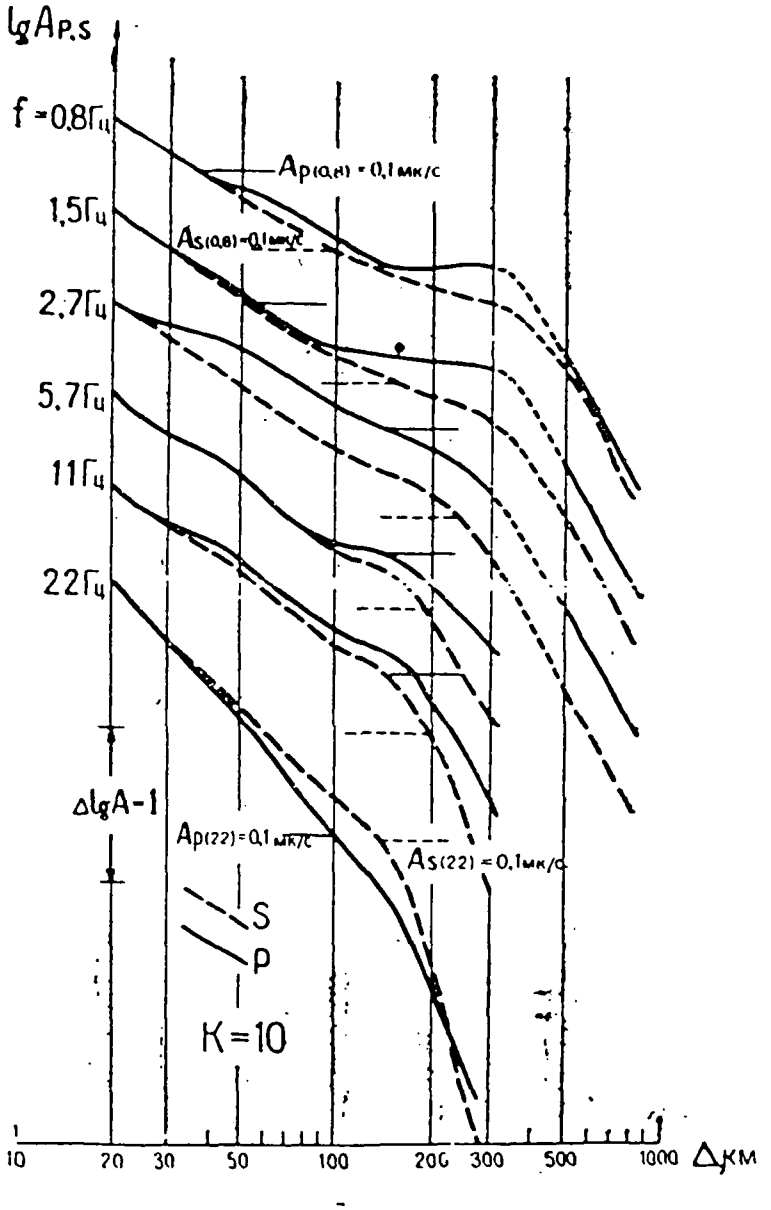

Figure 5. Family of amplitude curves of the form $A_i - \Delta$, for different frequencies (Nersesov, *et al.*, 1982).

0.6-0.7 and, increasing as a function of frequency, reaches n_{eff}=8 at 22 Hz. With increasing frequency, starting with the fourth channel (f = 2.7 Hz), this part splits into two shorter parts (100-160 km and 160-300 km). The steepness of the first part is weakly dependent on frequency, while that of the second part changes sharply with frequency.

"Thus, beyond 100-120 km on all amplitude curves there is a "flattening" at low frequencies or a decrease in slope at higher frequencies. The position of this feature on the distance axis changes in a regular way with frequency f. On the part of the curve from 300 to 800 km the slopes of both P and S curves are the same, essentially frequency-independent, n_{eff} = 3.6-3.8. It must be noted that our data are less reliable in this distance interval.

"From the set of amplitude curves for different frequencies we may draw some definite conclusions. First, the curves have characteristic shape, with the slope steepness changing systematically with frequency. The flattening of the curves at distances greater than 100 km is not accidental. It was noted earlier [by Rautian, 1960], and is connected with the appearance of strongly reflected waves, alternating later with the waves Pg and Lg, which dominate at distances of 250-700 km. The frequency content of these waves is different and as a result they behave differently (at distances of 100-160 and 160-300 km). In addition, the selective absorption of the medium leads to intensive absorption of the high-frequency components of the waves, which is clearly visible on the graphs."

- An earlier paper by Nurmagambetov (1974) contains much the same material, and appears to have been based on the same data, as the later paper by Nersesov et al. described above. The conclusions are the same -- flattening of the amplitude-distance curves for distances greater than 100-120 km and subsequent steepening to large distance and higher frequency. The author notes that for small distances the spectral peak for earthquakes of energy class K = 10 is at 13-15 Hz; for increasing distance this maximum gradually moves to lower frequencies, and for R = 570 km it is close to 0.8-1.5 Hz. Table 2, from Nurmagambetov, lists values for the coefficient of attenuation (n_{eff}) as a function of distance and frequency. Note that for the largest distance range (300-800 km) values of n are not listed for frequencies higher than 2.7 Hz.

Table 2. Change in n_{eff} with frequency for various distance ranges.												
R, km	Frequency, Hz											
	0.8		1.5		2.7		5.7		11		22	
	P	S	P	S	P	S	P	S	P	S	P	S
20-100	1.1	1.2	1.2	1.3	1.2	1.4	1.5	1.5	1.6	1.6	2.5	2.0
100-160						0.8	0.8	0.9	0.8			
160-300						2.5	2.2	3.6	3.9	5.3	5.1	8.4
120-300	0.	0.7	0.2	0.8	1.1							
300-800	3.6	3.7	3.6	3.7	3.7	3.8						

Note that the studies by Nersesov *et al.* (1982) and by Nurmagambetov (1974) both involve paths in an active seismic region of Central Asia. The *ChISS* data used in the study was recorded at Garm and Alma-Ata, and the source areas were at Talgar, Chilik, Khan-Tengri, Karakul', Alichur and Garm, in the Tadzhik, Khirgiz and southeast Kazakh Republics. According to a review of the Soviet DSS literature (Piwinski, 1979), structure of the crust and upper mantle in this region ranges from relatively simple layering to complex structure made up of heterogeneous blocks separated by deep fracture systems. The M-discontinuity ranges from flat to undulatory. In general, one would not expect the quality of high-frequency propagation in such a region to be as high as that in shield regions.

• Ringdal *et al.* (1986) present a "schematic illustration" of high-frequency *P*-wave spectra determined from digital recordings of a high-frequency seismic element (HFSE) in the NORESS array (*Figure 6*). The HFSE is configured as a dual sample-rate (125 and 250 sps) device and has a dynamic range of 120 dB. Spectra considered in the report show frequencies out to 62.5 Hz. *Figure 6* was compiled using data from about 100 events and represents average spectra over all azimuths, scaled to magnitude $M_L = 3.0$. The authors describe this figure as follows:

> "The figure illustrates the strong distance dependence of high-frequency signal energy. Of particular interest is the observation that the signal and noise spectra are aproximately parallel across the entire frquency band for distances out to about 500 km. Thus, within this distance range, the possibility of utilizing high frequencies for event characterization are excellent even at very low magnitudes. At further distances, the signal spectra start to merge with the noise (the crossover point being dependent on distance as well as magnitude). *E.g.*, at 900-1,000 km there seems to be significant SNR at M_L =3 for frequencies up to about 25 Hz.

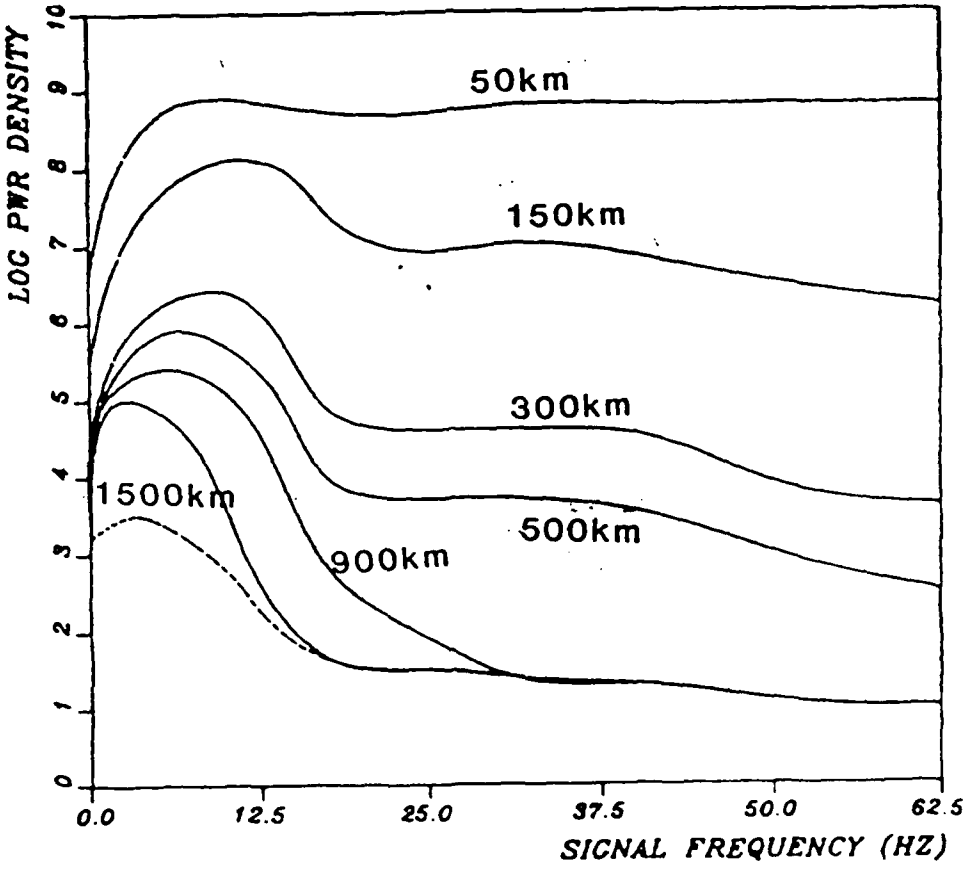

Figure 6. Average high-frequency *P*-wave spectra for events recorded at different distance ranges by the HFSE at NORESS (Ringdal, *et al.*, 1986).

"It must be noted that we have observed considerable spectral variability with source type and location, even within limited distance ranges. Thus Figure [5] must be interpreted accordingly."

Using equation (1), the ratio of amplitudes for different frequencies f_1 and f_2 at a given distance will be

$$\frac{A(f_1,R)}{A(f_2,R)} = \frac{A_0(f_1)}{A_0(f_2)}\, e^{\frac{\pi R}{Qv}(f_2-f_1)}. \tag{3}$$

If we assume that both f_1 and f_2 are greater than the corner frequency of the event, $f_2 > f_1 > f_c$, and that the high-frequency slope of the spectrum is equal to f^{-b}, then

$$\log\left(\frac{A_0(f_1)}{A_0(f_2)}\right) = b \log\left(\frac{f_2}{f_1}\right), \tag{4}$$

and from (2) and (3)

$$\log\left(\frac{A(f_1,R)}{A(f_2,R)}\right) = b \log\left(\frac{f_1}{f_2}\right) + \frac{0.4343\pi R}{Qv}(f_2-f_1). \tag{5}$$

Equation (5) can be used with measurements of spectral amplitudes at different distance ranges to solve for Q and b. The fact that the amplitude curves on *Figure 6* are almost parallel between 300 and 500 km can be interpreted as due to very high Q_α for P_n waves in that range, or perhaps as an artifact of averaging data over a wide range of azimuths and a relatively short range of distance. However, if we focus on a larger distance range -- 300-900 km or 500-900 km -- use of amplitude measurements for the frequency band 15-30 Hz in equation (5) yields Q of about 2,000. In this estimate, values of log power spectral density at 15 and 30 Hz -- respectively, 5.58 and 4.56 -- were measured from the curve for 300 km on *Figure 6*. The difference between these values, *i.e.*, the logarithm of the ratio of power spectral densities at the two frequencies, was divided by two and reduced by log f_1/f_2 to convert it to the logarithm of a spectral displacement ratio. Values were obtained in a similar way using the curves for 500 and 900 km on Figure 6, and these were substituted into equation (4) to obtain the following relationships for the three distance ranges, using a velocity of 8 km/sec for the P_n phase:

$$0.81 = -0.301\ b + 767.5\ Q^{-1}, \tag{6}$$

$$0.86 = -0.301\ b + 1{,}279\ Q^{-1}, \tag{7}$$

$$1.45 = -0.301\ b + 2{,}302\ Q^{-1}. \tag{8}$$

Equations (6) and (8) give $Q = 2{,}398$ and $b = 1.6$, while equations (7) and (8) give $Q = 1{,}734$ and $b = 0.4$.

3.4.5. Summary

Evernden *et al.* (1986) claim that Q_α = 9,000 for P_n waves propagating in stable shield/platform regions of the USSR. This claim is based on two lines of evidence -- (1) analysis of a high-frequency recording of an eastern Canada earthquake made at distance 190 km, and (2) a Soviet study of band-filtered Moho reflections made at distances less than 300 km. Their interpretation of the Canadian earthquake signal involves tradeoffs between Q and the assumed high-frequency slope of the source spectrum. Pulli (1986) shows that a value of $Q = 750\ f^{0.2}$, corresponding to Q = 1,200-1,400 for frequencies of 10-20 Hz, fits the data as well as the constant Q of Evernden *et al.*, if the source is assumed to have high-frequency slope of f^{-2} instead of f^{-3}. Support for the f^{-2} spectral slope is provided by results of a study by Chael (1986), who found that spectral ratios of the 1982 Miramichi, New Brunswick mainshock and aftershocks could be fit by theoretical curves if the source spectra had high-frequency slope of f^{-2} but not f^{-3}.

Interpretation by Evernden *et al.* of the Soviet results in terms of Q_α involves assumptions about the source spectrum and the structure of the M-discontinuity. The observations are certainly consistent with the Soviet interpretation of a boundary consisting of alternating high- and low-velocity thin lamellae, which would lead to reflection coefficients that change with frequency. If the coefficients are assumed to be frequency-independent then a crustal Q of around 2,000 is obtained, which is at the lower end of the range (1,500-7,000) given by Evernden *et al.* Use of this study to support the idea that high-frequency P_n signals could be recorded at large (1,000-2,000 km) distance ranges in shield/platform regions of the USSR should have been ruled out by any one of the following aspects of the study: the interpretation of the data was ambiguous, the waves were reflections rather than P_n arrivals, the study was carried out in a tectonic region, and the observations were made at relatively short (<300 km) distances.

Although a variety of high-frequency digital recordings now exist that could be used to estimate $Q(f)$, at least to frequencies of 20-30 Hz, only preliminary studies are available so far. One of these, by Hasegawa (1985), indicated that Q is about 1,500 for 10-20 Hz L_g signals propagating in the Canadian shield. Soviet studies (Nurmagambetov, 1974; Nersesov *et al.*, 1982) of central Asian earthquakes recorded by comb-filtered seismic systems indicate that attenuation increases for frequencies greater than about 15 Hz and distances greater than 300-500 km. The study was based on velocity amplitudes, and the change with frequency would be greater if the data were plotted as displacements. A study by Goncz and Dean (1986) of eastern US earthquakes recorded by RSTN stations involved the simultaneous determination of average source, path and receiver terms, and did not include a discussion of possible tradeoffs between these parameters. The calculations gave Q_β of 5,000-9,000 for the S_n phase, while Q_α was only 2,000-3,000 for P_n -- a result that is not physically reasonable.

Perhaps the most useful information published so far is a plot (Figure 6) given by Ringdal *et al.* (1986), showing average high-frequency P-wave power spectral density for

frequencies out to 62.5 Hz and distances to 1,500 km. In agreement with the central Asian studies cited above, Ringdal *et al.* conclude that high-frequency propagation is good out to a range of about 500 km, but merges with the noise for larger distances. Values of average power spectral density, measured at 15 and 30 Hz on the curves for 300, 500 and 900 km on Figure 6, indicate that Q_α is about 2,000 for P_n waves propagating in the Baltic shield to distances of 900 km.

Alan S. Ryall, Jr.
Jay J. Pulli

REFERENCES

Borcherdt, R.D., J.B. Fletcher, E.G. Jensen, G.L. Maxwell, J.R. VanSchaack, R.E. Warrick, E. Cranswick, M.J.S. Johnston and R. McClearn (1985). A general earthquake-observation system (GEOS), *Bull. Seism. Soc. Am., 75*, 1783-1826.

Braile, L.W. and C.S. Chiang (1986). The continental Mohorovicic discontinuity: results from near-vertical and wide-angle seismic reflection studies, *Am. Geophys. Un., Geodynamics Series, 13*, 257-272.

Chael, E.P. (1986). Spectral scaling of earthquakes near Miramichi, New Brunswick, manuscript, 30 pp.; Earthquake source spectra to 15 Hz, *Lawrence Livermore Lab., Proceedings of the 1986 RSTN/NORESS Research Symposium*, 422-438.

Davydova, N.I. and G.C. Mikhota (1973). Study of the fine structure of the Mohorovicic boundary on dry land, *Deep Seismic Sounding, Papers Presented at the All Union Conference on the Study of the Earth's Crust and Upper Mantle by Methods of Explosion Seismology*, "Nauka", Alma-Ata, 167-181 (Transl. by Addis Translations International).

Evernden, J.F., C.B. Archambeau and E. Cranswick (1986). An evaluation of seismic decoupling and underground nuclear test monitoring using high-frequency seismic data, *Rev. Geophys., 24*, 143-215.

Fuchs, K (1968). Das Reflexions- und Transmissionsvermoegen eines geschichteten Mediums mit beliebeger Tiefen-Verteilung der elastischen Moduln und der Dichte fur schraegen Einfall ebener Wellen, *Zeitschrift f. Geophysik, 34*, 389-413.

Goncz, J.H. and W.C. Dean (1986). Excitation, propagation and detection of L_g, S_n, and P_n seismic waves from EUS earthquakes by regression analysis of RSTN data, *Lawrence Livermore Lab., Proc. RSTN/NORESS Res. Symposium*, 389-412.

Hasegawa, H.S. (1985). Attenuation of L_g waves in the Canadian shield, *Bull. Seism. Soc. Am., 75*, 1569-1582.

Mitchell, B.J. (1980). Frequency dependence of shear wave internal friction in the continental crust of eastern North America, *J. Geophys. Res., 85*, 5212-5218.

Mitchell, B.J. (1981). Regional variation and frequency dependence of Q_β in the crust of the United States, *Bull. Seism. Soc. Am., 71*, 1531-1538.

Nersesov, I.L., A. Nurmagambetov and A. Sydykov (1982). *Detailed Study of the Seismic Regime of Kazakhstan and Adjacent Territories*, "Nauka", Alma-Ata, 158 pp (in Russian).

Nurmagambetov, A. (1974). Attenuation of seismic waves and energy classification of earthquakes using observations from ChISS instruments, in *Magnitude and Energy Classification of Earthquakes*, Akad. Nauk, Moscow, 164-173 (in Russian).

Piwinski, A.J. (1979). *Deep Structure of the Earth's Crust and Upper Mantle in the USSR According to Geophysical and Seismological Data, Part 1*, Lawrence Livermore Laboratory Rept. UCID-18099, 69 pp.

Pulli, J.J. (1986). A note on the spectral interpretation of regional seismic waveforms, *Center for Seismic Studies Technical Report 86-07*, 74-81.

Ringdal, F., B.Kr. Hokland and T. Kvaerna (1986). Initial results from the NORESS High Frequency Seismic Element (HFSE), *NORSAR Semiannual Tech. Summary, Rept. 2-85/86*, 31-39.

Singh, S. and R.B. Herrmann (1983). Regionalization of crustal Q in the continental United States, *J. Geophys. Res., 88*, 527-538.

4. SUPPORT OF THE DARPA PROGRAM

4.1. COMPARISON OF THE EASTERN KAZAKH AND NEVADA TEST SITES BASED ON m_b AND NUTTLI L_g MAGNITUDES

4.1.1. Introduction

Nuttli (1986a; 1986b) has reported a comprehensive set of L_g magnitudes for underground nuclear explosions at the Nevada Test Site (NTS) and the Soviet Eastern Kazakh Test Site (STS). The methodology used to make the L_g magnitude determinations (hereafter referred to as M_{L_g} is described by Nuttli in the above references and in an earlier work (Nuttli 1973). Briefly, peak values of amplitude read from WWSSN film records in the time window corresponding to a group velocity of 3.6 to 3.2 km/sec are corrected for attenuation using a coda scattering model and for distance using a formula which accounts for geometrical spreading and dispersion assuming propagation as higher-mode surface waves. Amplitudes are read from the short-period vertical component at a nominal period of 1 second.

Since L_g waves propagate as higher-mode surface waves confined to the continental crust they are not affected by absorption within the asthenosphere as are teleseismic P-waves. Because L_g waves are a superposition of higher-mode surface waves, their generation appears to be unaffected by near-source anisotropy and tectonic energy release which can alter the M_s values determined from long period fundamental-mode Rayleigh waves. Thus in principal, L_g waves offer an independent measure of explosion yield which is unaffected by the upper-mantle absorption which produces the regional bias in m_b and by tectonic release which can degrade the utility of M_s for yield estimation. An attempt has been made to test a fundamental assumption which underlies the use of L_g for estimating yields of underground explosions; namely that L_g is generated in the same way at the Soviet Test site as it is at NTS, permitting use of an M_{L_g}-yield relationship based on NTS experience to estimate yields for Soviet tests.

4.1.2. Nevada Test Site Explosions

Table 1 lists the US tests used in the analysis. The events in Table 1 were extracted from a larger set of explosions for which Nuttli has made M_{L_g} determinations, but which includes events in unsaturated rock or alluvium. All the events in Table 1 were detonated in saturated rock or alluvium, which is presumed to couple explosion energy like the rocks in which the Soviet tests are detonated. Table 1 also shows the area of the test site in which they were detonated and the M_{L_g} reported by Nuttli. The stations which Nuttli used in making the M_{L_g} determination are also shown in Table 1.

The yield range was limited to 10-400 kt, since the intent was to use the relationship derived to evaluate the m_b bias at yields near the 150 kt threshhold treaty limit. Lower-yield Rainier Mesa events are included in the data set because although they are reported as having been detonated in tuff above the water table, the tuff layers are generally saturated, the events are well coupled, and their inclusion permits a more robust estimation of the slope of the regression curve.

4.1.3. Soviet Test Data

Table 2 and Table 3 list the dates and M_{L_g} for the Shagan River Test Site and the Degelen Test Site, respectively. Also shown are the WWSSN stations used by Nuttli (1985; 1986) to make the L_g measurements. Although not shown, the m_b values used in the analysis were provided by DARPA and were derived from combined AFTAC and Worldwide station data using the maximum likelihood process

4.1.4. Discussion

A major assumption underlying the use of M_{L_g} for estimating yields at EKZ is that there are no systematic differences in the way in which L_g waves are generated by explosions at NTS as compared with STS. Since the M_{L_g} scale was defined to be equivalent to the m_b scale (Nuttli 1973), one way to test for systematic differences is to plot M_{L_g} versus m_b for events at each test site. Differences in slope between the two test sites would be suggestive of differences in L_g generation at the two locations, but systematic differences in P-wave generation cannot be ruled out and could account for observed slope differences. Plots of M_{L_g} versus m_b for NTS and for Shagan and Degelen combined are shown in *Figures 1* and *2*. The slope for the NTS data set is 0.79 and for the combined Shagan-Degelen set, 1.08. Thus, there does appear to be a significant difference between the test sites. Although the linear fits to both data sets appear statistically consistent, it could be argued that the Rainier Mesa and Degelen events should not be included because in both cases they are concentrated in a lower yield range and were detonated in a different geological setting. Excluding the use of events in Rainier Mesa on the grounds of differing geology (from Pahute Mesa) would be tantamount to rejecting the premise of transferability of L_g methods to other test sites. Furthermore, systematic differences between test sites in their P to L_g ratio in *any part* of the range of yields appears to be most logically attributable to fundamental differences in the generation of P or L_g at these test sites, and poses a dilemma as to which method to use for computing yields. Nevertheless, if the Rainier and Degelen data are excluded, then one obtains slopes of 0.56 and 0.94, respectively for NTS and Shagan. The slope difference remains substantial.

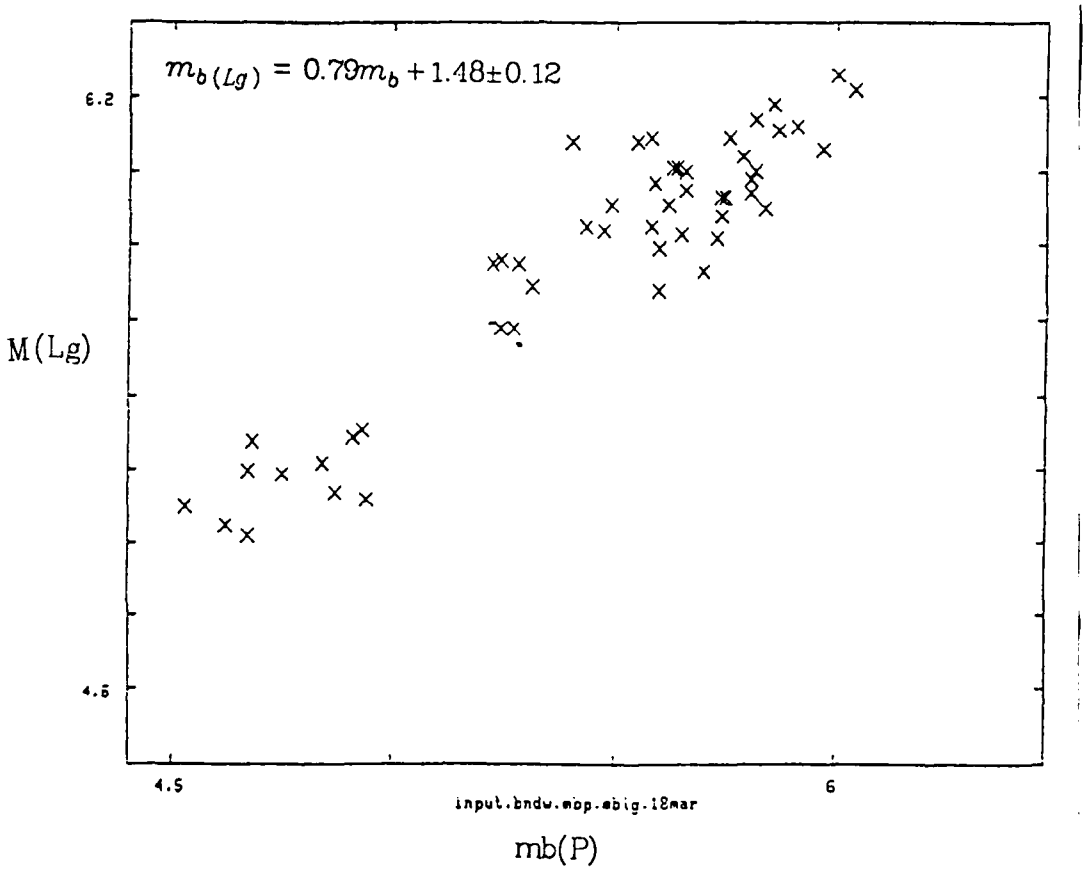

Figure 1. $M(L_g)$ *vs.* $m_b(P)$ **for NTS events below the water table.**

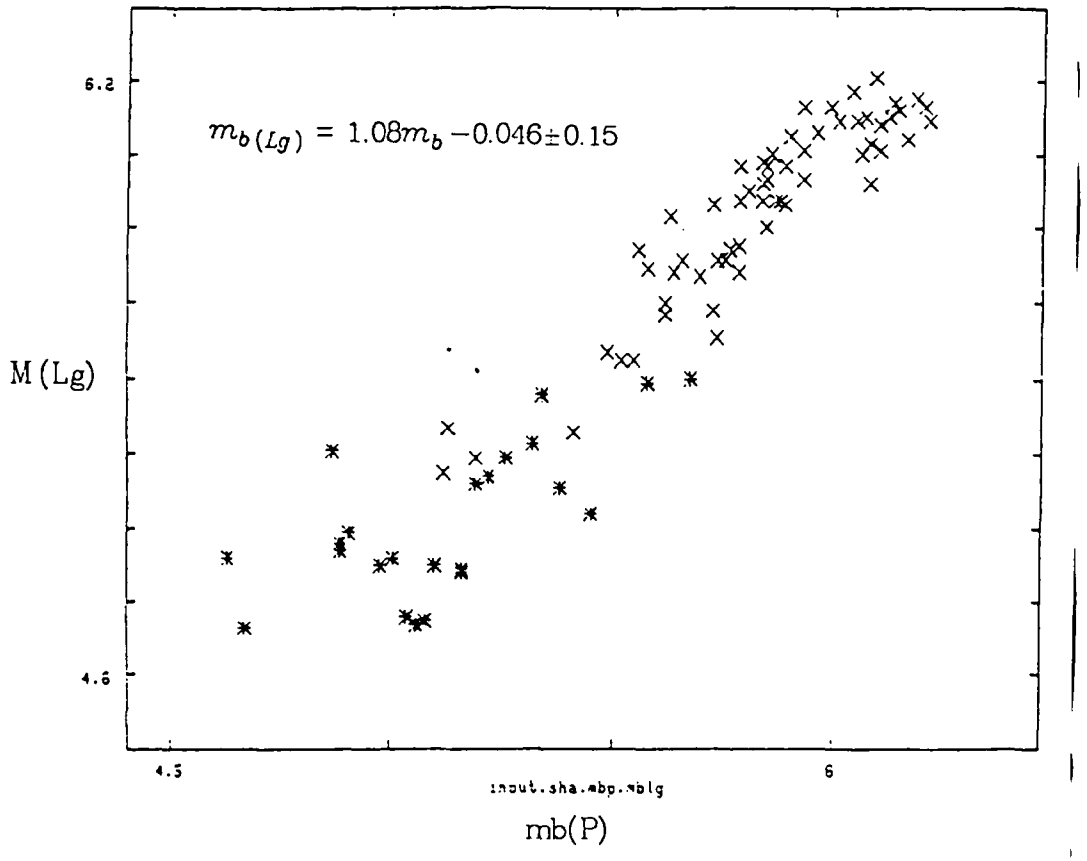

Figure 2. $M(L_g)$ *vs.* $m_b(P)$ **for combined Shagan and Degelen data set.**

The slope differences could be explained by depth of burial effects if Soviet practice differs from the US practice of increasing burial depth with yield. A review of the containment data (Howard, 1984) for the US events shows an increase in depth of burial from near 400 meters for the smallest yield to more than 1000 meters for the largest. Significantly, the containment data also predict a consistent increase in the two-way reflection time from about 0.3-0.8 second, based on seismic velocities in the rocks overlying the shot points.

George V. Bulin

REFERENCES

Alewine, R.W., G.B. Young, D.L. Springer, R.W. Klepinger (1977). Teleseismic P-wave magnitude-yield relations for well-coupled Nevada Test Site explosions, *AFTAC-TR-77-22*, 62 pp., SECRET.

Nuttli, O.W. (1973). Seismic S-wave attenuation and magnitude relations for eastern North America, *J. Geophys. Res., 78*, 876-885.

Nuttli, O.W. (1986a). Yield estimates of Nevada Test Site explosions obtained from seismic L_g waves, *J. Geophys. Res., 91*, 2137-2151.

Nuttli, O.W. (1986b). L_g magnitudes of selected East Kazakhstan underground explosions, *Bull. Seism. Soc. Am., 76*, 1241-1251.

Howard, N. and W. Richardson (1985). Selected Event Data In SI Units, *LLNL Rept. UCID-18532-85.*

Table 1. U.S. Tests Used in the Analysis

DATE	EVENT	$M(L_g)$	LOCATION
09/13/63	BILBY	6.09	Yucca
10/26/63	SHOAL	5.19	Granite
02/24/66	REX	5.28	Pahute
05/06/66	CHARTREUSE	5.76	Pahute
06/02/66	PILE DRIVER	5.84	Granite
06/30/66	HALFBEAK	6.26	Pahute
05/20/67	COMMODORE	6.04	Yucca
05/23/67	SCOTCH	6.08	Pahute
10/29/69	CALABASH	5.88	Yucca
12/17/70	CARPETBAG	6.14	Yucca
07/08/71	MINIATA	5.93	Yucca
04/26/73	STARWORT	5.85	Yucca
12/03/65	CORDUROY	5.91	Yucca
02/23/67	AGILE	5.91	Yucca
06/26/67	MIDI MIST	5.20	Rainier
08/31/67	DOOR MIST	5.05	Rainier
09/27/67	ZAZA	6.00	Yucca
10/18/67	LANPHER	6.09	Yucca
02/21/68	KNOX	6.01	Yucca
02/29/68	DORSAL FIN	5.14	Rainier
03/22/68	STINGER	6.00	Pahute
08/29/68	SLED	6.12	Pahute
09/06/68	NOGGIN	6.08	Yucca
09/24/68	HUDSON SEAL	5.22	Rainier
01/15/69	WINESKIN	5.58	Rainier
04/30/69	BLENTON THISTLE	5.84	Yucca
05/07/69	PURSE	5.98	Pahute
10/08/69	PIPKIN	6.06	Pahute
12/05/69	DIESEL TRAIN	5.23	Rainier
12/17/69	GRAPE A	5.79	Yucca
02/04/70	GRAPE B	6.00	Yucca
02/11/70	DIANA MIST	5.02	Rainier
03/23/70	SHAPER	5.69	Yucca
05/05/70	MINT LEAF	5.29	Rainier
12/18/70	BANEBERRY	5.21	Yucca
08/18/71	ALGODONES	5.58	Yucca

09/12/72	OSCURO	5.97	Yucca
03/08/73	MIERA	5.75	Yucca
06/05/73	DIDO QUEEN	5.12	Rainier
02/28/75	TOPGALLANT	5.93	Yucca
06/03/75	MIZZEN	5.83	Yucca
06/19/75	MAST	6.22	Pahute
12/20/75	CHIBERTA	5.93	Yucca
02/04/76	KEELSON	5.73	Yucca
02/04/76	ESROM	5.95	Yucca
02/14/76	CHESHIRE	6.18	Pahute
03/09/76	ESTUARY	6.06	Pahute
04/05/77	MARSILLY	6.01	Yucca
08/19/77	SCANTLING	5.68	Yucca
11/09/77	SANDREEF	5.94	Yucca
12/14/77	FARALLONES	5.82	Yucca
03/23/78	ICEBERG	5.79	Yucca
09/27/78	RUMMY	6.11	Yucca
06/11/79	PEPATO	5.95	Yucca
09/06/79	HEARTS	5.90	Yucca

Table 2. Shagan River Tests

DATE	$M(L_g)$	STATIONS
01/15/65	5.87	NDI,SHL
11/02/72	6.04	NUR
12/10/72	6.09	NDI,NUR
07/23/73	6.13	KBL,KEV,NIL,NUR,QUE,UME
12/14/73	5.87	NUR,SHL,UME
05/31/74	5.68	KEV,NUR,QUE,UME
10/16/74	5.26	KEV,NIL,NUR
12/27/74	5.69	KBL,MSH,NIL,NUR,QUE,SHL
04/27/75	5.47	KON,NDI,NIL,NUR
10/29/75	5.45	MHI,NDI
12/25/75	5.83	NDI,NIL,SHL
04/21/76	5.19	MHI
06/09/76	5.27	MHI,NDI,UME
07/04/76	5.90	MHI,NDI
08/28/76	5.60	KON,MHI,NDI,NUR,SHL
11/23/76	5.86	KBL,NDI,SHL
12/07/76	5.71	NDI,SHL
05/29/77	5.58	KEV,NDI,NUR,SHL,UME
06/29/77	5.15	MHI,NDI,NIL
09/05/77	5.51	KEV,MHI
11/30/77	5.71	KON,MHI,NDI,NUR,SHL
06/11/78	5.75	KBL,KEV,MHI,NUR
07/05/78	5.67	NDI
08/29/78	5.80	KEV,NDI,UME
09/15/78	5.87	KEV,NUR,UME
11/04/78	5.57	KBL,NUR
11/29/78	6.01	NIL,NDI,QUE,SHL
06/23/79	5.92	KEV,UME
07/07/79	5.87	KEV,NUR,UME
08/04/79	6.01	KEV,NDI,NUR,SHL
08/18/79	6.03	KEV,KON,NDI,NUR,SHL
10/28/79	6.06	KON,NDI,NUR,SHL,UME
12/02/79	6.05	KON,NUR
12/23/79	6.12	KON,NDI,NUR,QUE,SHL,UME
06/12/80	5.74	KBL,NDI,NIL,NUR,QUE
06/29/80	5.71	KBL,NIL,NUR,QUE,UME

09/14/80	6.09	KON,NDI,NIL,NUR,SHL
10/12/80	5.92	KEV,KON,NDI,NUR,QUE
12/14/80	5.93	KEV,NUR,SHL,UME
12/27/80	6.00	COP,KEV,NDI,NUR,QUE,SHL,UME
03/29/81	5.45	KBL,NIL
04/22/81	5.97	NIL,NUR,QUE,UME
09/13/81	6.10	KEV,KON,NDI,NUR,SHL,UME
10/18/81	6.09	KEV,KON,NDI,NUR,SHL
12/27/81	6.15	KEV,KON,NDI,NUR,SHL
04/25/82	6.13	COP,KEV,KON,NDI,NUR,SHL,UME
07/04/82	6.14	COP,KON
12/05/82	6.21	NUR,SHL
10/06/83	5.93	KEV,NUR
10/26/83	6.10	NUR
02/19/84	5.74	NUR
03/07/84	5.68	NUR
03/29/84	5.97	NUR
04/25/84	5.86	COP,NUR
05/26/84	6.00	KEV,NUR
07/14/84	6.17	COP,KEV,NUR
10/27/84	6.10	KEV,NUR
12/02/84	5.97	NUR
12/16/84	6.08	NUR
12/28/84	6.13	COP,NUR
02/10/85	5.98	COP

Table 3. Degelen Tests

DATE	$M(L_g)$	STATIONS
04/19/73	5.12	NIL,NUR
07/10/73	5.14	KBL,NIL
10/26/73	4.88	NIL
01/30/74	5.11	KBL,NIL
05/16/74	4.89	KBL,NIL
07/10/74	4.75	KBL,NIL
09/13/74	4.74	NIL
12/16/74	4.15	KBL,NIL
02/20/75	5.40	KBL,NDI,NIL
03/11/75	5.23	MSH,NIL
06/06/75	5.04	KBL,NIL
08/07/75	4.90	KBL,NIL
01/15/76	4.92	MHI,NIL
04/21/76	5.21	MHI
05/19/76	4.92	MHI,NIL
07/23/76	4.96	KBL,SHL
12/30/76	4.99	MHI
03/29/77	5.36	MHI,NDI,NIL,SHL
04/25/77	4.94	MHI,NDI
07/30/77	4.76	KBL,MSH,NIL
12/26/77	4.73	MHI,SHL
03/19/78	4.90	MHI,NIL
05/26/78	5.39	MHI,NDI,NIL,NUR,SHL
04/22/78	5.19	MHI,NDI,NUR,SHL

4.2. NOTE ON SEISMIC DISCRIMINATION AND THE 1 AUGUST 1986 NOVAYA ZEMLYA EVENT

4.2.1. Introduction

Some recent studies (*e.g.*, Evernden *et al.*, 1986) have concluded, primarily on the basis of theoretical calculations, that a network of about 25 stations inside and 15 stations outside the USSR will be capable of detecting, locating and identifying decoupled explosions of 1 kt, *i.e.*, down to about m_b 2.5. These studies assume that detection by a few stations equipped with high-frequency instruments will be sufficient to locate and discriminate decoupled nuclear explosions, mine blasts and small earthquakes, in all parts of the Soviet Union. For such events, the recording stations would be at regional distance ranges, *i.e.*, at least 500 km assuming an evader would not test in the immediate vicinity of a monitoring station, and not more than about 2,000 km along very favorable propagation paths. Discrimination in these studies is assumed to be based on differences in high-frequency energy radiated by earthquakes and explosions.

A less optimistic view of the monitoring problem was presented by Pomeroy *et al.* (1982), who reviewed the use of regional seismic data in test ban treaty verification, and concluded that the problem of identifying small earthquakes and explosions at regional distance ranges has been remarkably difficult to solve. Although a large number of empirical discriminants have been tested, most of them suffer from one or more problems, including azimuth and distance effects, regional variations in propagation, insufficient size of the populations analyzed, and lack of comparable earthquakes and explosions in the same areas for testing. Some discriminants that have proven useful for large events recorded at teleseismic distances (M_s:m_b ratio, first motion in P) cannot be used for small events at regional distances because the diagnostic phases are recorded poorly or not at all. Others, such as P/L_g amplitude ratio, excitation of S_n or high-frequency spectral content, may fluctuate depending on factors such as the character of attenuation along the path, source coupling, source radiation patterns, etc. In a more recent study by Henson and Bache (1986), spectral characteristics of Soviet mine blasts recorded at NORESS were found to be strongly dependent on differences in attenuation along the path, and spectral features of a nuclear explosion on the Kola Peninsula, filtered to simulate a decoupled shot, were indistinguishable from mine blasts along the same azimuth from NORESS, or from the spectra of earthquakes in other azimuths.

A current approach to the monitoring problem involves the use of *case-based reasoning* to identify the *signature* of events that occur frequently at the same location. Examples being studied at the Center for Seismic studies include repeated explosions at mines in the western USSR, underwater detonations presumably connected with naval exercises off the coast of Norway, and northern European earthquake sequences, all recorded at NORESS. In this investigation, a number of discrimination techniques (polarization, vespagram, spectral, cepstral and autoregressive analyses) are applied to regional seismic

LAT	LON	DATE	TIME	DEPTH	m_b	NDEF	SOURCE
73.40	54.90	Oct 27, 1966	05:57:57.7	0	6.3	217	CGS/NOAA
73.40	54.80	Oct 21, 1967	04:59:58.1	0	5.9	60	CGS/NOAA
73.40	54.86	Nov 7, 1968	10:02:05.3	0	6.0	134	CGS/NOAA
73.40	54.81	Oct 14, 1969	07:00:06.2	0	6.1	127	CGS/NOAA
73.31	55.15	Oct 14, 1970	05:59:57.1	0	6.7	157	CGS/NOAA
73.39	55.10	Sep 27, 1971	05:59:55.2	0	6.4	176	ERL/NOAA
73.34	55.08	Aug 28, 1972	05:59:56.5	0	6.3	70	ERL/NOAA
73.30	55.16	Sep 12, 1973	06:59:54.3	0	6.8	226	USGS/NOAA
70.76	53.87	Sep 27, 1973	06:59:58.0	0	6.0	106	USGS/NOAA
70.78	54.18	Oct 27, 1973	06:59:57.4	0	6.9	221	USGS/NOAA
70.81	53.23	Oct 27, 1973	08:03:56.3	0	4.2	9	USGS/NOAA
70.89	52.87	Oct 27, 1973	08:21:20.7	0	4.4	15	USGS/NOAA
71.30	51.88	Oct 27, 1973	09:13:51.3	0	4.8	18	USGS/NOAA
70.68	53.54	Jul 22, 1974	01:32:21.5	0	4.4	14	USGS/NOAA
73.37	55.09	Aug 29, 1974	09:59:55.5	0	6.4	110	USGS/NOAA
70.82	54.06	Nov 2, 1974	04:59:56.7	0	6.7	205	USGS/NOAA
73.37	54.64	Aug 23, 1975	08:59:57.9	0	6.4	210	USGS/NOAA
70.84	53.69	Oct 18, 1975	08:59:56.3	0	6.7	254	USGS/NOAA
73.35	55.08	Oct 21, 1975	11:59:57.3	0	6.5	102	USGS/NOAA
73.41	54.50	Sep 29, 1976	02:59:57.6	33	5.8	298	USGS/T/ISC
73.40	54.47	Oct 20, 1976	07:59:57.8	0	5.1	115	USGS/T/ISC
73.37	54.41	Sep 1, 1977	02:59:57.7	0	5.7	313	USGS/T/ISC
73.47	53.98	Oct 9, 1977	10:59:58.8	0	4.6	69	USGS/T/ISC
73.31	54.70	Aug 10, 1978	07:59:57.7	0	5.9	328	USGS/T/ISC
73.38	54.44	Sep 27, 1978	02:04:58.4	0	5.6	273	USGS/T/ISC
72.57	52.84	Nov 15, 1978	08:30:04.8	0		6	USGS/T/ISC
73.37	54.58	Sep 24, 1979	03:29:58.3	0	5.7	322	USGS/T/ISC
73.34	54.73	Oct 18, 1979	07:09:58.5	33	5.8	303	USGS/T/ISC
73.35	55.00	Oct 11, 1980	07:09:57.0	0	5.8	190	USGS/T
73.32	54.81	Oct 1, 1981	12:14:56.7	0	5.9	236	USGS/T
73.39	54.56	Oct 11, 1982	07:14:58.2	0	5.6	216	USGS/MON
73.38	54.91	Aug 18, 1983	16:09:58.6	0	5.9	263	USGS/MON
73.35	54.50	Sep 25, 1983	13:09:57.7	0	5.8	261	USGS/MON
73.37	54.96	Oct 25, 1984	06:29:57.7	0	5.9	269	USGS/MON
73.04	55.57	Aug 1, 1986	13:56:40.6	33	4.6	21	USGS/PDE

Table 1. Events listed in **events** database for 1965-1986

waves (P_n, P_g, S_n, L_g), and the results are parameterized to produce a "fingerprint" of events of a specific type from a specific location. Thus, while no single rule or set of rules can be universally applied at NORESS to identify source types, it appears feasible to construct an expert system that will automatically detect, locate and identify many events at regional distance ranges, *provided* that the events are sufficiently repeatable.

If the expert system approach succeeds in eliminating many, or even most, of the small events detected by regional monitoring networks, we will still be faced with the problem of identifying those events that are isolated in space and time and not part of a repeated series. For example, we will have to be able to conclude from analysis of seismic data that a particular isolated event was a chemical explosion or a small earthquake, rather than a clandestine nuclear weapons test. From experience to date it is not clear that this problem is tractable with current technology.

As an illustration of the difficulty of the discrimination problem, this note describes an attempt to identify an event of magnitude (m_b) 4.6, equivalent to that of a tamped underground nuclear test of a few kilotons, that occurred on Novaya Zemlya, not far from a well-studied Soviet weapons test site, during the recent Soviet nuclear testing moratorium.

4.2.3. Location and Previous History

At 13h 56m GMT on 1 August 1986 an m_b 4.6 event (hereafter "NZ86213") occurred at a location given by the US National Earthquake Information Service (NEIS) as 73.04° N and 55.57° E, near the east coast of Novaya Zemlya and south of Matochkin Shar strait, in the northern USSR. A search of the Center for Seismic Studies' **sov** database, containing Soviet earthquake catalogs for 1974-1979, produced no listed events for the region 70-76° N and 50-60° E. However, the Center's **events** database, containing NOAA, NEIS and ISC locations, had 34 events in this area for the period 1965-1984 (Table 1). With four exceptions, origin times of all the events were within a few seconds of 5-minute multiples after the hour (*i.e.*, 08:00, 07:10, 12:15, *etc.*), and are presumed to be explosions. Only one of the presumed explosions -- on 9 October 1977 -- had m_b comparable to NZ86213. Of the four events not presumed to be explosions, three occurred in 1973 near to, and within 135 minutes of, a large (m_b 6.9) underground explosion, and were most likely afterevents of that explosion. The fourth occurred in the same area nine months later, and could have been another afterevent of the same explosion. Thus, neither the **sov** nor **events** database appears to contain any natural earthquake activity within a radius of 150 km of NZ86213 and a period of 20 years prior to August 1986.

4.2.3.1. Relocation

P-wave arrival times for NZ86213 were available for fourteen seismic stations of the GDSN, and times were added for recordings obtained from the NORESS and GRF arrays

(Table 2). To relocate this event we used time corrections determined for a reference event. Arrival-time residuals were determined for nine of the stations that recorded a large, well-located Novaya Zemlya explosion on 25 October 1984, and these residuals were used to correct arrival times of NZ86213 at the same nine stations. Relocation of the event using the corrected times gave latitude and longitude of 73.02 ° N, 56.50 ° E, with standard errors of ±14.8 and ±19.7 km, respectively. Depth was fixed at the surface. The origin time was 13h 56m 36.0s GMT, with standard error ±0.6 second. *Figure 1* shows the original NEIS location and our relocation of NZ86213. The latter is near the eastern coast of Novaya Zemlya, with an error ellipse that would allow the epicenter to be either on- or off-shore.

Table 2. Data available for NZ86213.

Sta	Phase	Time: 14h+	Resid* sec	Delta deg	Az deg	A nm	T sec	m_b	M_s
NUR	iP	00:36.0		17.4	241	9.8	0.5		
DAG	eP	00:58.0		18.7	316				
HFS	iP	01:17.4		20.6	254	33	0.4	5.0	
	_LR	09:24				150	10		3.4
NRA1	iP	01:18.9		20.7	258				
PRU	eP	02:41.5	0.5	29.3	241				
EKA	_P	02:43.0	0.2	29.5	266	10	1.0	4.6	
KHC	_P	02:50.6	-0.1	30.3	242				
	ePP	03:30.2							
GRA1	eP	02:51.6	0.0	30.6	245				
MLR	eP	02:55.0	-0.4	30.8	224				
KBA	wP	03:09.2	0.6	32.2	241				
LOR	iP	03:26.9	0.1	34.6	252	7.7	0.7	4.7	
INK	eP	04:05.0		39.0	6				
COL	iP	04:25.0	0.6	41.6	15				
YKA	_P	04:48.3	-0.8	44.6	354	3.7	1.0		
GBA	_P	06:50.0		60.5	156	2.1	0.5	4.5	
LIC	eP	08:23.5		75.8	244				

* -- Residuals are given only for those stations used in the relocation, and are relative to the arrival time in the table plus a correction based on P-wave residuals for a reference event.

4.2.4. Character of the Data

Short-period digital recordings of NZ86213, at GDSN and RSTN stations, as well as the NORESS and GRF arrays, have been analyzed in an attempt to determine the nature

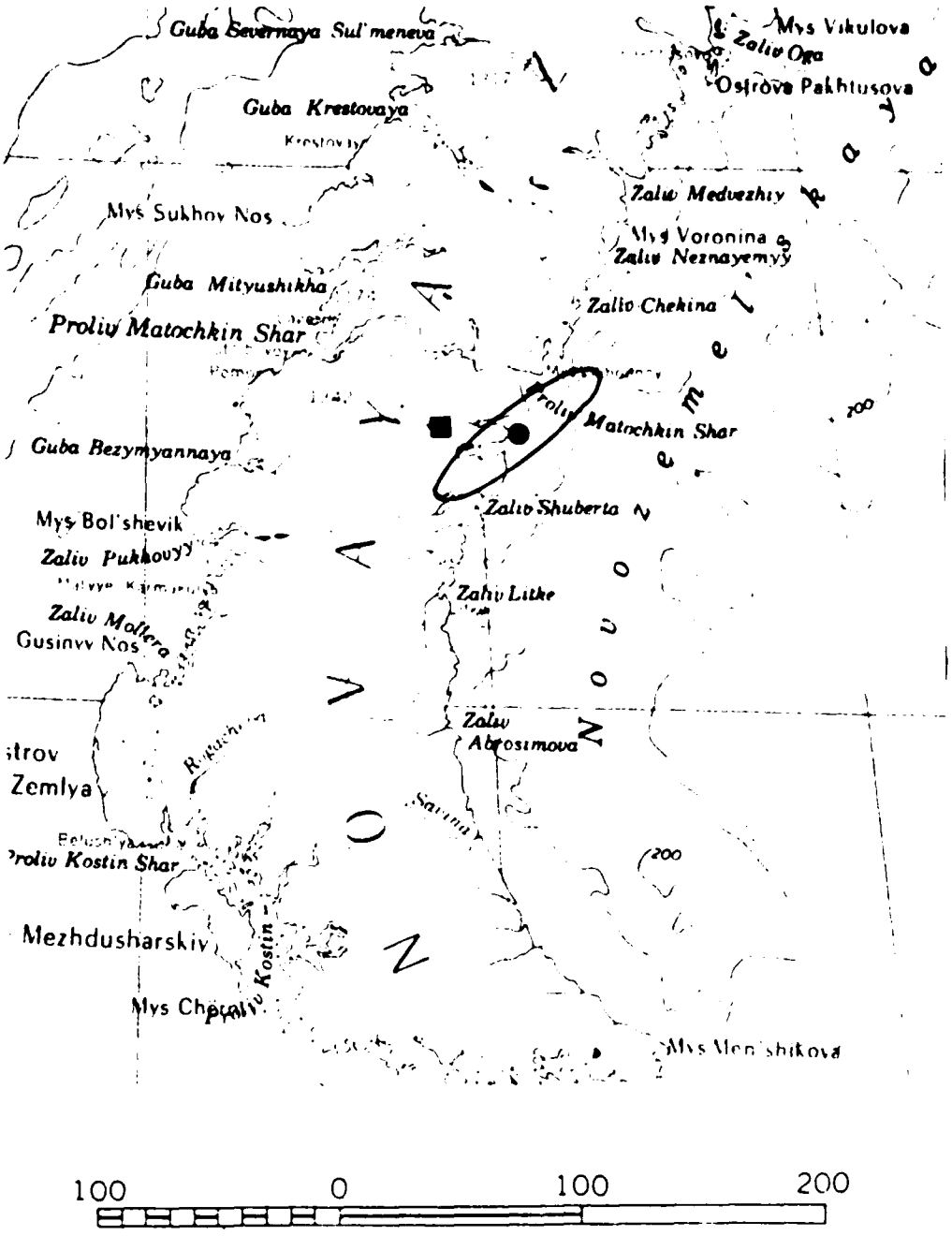

Figure 1. Map of Novaya Zemlya, showing NEIS location (square and our relocation (dot) of NZ86213. Error ellipse is shown for the relocation.

of the source. Inspection of the data bandpassed over several frequency intervals has shown that for most of the GDSN and RSTN recordings the signals are either not observed or were barely above the noise in a narrow band. On the other hand, the NORESS recordings show very strong short-period signals.

The only useful GDSN short-period records were obtained at COL in Alaska and BCAO in the Central African Republic. Signals were not observed above the noise for any other stations examined. *Figure 2* shows the short-period vertical-component seismograms for COL and BCAO bandpassed in several frequency passbands. The predicted P-wave arrival times are indicated at 20 seconds. The P-wave arrivals are clearly visible around 2 Hz. COL shows a build-up and decay in amplitude over 15 seconds with some later arrivals in the following P coda. BCAO has most of the energy arriving impulsively at the predicted P time.

The only RSTN stations to show any short-period signal at the predicted time were RSSD and RSON. *Figure 3* shows the sz channels for these stations in several frequency passbands. The predicted P-wave arrival time is at 20 seconds on the figure. RSSD contains a strong pulse in the 1-2 Hz band about 15 seconds after the predicted time. This signal is dominant on the vertical component. RSON contains some energy in the 4-8 Hz band which may be associated with this event or may not. Little signal is seen at RSON at the predicted time at lower frequencies. These four GDSN and RSTN recordings contain no information about the polarity of the P onset, and the character of the P wavetrain is different on the different recordings. Thus, any conclusions about the source are difficult to make.

Good short-period recordings of this event were obtained at NORESS, ($\Delta = 20.7^\circ$), and the event was also detected by arrays at Grafenberg (GRF, $\Delta = 30.6^\circ$) and Eskdalmuir (EKA, $\Delta = 29.6^\circ$). *Figure 4* shows the vertical channel at NRC2 bandpassed at several frequency intervals. The signals in this figure show a very impulsive first arrival at 1 Hz. The P onset polarity at low frequencies indicates the initial pulse is probably a compression. The higher frequencies show a more gradual build-up of energy over the first 4 seconds. This is likely due to scattering of the high-frequency energy, delaying it in time relative to the low frequency. The P coda is relatively complex, with several bursts of energy arriving within 60 seconds. Plots of seismograms from the entire 25 elements of the array indicate that this coda energy is quite planar and coherent across the array. This implies that local scattering effects are not dominating the coda. It is not unexpected to see coherent phases in the short-period P-coda at these distances, which are likely associated with secondary crustal reflected phases and "near-source scattering".

Figures 5 and *6* compare the character of P-waves recorded by NORESS/NORSAR and GRF for NZ86213 and the presumed nuclear test on 9 October 1977 which also had m_b 4.6 (Table 1). On *Figure 5*, a NORSAR recording of the 1977 explosion had less energy in the P-coda and a smaller onset than a nearby NORESS recording of NZ86213. Spectral characteristics of the two events are similar in the range 1-5 Hz. For lower

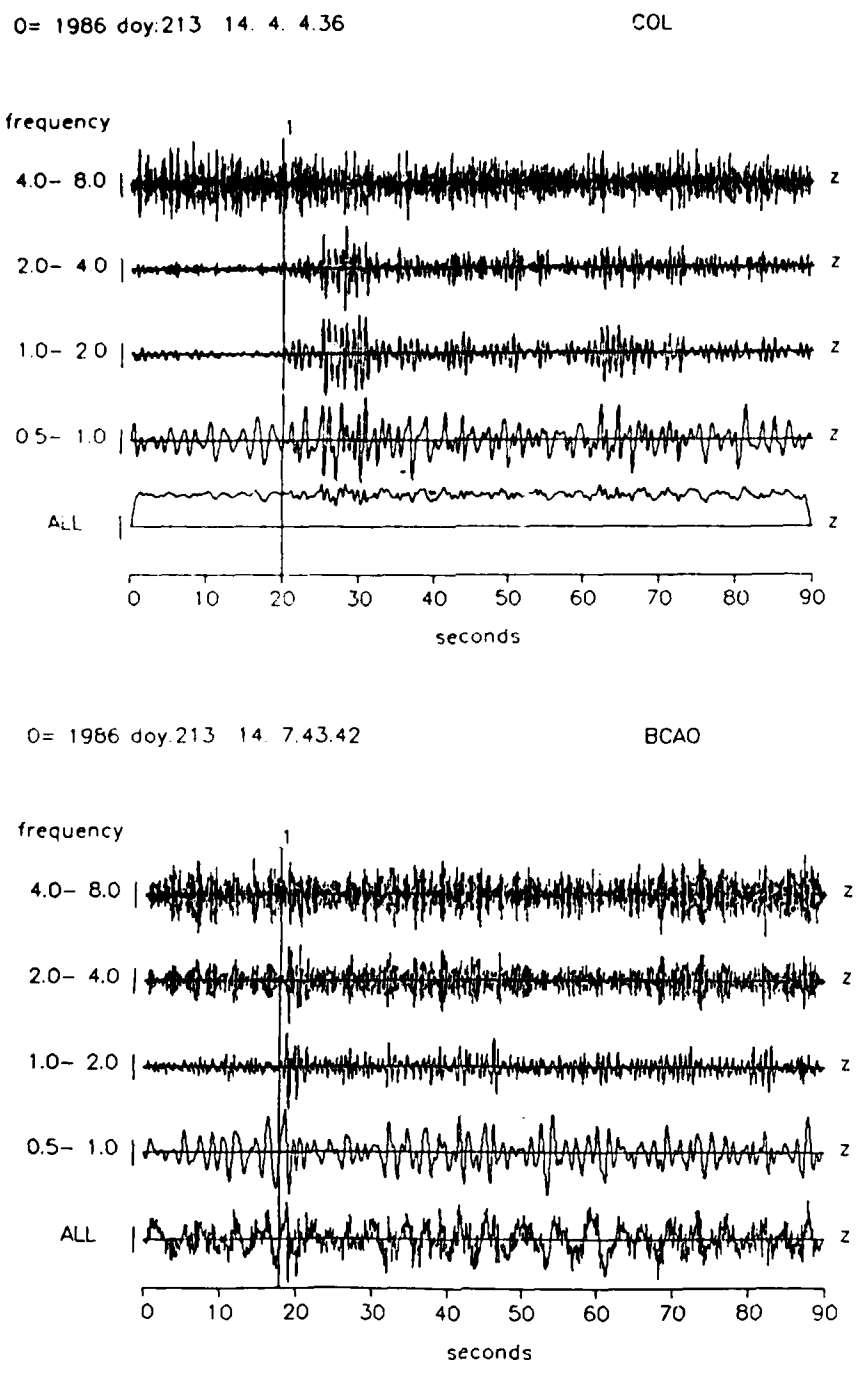

Figure 2. SPZ recordings at GDSN stations COL and BCAO, in several frequency passbands. Not corrected for instrument response.

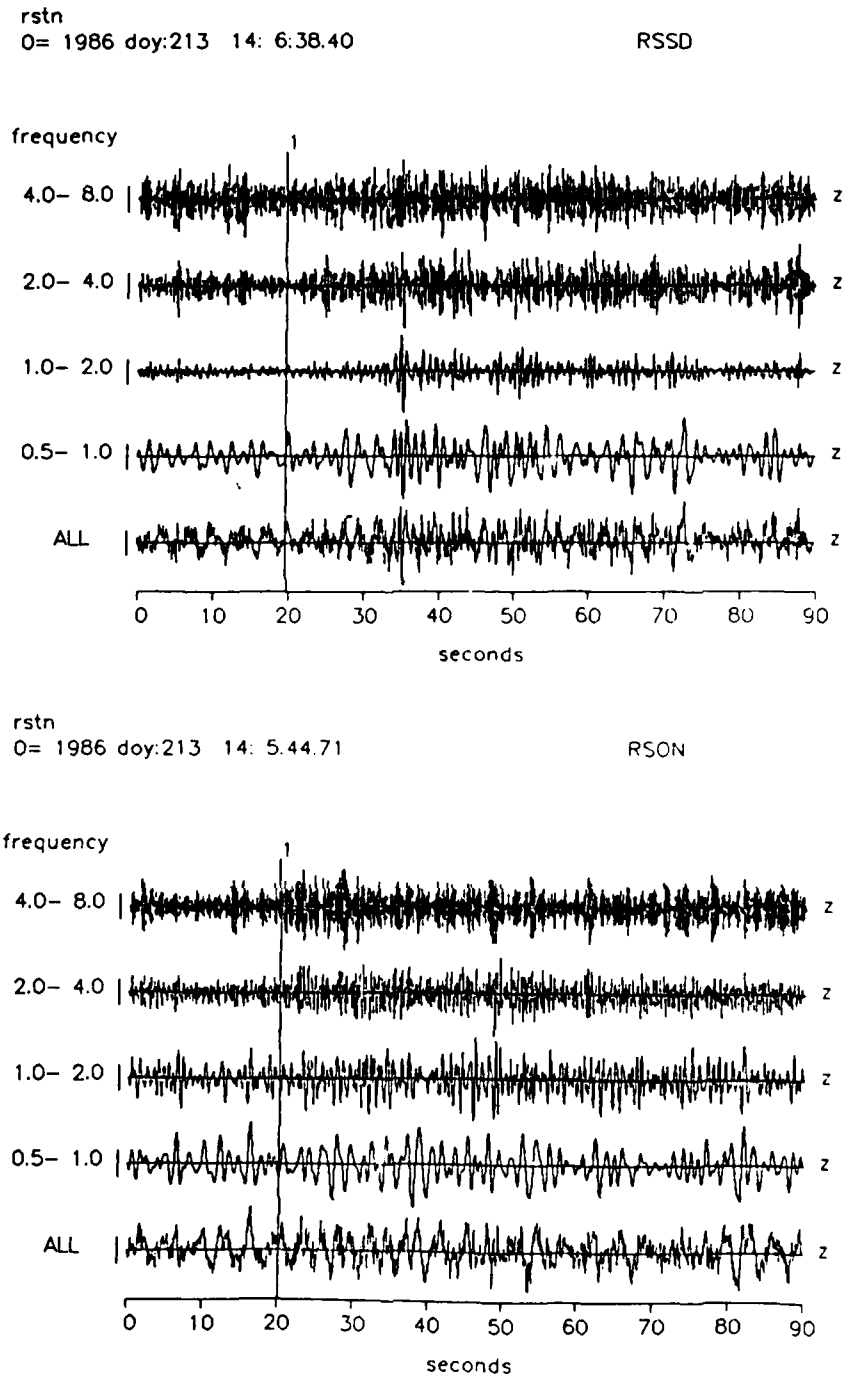

Figure 9. SPZ recordings at RSTN stations RSSD and RSON, in several frequency passbands. Not corrected for instrument response.

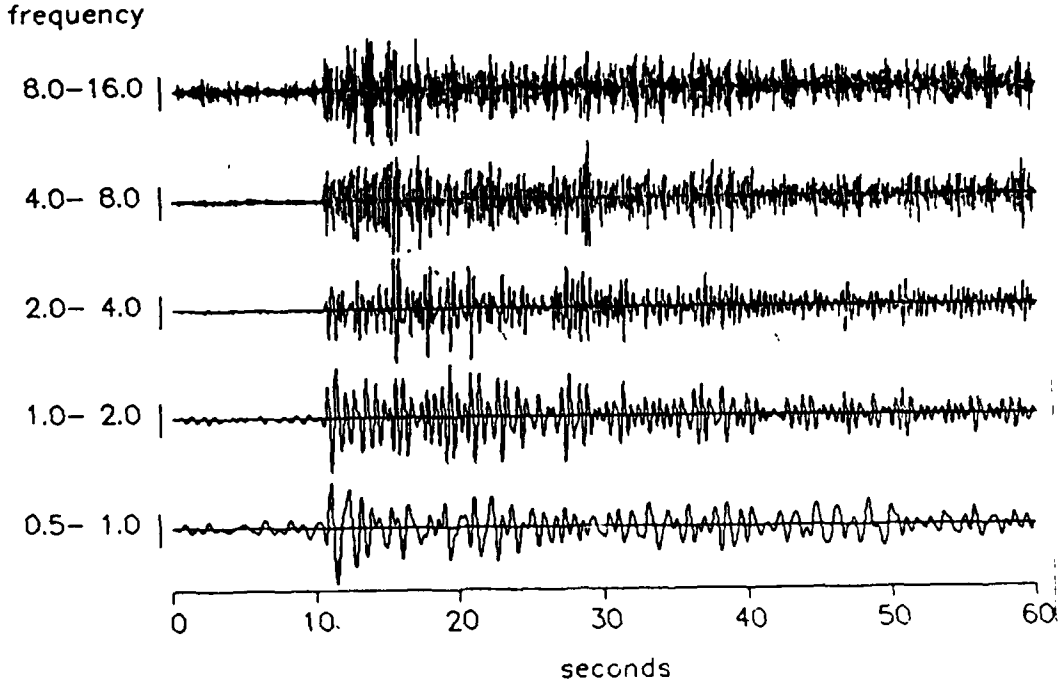

Figure 4. SPZ recording at NORESS element NRC2 in several frequency passbands. Not corrected for instrument response.

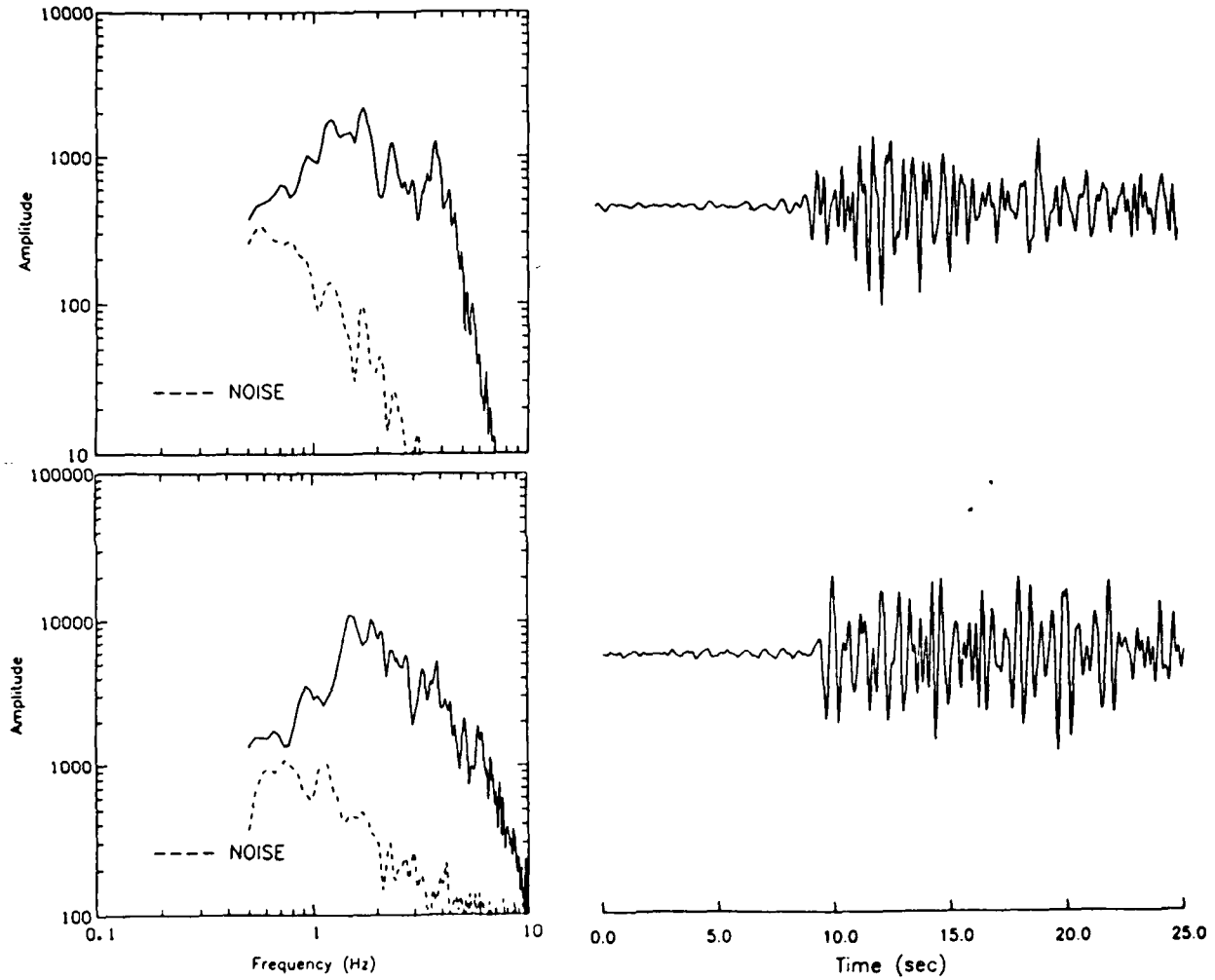

Figure 5. Top -- Spectrum and bandpass-filtered (0.8-5 Hz) NORSAR (N06C2) recording of 9 October 1977 Novaya Zemlya presumed underground nuclear test; bottom -- same for NORESS (NRA1) recording of NZ86213.

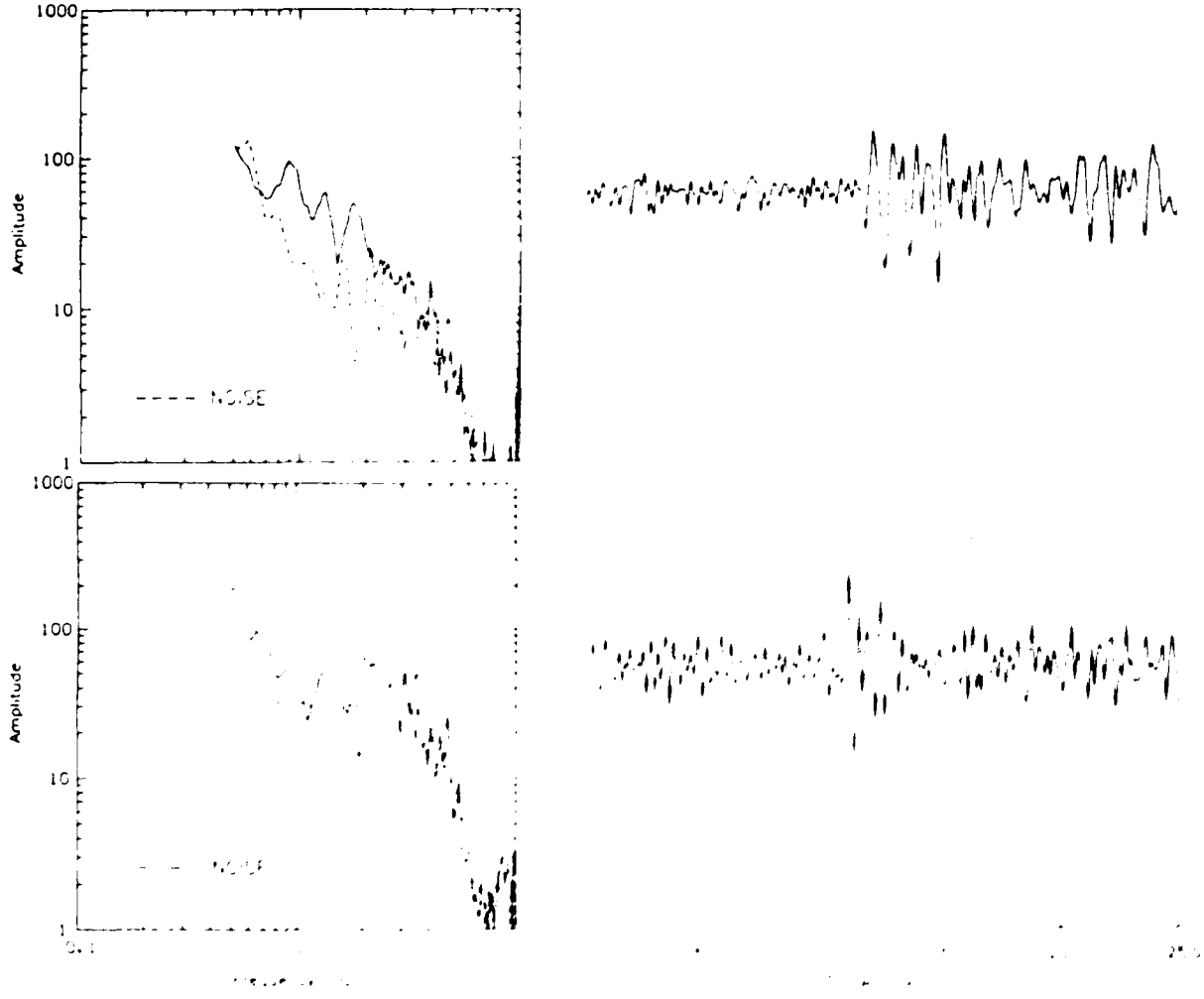

Figure 6. Top -- Spectrum and bandpass filtered (0.8-5 Hz) GREAT recording of 3 October 1977 Novaya Zemlya presumed underground nuclear test. Bottom -- same for N780213

frequencies the signal-to-noise ratio (SNR) is poor, and the NORSAR recording lacks high-frequency response due to an anti-aliasing filter at 5 Hz.

Figure 6 compares GRF recordings and spectra for the two events. The waveforms are somewhat different, with the 1977 event having more energy in the 0.7-2 Hz band than NZ86213. This might have been due to a 1978 change in instrumentation from a Sprengnether to a Wielandt system, although response for the two systems was supposed to have been identical. Above 3 Hz, both signals are in the noise. The 1977 event appears to have somewhat more energy in the P-coda than NZ86213.

4.2.5. Discriminants

None of the features discussed above identify NZ86213 as an earthquake. The event location is near the coast, with standard error such that it could be either on- or off-shore. The P-wave signature at NORESS has a complex coda, which could be a result of structure in the source region or in the upper mantle. The signature of NZ86213 at GRF is less complex than that of a presumed underground explosion of the same size in 1977, and the 1986 event appears to have relatively more high-frequency energy than the 1977 explosion, a feature that would not generally be expected for an earthquake.

We have applied several additional analysis techniques to the NORESS short-period signals in an attempt to identify possible depth phases, source complexity or source type. Our exprience with NORESS data so far has been limited to small events within a range of 10°. Analysis results for events with $m_b > 4.0$ around 20° are not available for comparison.

A velocity analysis was carried out using all 25 array elements to determine the coherency and plane-wave phase velocity as a function of time in several passbands. Results are shown in *Figure 7*. The coherency of plane-wave energy as a function of time is plotted in three passbands (amplitude has been scaled out). At frequencies of 2.5 and 5 Hz more than 10 wave groups within the first 40 seconds of P coda exhibit a coherency and horizontal phase velocity comparable to the initial P wave. The horizontal phase velocities of all these groups are between 10 and 14 km/sec. At 10 Hz, the coherency of the coda waves has dropped considerably below that of the initial P wave. A delayed second event or strong pP depth phase would be expected to generate a strongly coherent arrival within the P coda, and would be visible on this plot if the time lag were between, say, 3 and 40 seconds. The possibility remains, however, that a depth phase may have lost high-frequency energy along its up-down crustal path and so may appear as coherent energy at 2.5 and 5 Hz but not at 10 Hz.

Three-component analysis of the short-period signals was also carried out in several passbands. Results are shown in *Figure 8*. *Figure 8a* shows several particle-motion attributes plotted as a function of time in 3 passbands. The three-component analysis results were consistent with the velocity analysis. The 2.5 and 5 Hz signals had quite rectilinear

AD-A179 377 TECHNICAL REPORT FOR THE PERIOD 1 OCTOBER-31 DECEMBER 1986(U) SCIENCE APPLICATIONS INTERNATIONAL CORP ARLINGTON VA CENTER FOR SEISMIC STUDIES FEB 87

2/2

UNCLASSIFIED SAIC-87/1504 MDA903-84-C-0028 F/G 8/11 NL

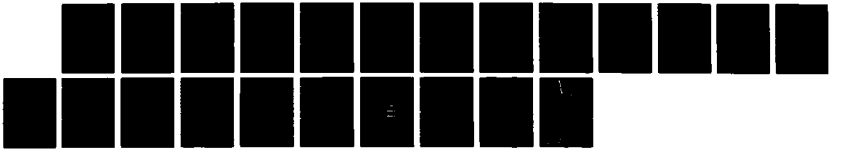


1.0
1.1
1.25
1.4
1.6
1.8
2.0
2.2
2.8
3.2
3.6
4.0

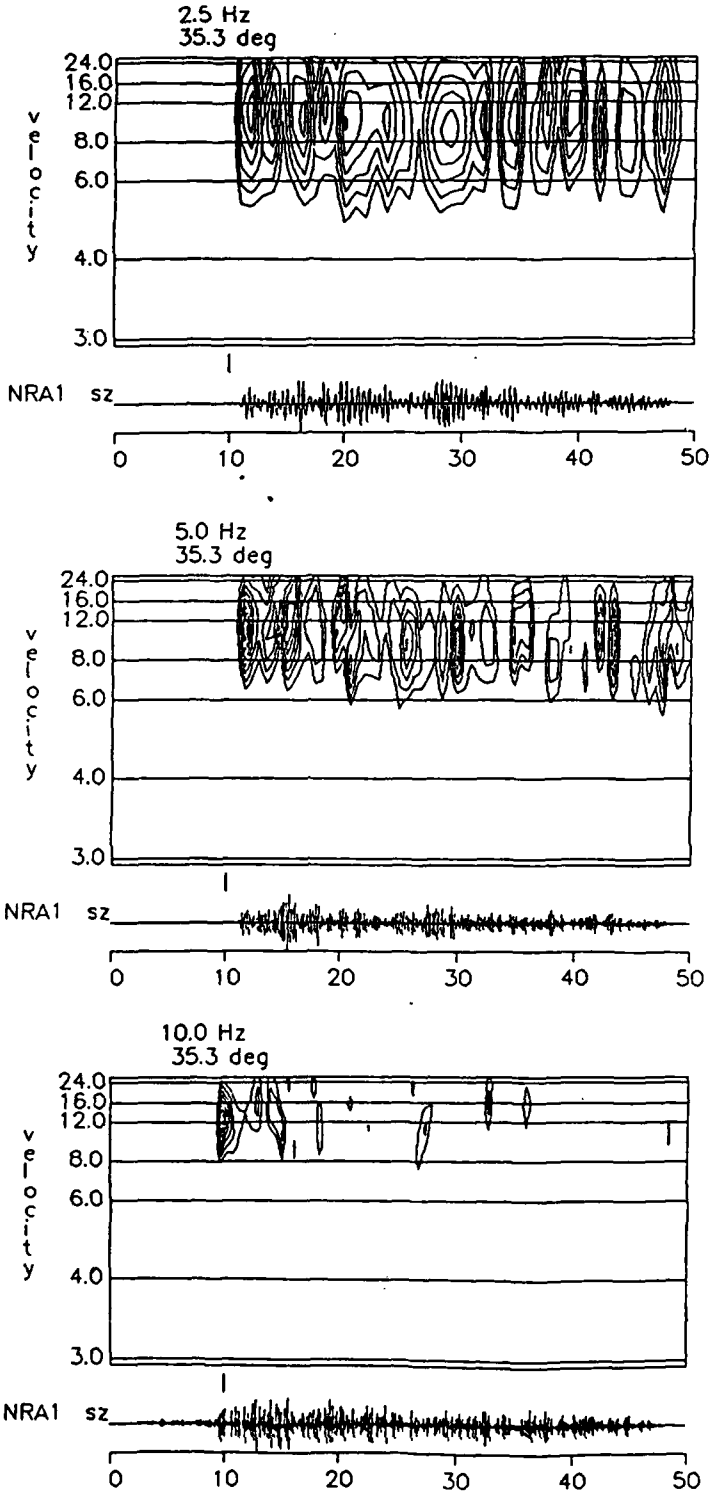

Figure 7. Vespagram analysis using 25 elements of the NORESS array to determine wave coherency as a function of velocity and time. Top -- bandpass centered on 2.5 Hz; middle -- 5 Hz; bottom -- 10 Hz.

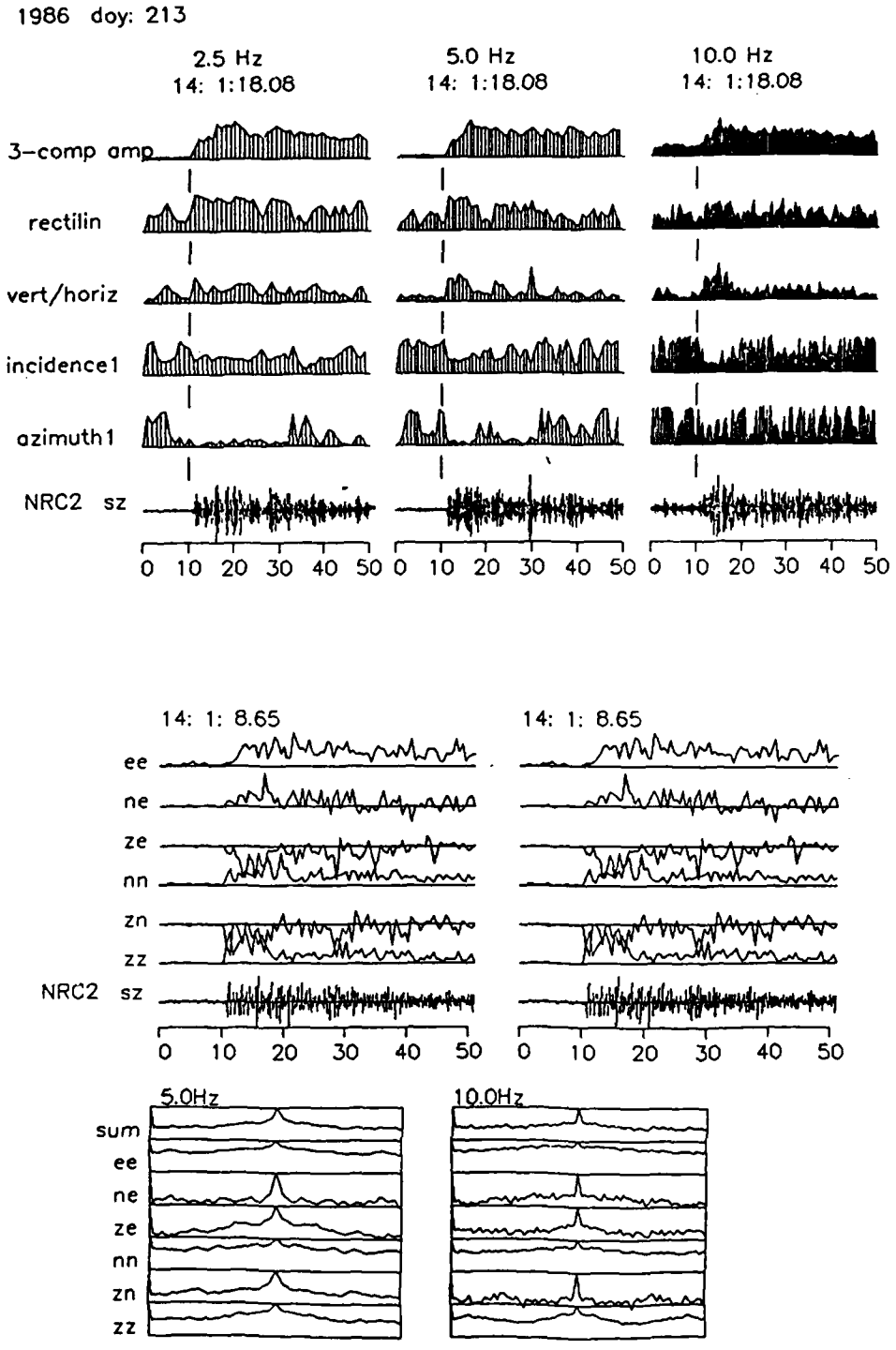

Figure 8. Three-component polarization analysis of NORESS data. Top -- particle-motion attributes in three passbands; bottom -- autocorrelation signatures and autocorrelations for 5- and 10-Hz passbands. For explanation of parameters shown, see Jurkevics (1986).

motion for the first 30 seconds of P coda, oriented in the source-receiver azimuth. However, the 10-Hz band showed strong P-wave motion for an interval of only about 8 seconds following the first arrival, after which the motions became quite random. Thus the P-coda has strongly P-polarized motion for more than 20-30 seconds at low frequency, but at higher frequencies the P motion is confined to a short interval following the first arrival. *Figure 8b* shows an autocorrelation of the particle-motion signature for a 50-second segment of P coda. The upper traces in this figure show the polarization signature and the bottom part shows the autocorrelations for 2 frequency bands. If the signal contained a double event or a strong depth phase, the autocorrelation would have a double peak separated by the time lag. The single peak of the autocorrelation suggests that such a "double source" is not present. This result is somewhat preliminary, as this technique is still in its research phase and is not well tested yet.

A final analysis carried out on the NORESS signals was a spectral parameter extraction using autoregressive (AR) analysis. The AR technique has shown promise in distinguishing between earthquakes and explosions within 10° of NORESS, in work at both the Center and NORSAR. *Figure 9* shows the AR parameters corresponding to the initial Pn arrival plotted for several earthquakes and mine explosions recorded at NORESS. The x's and crosses are for events within 10°, and most of the events were at distances less than 4°. The solid dot is for event NZ86213. Based on the spectral parameters, it falls in the earthquake population. However, a very strong qualifier needs to be applied to this result. The greater distance of the Novaya Zemlya event causes more of the high-frequency energy to be absorbed which changes the AR parameters; the m_b 5.9 presumed explosion on 25 October 1984 (Table 1) had similar AR parameters to those shown for NZ86213, and its spectrum (solid line on *Figure 10*) was similar to that (dotted line on *Figure 10*) for NZ86213.

In the NEIS list of observations, station HFS (Hagsfors, Sweden) obtained m_b of 5.0 and M_s of 3.4 for NZ86213. The position of this point on an M_s:m_b plot for Eurasian earthquakes and explosions recorded at HFS (Dahlman and Israelson, 1977; solid dot on *Figure 11*) puts it between the explosion (stars) and earthquake (open circles) populations on the plot, but closer to the latter.

4.2.6. Summary

Several analysis techniques have been applied to GDSN, RSTN and NORESS recordings of the NZ86213 event, which was located south of Matochkin Shar strait, near the eastern coast of Novaya Zemlya. The study was based on a limited amount of digital data, and at the time of this writing we are waiting for photographic copies of additional WWSSN records to be sent by the NEIS; as a result, our conclusions should be considered preliminary. The location of NZ86213 would not rule out the possibility of it being an explosion, and a comparison of P-wave signatures and spectra for this event and a presumed small underground explosion in 1977 was inconclusive for purposes of

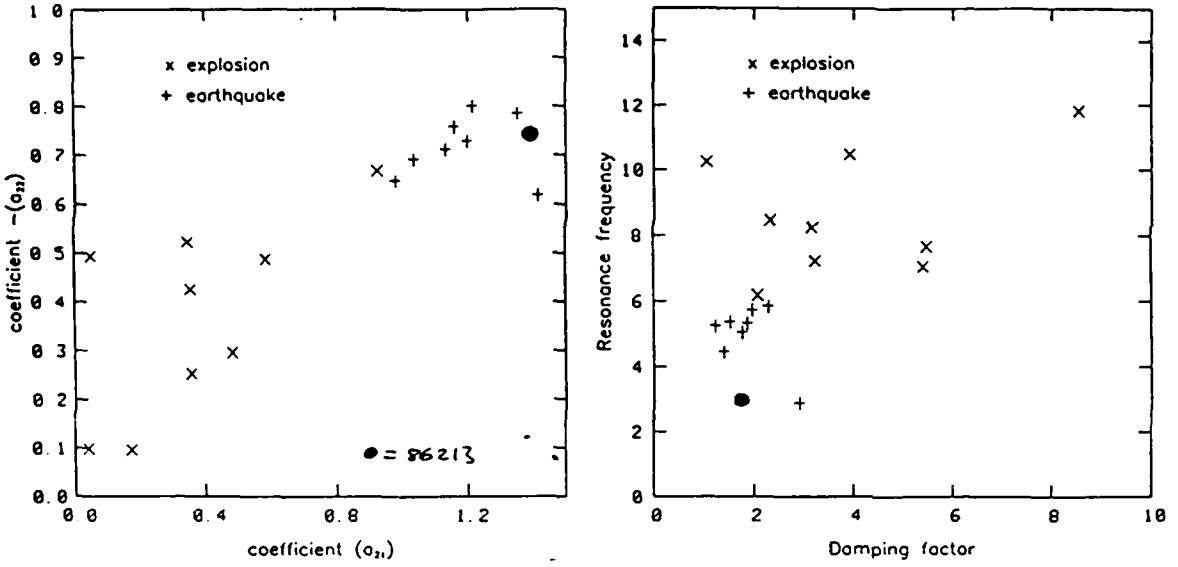

Figure 9. Left -- Second-order prediction coefficients for NORESS recording of NZ86213; right -- resonance frequency *vs* damping factor for same event. For explanation of parameters shown, see Dysart (1986).

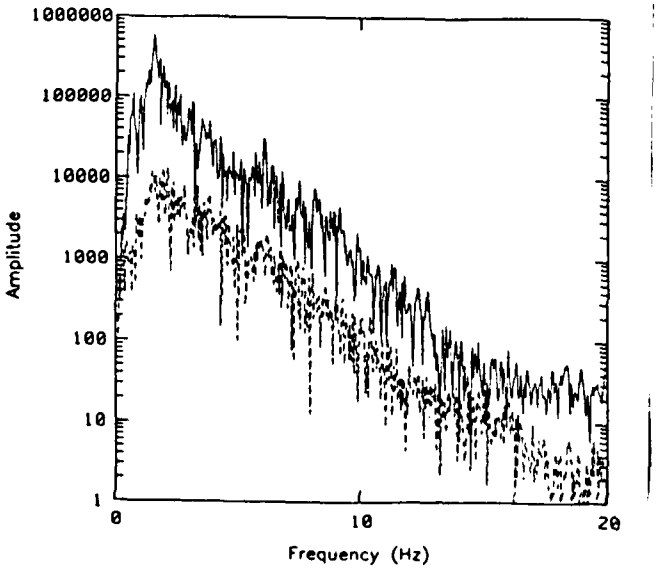

Figure 10. Spectra for NZ86213 (dotted line) and 25 October 1984 underground nuclear explosion (solid line), uncorrected for instrument response.

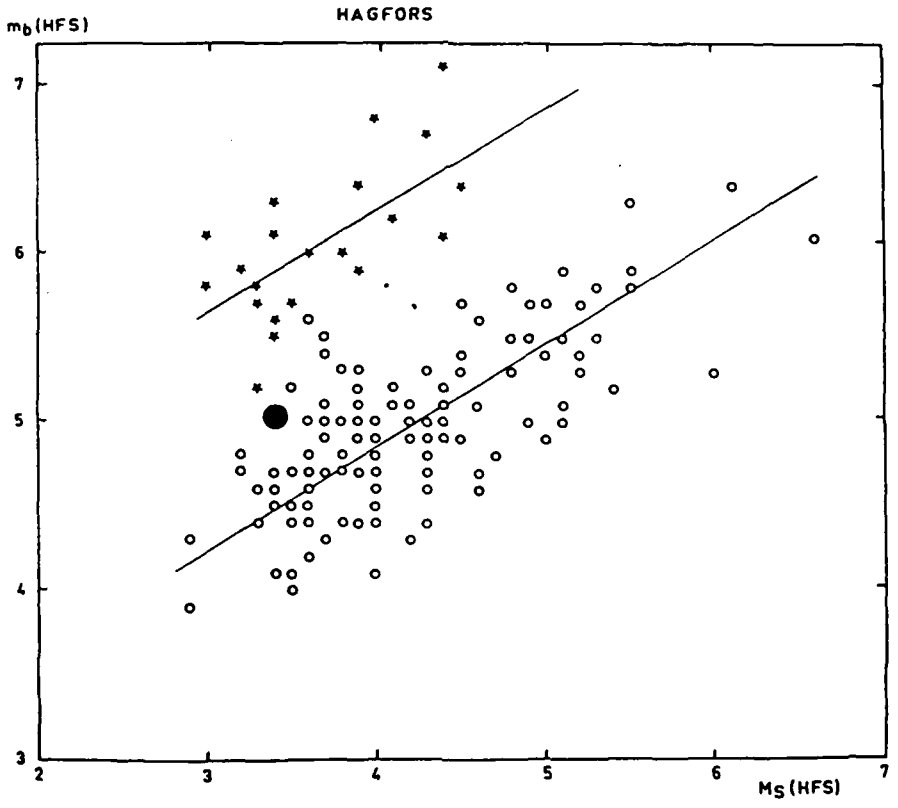

Figure 11. M_s:m_b plot for the HFS station (Dahlman and Israelson, 1977). Dot -- NZ86213; stars -- Eurasian explosions; crosses -- Eurasian earthquakes.

identification. AR parameters for NZ86213 are similar to those for small earthquakes at distances less than 10°, but are also similar to a larger explosion at the Novaya Zemlya test range. On an M_s:m_b plot the ratio of body- to surface-wave magnitudes determined by station HFS for NZ86213 was between the explosion and earthquake populations but closer to the latter. No evidence was found for a pP reflection that might have identified the event as a crustal earthquake.

These results illustrate the difficulty of identifying a well-recorded seismic event, with magnitude equivalent to a tamped underground nuclear explosion with yield of a few kilotons, locate in a stable geologic region near a well-studied test site. Far greater difficulties would certainly be encountered in attempting to use a limited number of seismic stations to detect, locate and identify much smaller earthquakes, mine blasts and possible decoupled nuclear explosions in all parts of the USSR.

Alan S. Ryall, Jr.
Andy Jurkevics
Paul S. Dysart
Jay J. Pulli

REFERENCES

Dahlman, O. and H. Israelson (1977). *Monitoring Underground Nuclear Explosions*, Elsevier Pub. Co., NY, 440 pp.

Dysart, P.S. (1986). Autoregressive analysis of regional seismograms from earthquakes and explosions, *SAIC Tech. Rept. C86-07*, 82-99.

Evernden, J.F., C.B. Archambeau and E. Cranswick (1986). An evaluation of seismic decoupling and underground nuclear test monitoring using high-frequency seismic data, *Rev. Geophys., 24*, 143-215.

Henson, A.S. and T.C. Bache (1986). *Spectral Characteristics of Regional Phases Recorded at NORESS, Technical Rept. SAIC-86/1967*, 83 pp.

Jurkevics, A. (1986). Polarization analysis using an array of three-component sensors: theory and application to NORESS, *SAIC Tech. Rept. C86-07*, 48-73.

Pomeroy, P.W., W.J. Best and T.V. McEvilly (1982). Test ban treaty verification with regional data – a review, *Bull. Seism. Soc. Am., 72*, S89-S130.

4.3. EVALUATION OF THE RSTN SYSTEM

4.3.1. Introduction

There was a dichotomy in the principal objectives of the RSTN system, at least as these objectives have evolved in practice. On the one hand the system should model an operational network having the primary characteristics of a potential system of U.S. monitoring stations inside the U.S.S.R., and on the other hand the system should also be a source of high quality data for research on propagation, detection and identification problems. The program was successful in the main in addressing both objectives, although conflicts between technical requirements for the two objectives limited what could be achieved in the program. We have included comments on both aspects of the network in the following sections of this report.

Sections 4.3.2, 4.3.3 and 4.3.4 address selected questions raised under the three categories outlined in a DARPA memo of August 18, 1986. Section 4.3.5 contains additional comments and summary material.

4.3.2. Site Selection and Performance

The quality of seismic recordings from the RSTN network varies greatly from station to station. Reasons for this include variations in the local geology, crustal structure, noise environment (both natural and man-made) and installation. Of course, if one were designing an ideal regional seismic research network, sites would be chosen for their low noise, simple crustal structure, and minimal local effects. However, in its role as a prototype network for nuclear monitoring within the Soviet Union, where station site selection may be severely restricted for the designers, the RSTN serves as a testbed for gaining experience with less than ideal sites and data. If a new generation RSTN network is to be installed, this consideration should be included.

Specific site problems included:

- **High noise at RSCP.** High-frequency noise at this site was about an order of magnitude greater than at other stations, even at relatively quiet times, (*Figure 1*). While this site may be representative of some locations that might be designated by the U.S.S.R. for use by the U.S., it would never be a site of choice for a test ban monitoring system given reasonable alternatives. Because of high noise, the data were unsuitable for several aspects of seismological research on verification problems.

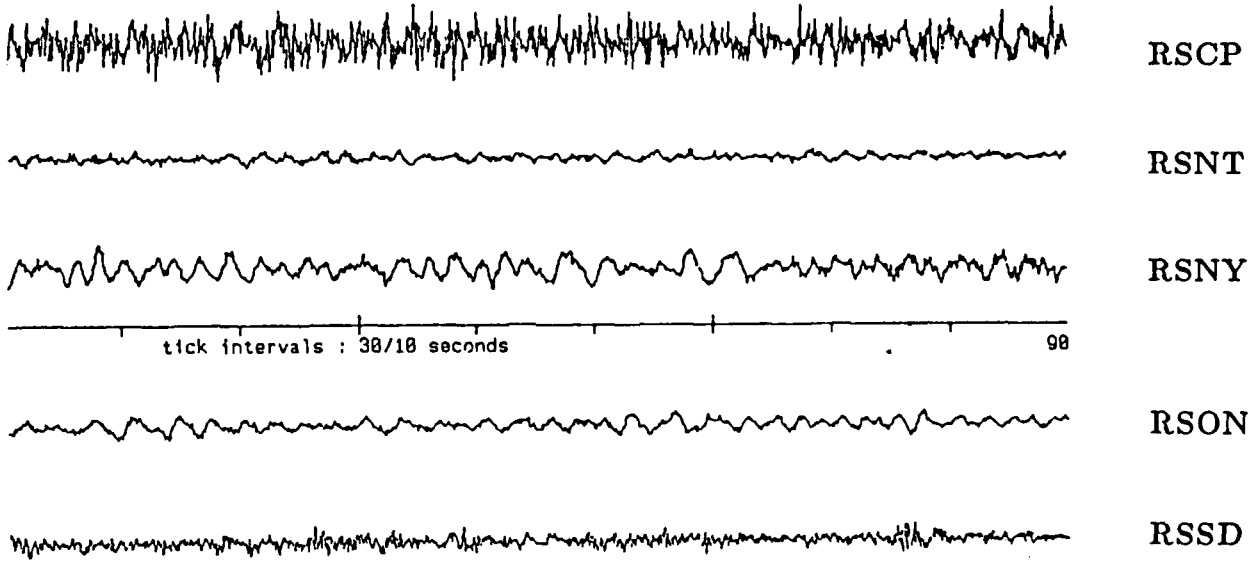

Figure 1. RSTN stations at constant gain showing noise, and local event on RSSD.

- **Mining/quarry blasts.** All sites were adversely affected by interference from mining and/or quarry blasts--RSSD more so than others. Some of these might have been usable for seismological research if the RSTN program had been supported by a supplementary program to obtain times, locations and energies of a significant number of representative blasts, but without such a program these events merely constituted noise (see RSSD trace on *Figure 1*, which shows one of the smaller blasts recorded at that site). Interference was also experienced at RSON at times by local events attributed to "ice-quakes."

- **"Crustal complexity" at RSSD.** Although the cause was not clearly isolated, RSSD exhibited characteristics commonly attributed to crustal complexity. There were reports that signals from the west were diffuse and difficult to interpret. The short-period data recorded at RSSD also show reverberations attributable to site geology. The vertical short-period data (*P* wave and coda) for two nuclear explosions at Semipalatinsk is shown in *Figure 2* as an example. This effect would certainly bias results obtained from station averages, or could produce artificial results in some kinds of analyses; e.g., secondary arrivals could be misinterpreted as depth phases. Three-component analyses of seismic signals above 1-2 Hz at RSSD were so perturbed, apparently by local effects, that the particle motions in the short-period band were not useful for determining source azimuth.

The first two problems are easily detectable (and avoidable) through a suitable site selection procedure involving the use of portable seismographs to measure noise and local disturbances prior to installation of more permanent equipment; the third is probably unavoidable in some cases in practice, although the evidence reinforces the long standing idea that massive, geologically homogeneous formations and regions are preferred for station sites.

We have not noted instances of interference from wind generated noise in the passband of interest for teleseismic detection. From this point of view the borehole installations were successful. As far as we know, possible wind effects at the high frequency limit of the system have not been adequately studied.

Polarities of the seismometers were neither fully consistent from site-to-site, nor consistent with generally accepted seismological standards (compressional motions of the earth had a negative sign, for instance). This caused erroneous reports and interpretations to be made, and required extra steps and computing time in converting this data to conform to our database (and normal seismological) standards.

There are reports of possible misorientations of horizontal components at RSNY and RSON based on analyses of the direction of arrival of seismic *P* waves. Our three-component analyses of RSCP, RSNT and RSNY were consistent with correctly oriented instruments (RSSD could not be adequately analyzed for instrument orientation as

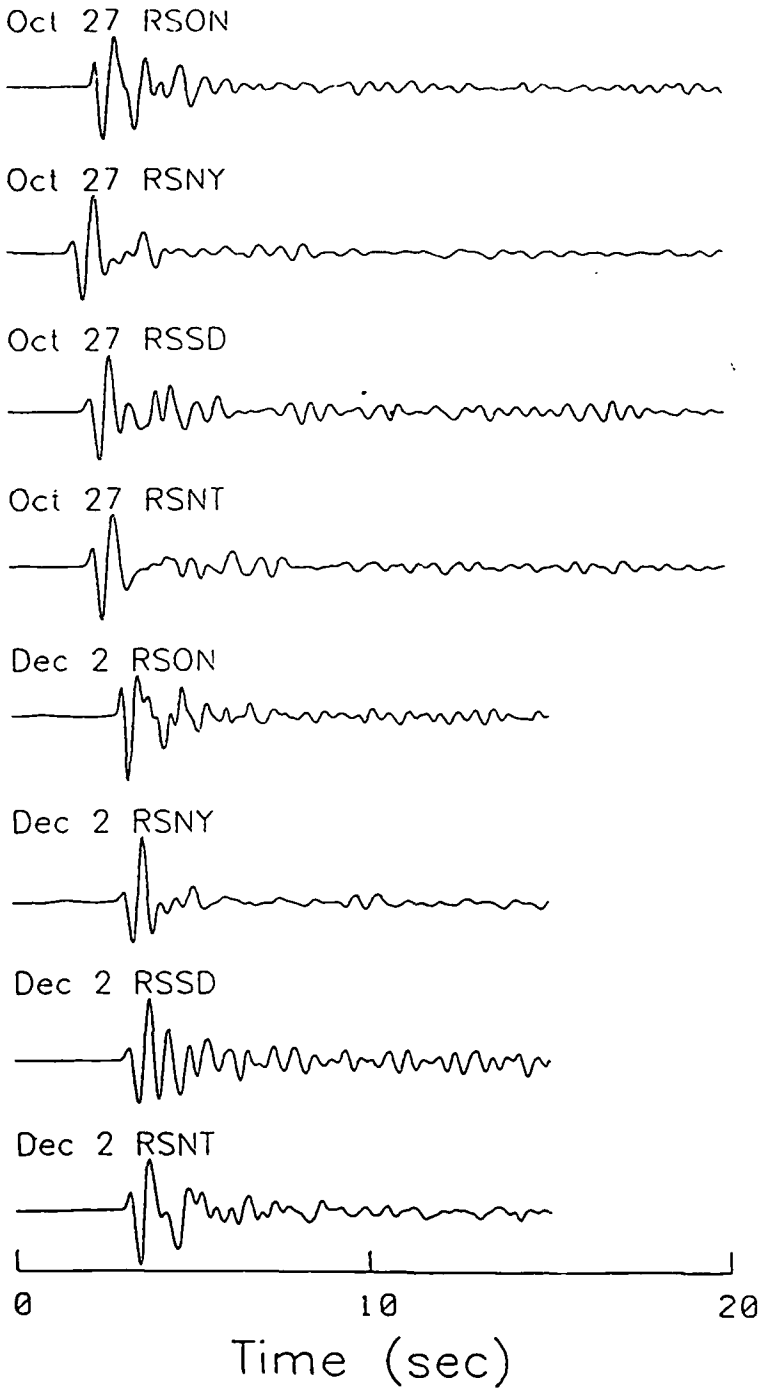

Figure 2. Two explosions at Semipalatinsk recorded in 1984 at RSTN stations. Note extended coda at RSSD relative to other sites.

previously noted), but RSON horizontals appear misoriented by 15 or 20 degrees, as also noted by others. However, these latter effects might well be caused by geological structure under the site and compass measurements within the borehole are needed to distinguish between engineering and geophysical causes. (Note: compass measurements by Sandia National Laboratories subsequently indicated that RSNY horizontals were misoriented by 17°)

For future systems, it is probable that higher frequency data will be required (see the next section of this report). The resulting shorter wavelengths will increase the desirability of establishing stations in geologically simple structures, and increase the need for protecting the seismometers from environmental and man-made interference. The preferred solution will continue to be borehole installations.

However, when a seismometer is located in a borehole, the downgoing surface phases Pp and Ps_v produce an interference effect on the observed ground motions. The interference is a function of frequency and depends on the instrument depth, seismic velocity and angle of the arriving wave. This interference is manifested not only as the well-known "scalloping" of the amplitude spectrum, but also the orientation and character of the vector particle motion become a strong function of frequency. *Figure 9* shows the theoretical interference effects of the surface phases Pp and Ps_v on an upcoming planar P wave incident at 30°. The crustal structure is assumed to be homogeneous with a P wave velocity of 5.0 km/sec and results are shown for four different receiver depths. When the receiver is on the surface, the particle motion is uniform with frequency. As the receiver is situated further downhole, the interference effects migrate to lower frequencies since the time delay of the reflected phases increases. The theoretical results shown in *Figure 9* have been confirmed by analyzing three-component short-period recordings at NORESS, where one instrument is located at the surface and another 60 meters directly below. If the crustal structure at the receiver is simple, these interference effects can be deterministically corrected to some degree. Nevertheless, it is evident that there will be a trade-off between deep burial for protection from surface generated noise and shallow burial for signal quality. This needs further study before specifying an optimum emplacement depth.

Modal structure of the noise also produces effects that vary with depth, but these effects are probably too complex to determine in any practicable site selection or instrument installation procedure. General rules guiding emplacement depth to minimize propagating noise may perhaps result from ongoing analysis at NORESS and elsewhere, but probably not in the near term.

4.3.3. Instrumentation Characteristics

4.3.3.1. Monitoring Functions

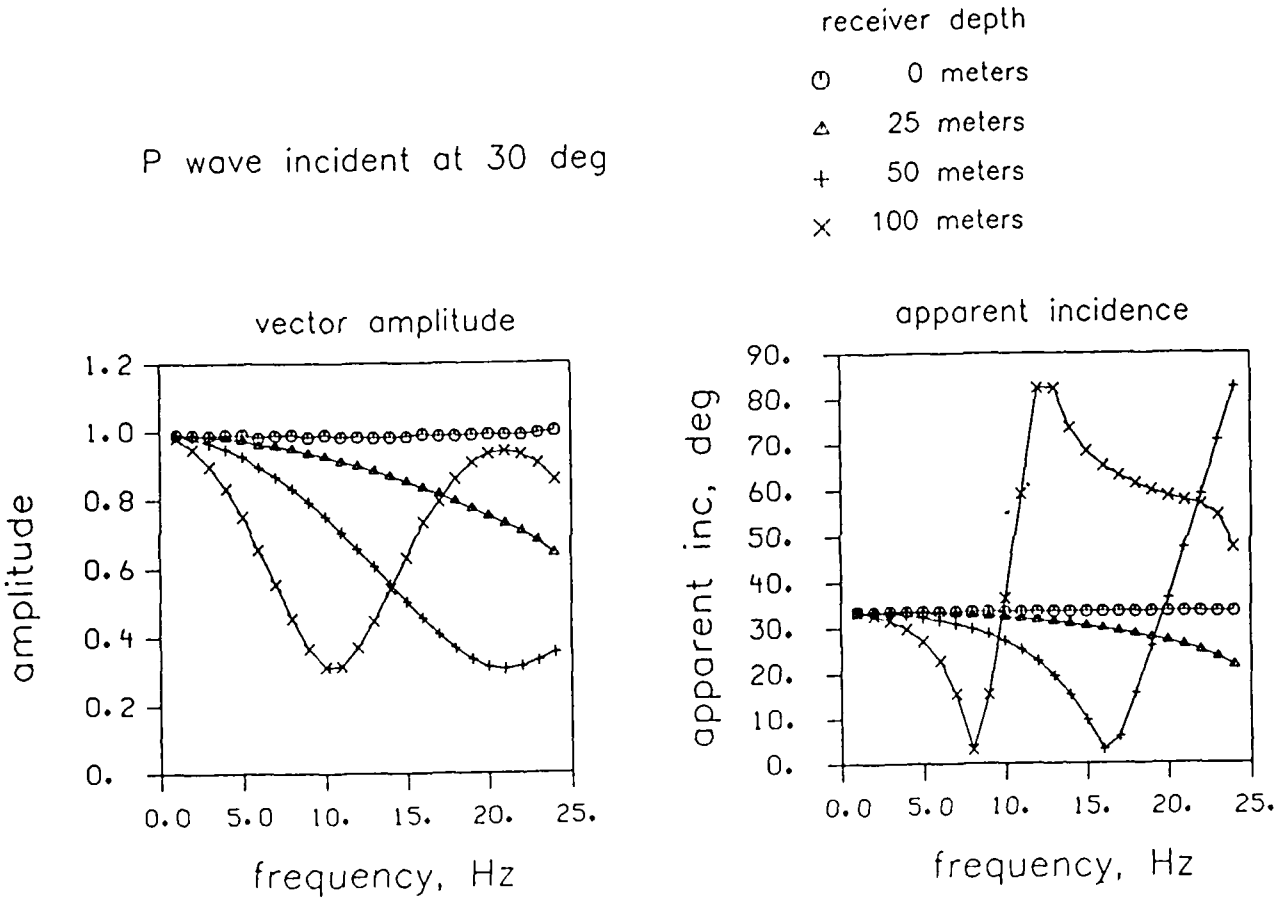

Figure 8. P + Pp + Ps interference effect vs receiver depth.

In general, the instrumentation met the overall design as established in 1977-78 for functioning as a prototype nuclear test monitoring system. That is to say, all of the standard processes relating to detection and identification of seismic events could be accomplished without significant limitations due to bandwidth, sampling rate, dynamic range, non-linearities, internal noise or other characteristics of the equipment *per se*.

Reliability was generally high: during the two months of the GSETT, for example, only six hours of outage or seriously impaired data could be definitely linked to the three stations analyzed by the Center and their transmission systems (RSSD, RSNY, and RSON). The primary impairment, however, exposed a weakness in the system since all stations were seriously impaired simultaneously (no time signals received) because of snow on the antenna at Sandia. Future stations should be more nearly autonomous. During this same period, however, RSCP was out for the entire time and RSNT had an outage of roughly 90 hours. Excluding RSCP, the average known outage for the four stations was about 24 hours ($\simeq 1.6\%$).

The inability to derive satisfactory short-period channels from the KS-36000 seismometers was adequately compensated for by using the auxiliary S-750 instruments. A similar redundant set of sensors should be included in follow-on systems.

Partitioning the data into three frequency bands imposed no problems: to date there are no monitoring functions that require recombining the data in a broad-band channel. The mid-period channels contributed little; gains were necessarily low because of the 6-second microseisms in the passband, and their utility was primarily limited to aiding an analyst in interpreting large regional events. The long-period and short-period channels had well chosen passbands for accomplishing monitoring functions, as illustrated by the fact that they provided virtually all of the required data for the GSETT. Preliminary research results have indicated that useful data might be obtained by extending the short-period band to higher frequencies, but as previously noted, currently validated monitoring methods do not require this.

One of the contemplated functions of a monitoring system would be to detect small, high-frequency events mixed with signals from large low-frequency events to guard against hide-in-earthquake evasion methods. This appears to be the only monitoring function that could be used to argue convincingly for a 24-bit system (although see comments in Section 4.3.3.2).

4.3.3.2. Research Functions.

The instruments were successful for the most part in producing high quality data needed for research on regional events. Sampling rates and the anti-aliasing filters were properly matched to the passbands. However, the instruments exhibited a non-linear response to moderate-to-large regional events. An example is shown in *Figure 4*, produced by a magnitude 5 earthquake in Ohio on January 31, 1986, at an epicentral

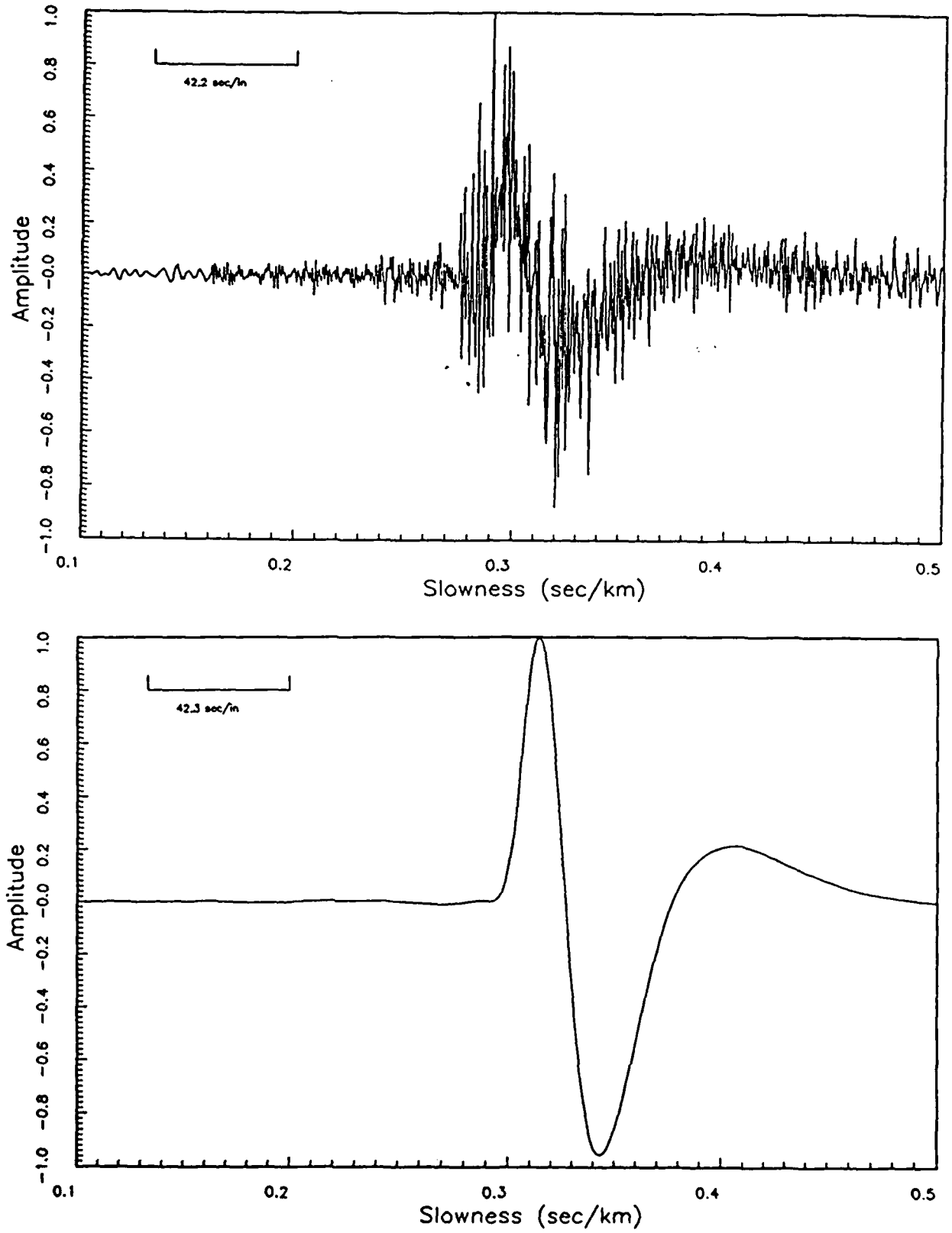

Figure 4. Mid-period and long-period response to Ohio earthquake of 31 January 1986, as recorded at RSNY.

distance of 5.7°; the impulse response of the seismometer appears to predominate, rather than the crustal/mantle response normally seen at this distance from smaller events.

Pn waves in the eastern U.S. have been observed to include frequencies up to approximately 50 Hz out to distances of at least 200 km. A number of studies at the Center and elsewhere have shown that these high frequencies contain information that can be used to discriminate between the different seismic phases that propagate to regional distances, (see *Figure 5*) and there are promising indications that identification of events may also be aided by the use of high frequencies. Three-component data is required for some of these methods. Further research is needed to determine the useful upper frequency bound for detection and identification of events in a network having the station density contemplated for use in the U.S.S.R.

For research purposes, digital resolution of 24 bits may be needed to eliminate the necessity of gain-ranging, which has been shown to contaminate some of the high frequencies at RSTN stations.

4.3.4. Communications

4.3.4.1. Transmission/Reception

The Center had no capability to measure bit error rates *per se*, since this would require complete knowledge of what was actually transmitted in addition to what was received. However, the authenticator provided direct information on the numbers of defective one-second data frames received, which was another measure of the quality of communications. Bit errors, drop-outs, noise, or any other causes of change in the data stream following the station authenticator caused the data frame to fail to authenticate at the Center.

Results were highly variable. There were day-long intervals of essentially perfect reception. An analysis of recent data from 1754 GMT September 2, 1986 through 0523 on September 8, 1986, showed that daily rates of defective frames ranged from about 50 to about 10,300 (includes all errors from five stations). The latter figure corresponds to 97.6% perfect reception rate for one-second frames assuming that all transmitted frames were actually received and checked for authenticity. Since many of the problems that caused frames to fail to authenticate were probably single bit errors or other transient effects, the reception rate per channel may have been higher in terms of bit errors or other conventional communications measures. This appears to have been the case during intervals of low error rates, but the reverse may have been true during high error rates, as discussed in the following two paragraphs.

Bit error rates or measured authentication rates, however, do not tell the story from the standpoint of a seismologist, or of a data management system like that at the Center. During intervals when one or two defective frames per hour were received from each

station, our data quality was very high. In many (perhaps most) cases, the defective frame was replaced with the delayed frame with no loss in data. In other instances, spikes or short dropouts were noted on one or more sensor channels, indicating that neither the first nor the second transmitted frame was perfect; such instances normally caused little trouble for visual analysis by a seismologist, nor would they be serious for use in research after "de-glitching." However, they caused problems for automatic analyses (to be elaborated subsequently).

During intervals having substantially greater error rates the consequences for the data management system became important, if not overwhelming. For example, during a period of 4.25 hours when the measured frame error rates were about 35 per hour per station ($\simeq$ 1%), major gaps occurred in the data recorded, resulting in an actual data loss ranging from 23% at RSON to 78% at RSNT (ignoring fragmented brief segments of received data). The reasons are not fully understood, but it appears that the communications interface system repeatedly lost synchronization with the incoming data stream, and could not reinitialize its data management programs during the intervals of clean data. If this is correct, it seems likely that the *measured* frame defect rate was not an accurate indication of the *actual* defect rate, which could have been much higher than 1%. Whatever the actual rate was, the lesson seems clear: above some threshold rate, a complex system like the Center's that attempts to do *on-line* demultiplexing, quality control, logging for Ingres records, replacing defective data with data from the delayed transmission, reformatting and archiving the data, etc., may founder. This should not be the case for a system that simply receives and writes the incoming signal to tape.

Fortunately, intervals with error rates of the magnitude just described were uncommon. During the 60+ days of the GSETT, for example, the Center was able to receive and archive 100% of the data during most days. However, from time to time the data contained transients, typically appearing as short dropouts or spikes on one or more channels. Usually the rate was low enough that the waveforms were acceptable for visual analysis. However, such occurrences did adversely affect the automatic event detector: the spikes perturbed the short-term and long-term averages and at times produced a false "trigger," and the dropouts required the detection processor to reinitialize. In either case the consequence is an interval of loss in the effectiveness of the processor until the noise statistics again stabilize. In practice during the GSETT, there were no known failures to detect valid teleseismic events following such transients, indicating that the rate of occurrence was acceptably low. Other potential automated processes (e.g., complexity) and standard off-line waveform analyses (e.g., spectra) could also be adversely affected.

4.3.4.2. Authentication

The authentication process worked well, and was used to replace defective frames from the first transmission with corrected data received in the delayed transmission. Authentication is a very sensitive method for accomplishing an extremely valuable function: *error detection.* This information can be applied to greatly reduce costly

frame-by-frame and channel-by-channel quality control and bookkeeping computations in the data management system and, potentially, in some of the automatic signal analysis processes. To be fully effective, time, channel identification and seismic data must all be authenticated.

4.3.4.3. Time Standard

Establishing the primary system time standard at Sandia proved to be troublesome. Transmission failures at Sandia left the entire network without the primary time source. Experience led the users to rely more heavily upon the "counter" at each station. A future system should have a primary time source at each station, obtaining periodic corrections from a suitable radio time standard. Time should be encoded twice in each data frame--or at least seconds and tenths should be included a second time.

4.3.4.4. Format

The basic format was satisfactory. We suggest changing the flag that now indicates when hard clipping occurs to indicate soft clipping (clipping at any stage of the signal path from seismometer through the digitizer). As used currently, the clipping flag is redundant since hard clipping is easy to see on a seismogram; soft clipping is difficult to detect in narrow-band channels.

4.3.5. General and Summary Comments

For any follow-on development, the objectives need to be clearly defined, especially with respect to development of a prototype nuclear test monitoring system *versus* a system to be deployed to obtain data for general research (i.e., research on source characteristics, propagation, or other matters not directly focused on station or network performance in a monitoring context). Questions related to generation, frequency content, attenuation, or other characteristics of regional phases for instance, are much more effectively and economically conducted with mobile stations of far less complexity than RSTN-type stations (or arrays). The additional general comments and summaries that follow deal chiefly with the development of stations and systems for nuclear test monitoring.

4.3.5.1. Site Selection/Installation

Experience with the RSTN has again confirmed the dependency of a station's quality upon the site selection and installation practices that were followed. Theoretical advantages of precise network geometry or deployment relative to potential evasive test sites can be offset by local site effects--noise, numerous local events, seasonal effects such as "ice-quakes," geological/geophysical complexity and perhaps modal structure of the noise. Installation of sensors in boreholes still appears to be optimal, although the proper

depth may be a function of site location, and more investigation is needed to define how to optimize depth. Site surveys for selecting a precise location for the borehole should include seismometers for obtaining field measurements of noise and signals covering the full range of the short-period spectrum, and the surveys should encompass seasonal as well as diurnal changes, if possible. While it is unclear how much latitude the U.S.S.R. would permit in the site selection process, it would seem to be prudent to define the operational and analytical steps that the U.S. recommends for use in an actual deployment.

4.3.5.2. Station Instrumentation and Communications

Three-component short- and long-period seismometers each have well-established functions to perform in a monitoring system, and should be included in a new system. The 6-second microseismic band is a natural place to separate long- and short-period channels, and doing so reduces dynamic range requirements on parts of the system. There has been no convincing demonstration of the need either for mid-period channels or for a single sensor or channel encompassing the entire seismic spectrum. Separate short- and long-period seismometers are probably the most economical way to obtain the required data, and the thoroughly demonstrated stability and reliability of short-period sensors should improve overall system reliability over that provided by broad-band sensors alone.

The short-period sensors should have their response extended to higher frequencies, although ongoing research has not established an upper frequency bound that could be well-defended against arguments by the Soviets to restrict the bandwidth. A compromise between interests of researchers and what is actually known about the value of higher frequencies for monitoring might be a sampling rate of 60 samples per second with an anti-aliasing filter at 25 Hz. (This is the sampling rate currently used by the Eastern Canadian Telemetered Network, or ECTN.) It would also provide enough high-frequency signal to do phase identification based on frequency content (*Figure 5*), and may be close to the high-frequency limit for observations at about 1000 km, based on NORSAR reports.

The relative values of higher frequencies, higher dynamic range, and high transmission reliabilities need to be weighed against the almost certain pressure of the Soviets to restrict the transmission rate from the sites. Anticipating a Soviet rejection of the quadruply redundant RSTN 9.6K bit transmission system, or at best accepting 9.6K bit but balking at higher rates to accommodate higher frequencies, a main thrust of any new development should be to devise an effective transmission system capable of passing more *seismic* information using a lower transmission rate.

A possible avenue is to routinely transmit only once, reserving part of the transmission channel--perhaps one frame in ten--for retransmission of seriously garbled frames as determined by inspection and requested via commands from the receiving site. Only frames that fail to authenticate during the first transmission need be inspected, exploiting the authenticator's error detection capabilities as well as its role in ensuring

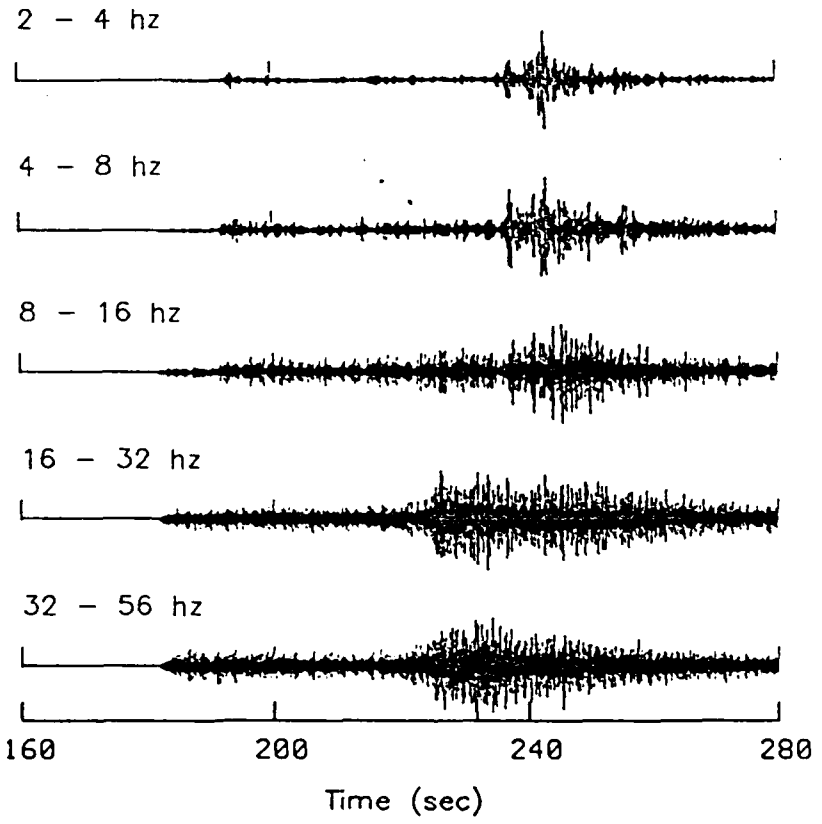

Figure 5. Filtered seismograms from regional event recorded at NORESS showing separation of P_n, P_g, S_n and L_g based on frequence.

data integrity. The criteria for commanding retransmission should be seismological rather than being based on conventional communications measures. This would allow the system to ignore bit errors in moderate numbers and other transients of no consequence to the user of the data, to concentrate on the more extended outages that do interfere with seismic monitoring, and to exploit the inherent redundancy and short-term predictability of seismic signals and noise. Some of the bandwidth saved by *not* requiring arbitrarily small bit error rates could be devoted to more seismic data. Such a design is conceptually no more intrusive than the RSTN since the short-term memories at the stations and the two-way communications that would be needed do not differ in any fundamental way from features already embodied in the RSTN design. A more extended study based on the actual *seismological* needs, and including the RSTN experience, is recommended.

Other approaches exist. High-frequency channels (or high sampling rates) could be transmitted only when triggered, for instance. Or data compression methods should be considered--simple, commonly available data compression methods tested at the Center on waveform data have given 40% reductions, and methods specifically tailored to seismic data might yield further compression. Or the design might consider that higher dynamic range (and the associated need for increased bandwidth) is not the only approach to counter hide-in-earthquake evasion: filtered channels and the design of the monitoring network itself need to be examined--all possible capabilities need not reside in each single station. Each of these concepts should be considered in a more extended study based on the actual seismological needs of the entire monitoring *system*, and drawing upon experience with the RSTN.

4.3.5.3. Data Processing and Archiving

Although station/transmission outages were the primary known causes of lost RSTN data, secondary causes were in the computer and software systems at the Center. The basic design of the Center's system, utilizing then-existing equipment, included two computers and the connecting Proteon network. As a result, the receiving and processing system was vulnerable to problems on all three subsystems, to software problems associated with the system's complexity, and, of course, to losses occasioned by scheduled maintenance and system tests on all three components. During the 63-day GSETT period, for example, losses at the Center accounted for 15 hours per station (average for RSTN, RSSD, RSNY, and RSON), or about 1%, as compared with station/transmission losses of 24 hours per station (excluding RSCP, which was out the entire time--1464 hours). Approximately five of the 15 hours of data loss at the Center were caused by computer crashes and network losses, while most of the remainder occurred during the period between a failure and the restart of the data input program. Most of the data losses at the Center were thus simultaneous at all stations.

Future systems can give improved reliability by accomplishing the data acquisition with single computers (as is being done for NORESS data at the Center), by employing backup computers, and by separating channels from each station and processing them

independently. This is another area where a trade-off study would be desirable. In addition, advances in operating systems, as well as software "lessons learned" in acquiring RSTN data, should lead to a more robust data acquisition system.

4.3.5.4. Network Monitoring Capability

The RSTN was not well-sited for exploring the capability of such a network. Although inter-station spacings were appropriate for modeling the proposed network inside the U.S.S.R., a more optimal network should include stations near or surrounding areas with dense local networks--like la Malbaie area of eastern Quebec, the area around New Madrid, eastern Tennessee, etc.--so that these local networks could provide epicenter, focal depth and mechanism for events recorded by the RSTN stations. Research using the RSTN data could then concentrate on development and testing of new methods to locate and identify events within the network, making use of the control provided by the dense local networks.

A thorough network monitoring experiment was never done. Perhaps the nearest was the Center's work during the GSETT, although the GSETT objectives were far more narrow than those that would be included in a thorough study. Specifically, data from all stations should be included, the experiment should attempt to detect and *identify* all events (including local, quarry blasts, etc.), and "ground truth" data from existing and supplementary seismic networks should be included to validate the estimated capabilities of the RSTN network. Research bearing on certain facets of such an experiment has been done, e.g., the work of Dean and Goncz, Blandford et al. (TGAL-TR-83-5), and work by the Center's staff. However, such an experiment would help provide a basis for assessing how problems or improvements in components or subsystems of a monitoring network effect the network's nuclear test ban *monitoring capability*. The latter is very difficult to do by evaluating components independently.

C.F. Romney
H. Israelsson
A. Campanella
J.J. Pulli
A. Jurkevics

END

5-87

DTIC